

ABUNDANCES AT HIGH REDSHIFTS: THE CHEMICAL ENRICHMENT HISTORY OF DAMPED LYMAN-ALPHA GALAXIES

Limin Lu¹, Wallace L. W. Sargent, & Thomas A. Barlow
California Institute of Technology, 105-24, Pasadena, CA 91125

ABSTRACT

We study the elemental abundances of C, N, O, Al, Si, S, Cr, Mn, Fe, Ni, and Zn in a sample of 14 damped Ly α systems (galaxies) with H I column density $N(\text{H I}) \geq 10^{20} \text{ cm}^{-2}$, using high quality spectra of quasars obtained with the 10m Keck telescope. To ensure accuracy, only weak, unsaturated absorption lines are used to derive ion column densities and elemental abundances. Combining these abundance measurements with similar measurements in the literature, we investigate the chemical evolution of damped Ly α galaxies based on a sample of 23 systems in the redshift range $0.7 < z < 4.4$. The main conclusions are as follows.

1. The damped Ly α galaxies have (Fe/H) in the range of 1/10 to 1/300 solar, clearly indicating that these are young galaxies in the early stages of chemical evolution. The $N(\text{H I})$ -weighted mean metallicity of the damped Ly α galaxies between $2 < z < 3$ is $(\text{Fe}/\text{H})=0.028$ solar. There is a large scatter, about a factor of 30, in (Fe/H) at $z < 3$, which we argue probably results from the different formation histories of the absorbing galaxies or a mix of galaxy types.

2. Comparisons of the distribution of (Fe/H) vs redshift for the sample of damped Ly α galaxies with the similar relation for the Milky Way disk indicate that the damped Ly α galaxies are much less metal-enriched than the Galactic disk in its past. Since there is evidence from our analyses that depletion of Fe by dust grains in the sample galaxies is relatively unimportant, the difference in the enrichment level between the sample of damped Ly α galaxies and the Milky Way disk suggests that damped Ly α galaxies are probably not high-redshift spiral disks in the traditional sense. Rather, they could represent a thick disk phase of galaxies, or more likely the spheroidal component of galaxies, or dwarf galaxies.

3. The mean metallicity of the damped Ly α galaxies is found to increase with decreasing redshift, as is expected. All four of the damped Ly α galaxies at $z > 3$ in our sample have (Fe/H) around 1/100 solar or less. In comparison, a large fraction of the damped Ly α galaxies at $z < 3$ have reached ten times higher metallicity. This suggests that the time around $z = 3$ may be the epoch of galaxy formation in the sense that galaxies are beginning to form the bulk of their stars. Several other lines of evidence appear to point to the same conclusion, including the evolution of the neutral baryon

¹Hubble Fellow

content of damped Ly α galaxies, the evolution in the quasar space density, and the morphology of $z > 3$ galaxies.

4. The relative abundance patterns of the elements studied here clearly indicate that the bulk of heavy elements in these high-redshift galaxies were produced by Type II supernovae; there is little evidence for significant contributions from stellar mass loss of low-to-intermediate mass stars, or from Type Ia supernovae.

5. Although earlier studies have attributed the overabundance of Zn relative to Cr or Fe found in damped Ly α galaxies to selective depletion of Cr and Fe by dust grains, such an interpretation is inconsistent with many of the other elemental abundance ratios seen in these galaxies, most notably N/O and Mn/Fe. Several other tests also indicate that there is no significant evidence for dust depletion in these galaxies. We suggest that the overabundance of Zn relative to Cr in damped Ly α galaxies may be intrinsic to their stellar nucleosynthesis. If this interpretation is correct, it will provide important new information to the theory of stellar nucleosynthesis.

6. The absorption profiles of Al III in damped Ly α galaxies are found to resemble those of the low-ionization lines. The profiles of Si IV and C IV absorption, while resembling each other in general, are almost always different from those of the low-ionization absorption lines. These results suggest that Al III is probably produced in the same physical region as the low-ionization species in the absorbing galaxies, while the high-ionization species (Si IV and C IV) mostly likely come from distinct physical regions.

7. We discuss possible ways to obtain information on the history of star formation (i.e., continuous or episodic) in damped Ly α galaxies, and on the shapes of the stellar initial mass functions.

8. We review the evidence for, and against, the hypothesis that damped Ly α galaxies are disks or proto-disks at high redshifts, and discuss the implications.

9. We determine upper limits on the temperature of the cosmic microwave background radiation at several redshifts using absorption from the fine structure level of the C II ion. These upper limits are consistent with the predicted increase of T_{CMB} with redshift.

Subject headings: cosmology: cosmic microwave background - early universe - galaxies: abundances - galaxies: ISM - nucleosynthesis - quasars: absorption lines

1. INTRODUCTION

A fundamental question in the study of galaxy formation and evolution is: what is the chemical evolutionary history of galaxies? While some information pertaining to the general question of galactic chemical evolution has been obtained from studies of stellar populations and

the interstellar medium in the Milky Way and in nearby external galaxies, *direct* observations of the chemical evolution of galaxies in the early universe has been lacking. The situation changed when it was recognized that the narrow absorption lines in the spectra of high-redshift quasars can be used to probe conditions in the early universe. One of the most important developments along this direction has been the recognition of “damped Ly α absorption systems” as a significant population of quasar absorbers and the subsequent systematic studies of their basic properties, which demonstrate that damped Ly α galaxies are likely to be the progenitors of present-day galaxies (Wolfe et al. 1986; Wolfe 1995; Lanzetta, Wolfe, & Turnshek 1995).

The pioneering work by Meyer, Welty, & York (1989) and by Pettini, Boksenberg, & Hunstead (1990) clearly demonstrated that one can extract significant information on the abundances of chemical elements in damped Ly α galaxies through the analysis of the absorption lines in quasar spectra. Pettini et al. (1994) conducted the first systematic survey of elemental abundances in damped Ly α galaxies, though, for practical reasons, the study was limited to the elements Zn and Cr. Nonetheless, their study revealed the important fact that damped Ly α galaxies are generally metal poor (mean (Zn/H) \sim 1/10 solar), confirming that these are young galaxies in the early stages of chemical enrichment. It was also noted that the element of Cr is generally less abundant than Zn relative to their solar proportion. Since Zn and Cr are thought to be made in solar proportions throughout the Milky Way based on their abundances in Galactic disk and halo stars (see discussion in §4.3), the overabundance of Zn relative to Cr found in damped Ly α galaxies was taken as evidence that some Cr was depleted from the gas phase by dust grains.

The large collecting power of the 10m Keck telescope has made it feasible to study elemental abundances in damped Ly α systems in much more detail (Wolfe et al. 1994; Lu et al. 1996a). The improvements come in three facets. The first is the higher spectral resolution (FWHM $<$ 10 km s $^{-1}$), which allows one to see more component structure in the absorption. The second is the much improved S/N of the spectra, which makes it considerably easier to study the weak absorption lines. Weak absorption lines are crucial for the determination of elemental abundances since they do not suffer nearly as much as the strong lines from line saturation. The third has to do with the large spectral coverage of the Keck High Resolution Spectrometer (HIRES), which enables the study of many elements simultaneously. This is important because the relative abundances of elements contain valuable information about the nature of the stellar nucleosynthesis that made these elements (cf. Wheeler, Sneden, & Truran 1989).

For a number of years, we have been collecting high quality spectra of quasars using the Keck HIRES in order to carry out a comprehensive analysis of the various absorption phenomena. One particular aspect of this program is the study of elemental abundances in damped Ly α systems and their implications for galactic chemical evolution and for stellar nucleosynthesis. Some preliminary results of this nature have been reported in Lu, Sargent, & Barlow (1995a). The current paper presents the full analyses. The results described here supersede the earlier results reported in Lu et al. (1995a).

In §2 we describe the observations, data reduction, and the methods used to estimate equivalent widths and column densities. Abundance determinations for the 14 damped Ly α systems studied here are discussed in §3. These abundance measurements are combined with similar measurements in the literature to study the chemical evolution of damped Ly α galaxies over the redshift range $0.7 < z < 4.4$ (§4). In §5 we discuss other observed properties of damped Ly α galaxies and implications for their nature. The redshift dependence of the temperature of the cosmic microwave background as estimated from the C II* $\lambda 1335$ fine structure line is discussed in §6. §7 summarizes the main conclusions.

Throughout this study, we will assume $q_0 = 0.1$ and $H_0 = 50 \text{ km s}^{-1} \text{ Mpc}^{-1}$. We will use z for general references of redshift, z_{em} for the emission redshift of quasars, z_{damp} for the redshift of damped Ly α systems, and z_{abs} for any other absorption systems or for absorption systems in general.

2. OBSERVATIONS, DATA REDUCTION, AND MEASUREMENTS

2.1. Observations and Data Reduction

Table 1 gives the journal of the Keck HIRES observations. A 0.86" slit width was used in all cases to yield a resolution of FWHM=6.6 km s $^{-1}$ with roughly 3 pixels per resolution element. The echelle format of HIRES is such that one can only get complete coverage of the free spectral range for $\lambda < 5100 \text{ \AA}$ in a single setup with the current TeK 2048x2048 CCD. Except in a few cases, we used two partially overlapping setups for each wavelength region in order to get complete spectral coverage. Data reductions were done using a software written by T. A. Barlow. After the echelle orders were optimally extracted and wavelength- and flux-calibrated, they were resampled to 2 pixels per resolution element, scaled to the same flux level, and added together weighted according to their S/N. Because some spectral regions have more exposures than others due to the overlapping-setup scheme, the S/N of the spectrum from even a single object can show quite large variations from one region to another.

Most metal lines associated with damped Ly α systems are blended with Ly α absorption lines if they occur in the Ly α forest. Thus our analyses will primarily rely on measurements made redward of the Ly α emission line. We estimate the continuum level redward of the Ly α emission by fitting cubic splines to regions deemed free of absorption lines using the IRAF task *continuum*. In rare cases, we may also use measurements made in the Ly α forest if the lines are reasonably clean. In such cases, the continuum level is estimated by picking out small “peaky” regions in the spectral region of interest that are free of obvious absorption lines and interpolating them with low-order cubic splines. The resulting continuum appears to describe the data quite well.

2.2. Equivalent Width and Column Density Measurements

For each damped Ly α system studied here, we give a table listing the absorption lines detected, the measured equivalent widths, and column densities (see §3).

To carry out the measurements for a given damped Ly α system, we first plot the continuum-normalized profiles of the absorption lines in velocity space for an adopted redshift for the system (which generally corresponds to the strongest component in the low ion absorption). Equivalent width for each line is then estimated by integrating the observed spectrum over the width of the absorption line defined by two limiting velocities: v_- and v_+ . The 1σ uncertainty associated with the measured equivalent width is also calculated including both the effects of statistical noise and of uncertainties in the placement of the continuum level (cf. Savage et al. 1993). Only features over the 4σ significance level will be considered a real detection.

To obtain column densities, we use the apparent optical depth method (cf. Savage & Sembach 1991). We first convert the normalized absorption line profiles, $I(v)$, into measures of the apparent optical depth per unit velocity, $\tau_a(v)$, through the relation $\tau_a(v) = -\ln[1/I(v)]$, which can then be converted into the apparent column density per unit velocity, $N_a(v)$, in units of atoms cm^{-2} (km s^{-1})⁻¹ through the relation

$$N_a(v) = 3.767 \times 10^{14} \frac{\tau_a(v)}{f\lambda}, \quad (1)$$

where λ is the rest wavelength in \AA and f is the oscillator strength. The total column density, obtained by integrating $N_a(v)$ over the width of the absorption profile, should represent the true column density to within the measurement uncertainty if the absorption line contains no unresolved, saturated components². In the case that the absorption line does contain unresolved, saturated components, the integrated $N_a(v)$ only gives a lower limit to the true column density. For an ion species for which several absorption lines with different $f\lambda$ values are observed, comparisons of their integrated $N_a(v)$ will generally allow one to infer if unresolved saturated components are present. This is because lines with larger $f\lambda$ values will yield lower integrated column densities than lines with smaller $f\lambda$ values in such cases. This technique was explored in details by Savage & Sembach (1991). Examples of applications may be found in Lu et al. (1995b).

Empirically, we find that, given the spectral resolution and S/N typical of the data used in this work, absorption lines with peak absorption depth less than $\sim 80\%$ (i.e., peak optical depth $\tau_0 < 1.6$ if the lines are resolved) show no evidence of unresolved saturation that would render invalid the column densities derived from $N_a(v)$ integrations. For example, the Fe II $\lambda\lambda 2249, 2260$ lines differ in their $f\lambda$ values by a factor of 1.3, and they yield the same $N(\text{Fe II})$ for several systems in Q 0449–1326, Q 0450–1312, and Q 0454+0356 even though the intrinsically

²In principle, one can measure the column density of a saturated absorption line if the absorption line is fully resolved, *and* if the S/N is good enough to clearly indicate that the flux in the center of the absorption line does not go to zero. In practice, this rarely happens due to limited S/N in real data.

stronger $\lambda 2260$ absorption lines are 60-75% deep. Similarly, the Si II $\lambda\lambda 1304, 1526$ absorption lines, which differ by a factor of 1.5 in their $f\lambda$ values, yield consistent $N(\text{Si II})$ in several systems in Q 1946+7658, Q 2212–1626, and Q 1202–0725 (Lu et al. 1996a) even though the intrinsically stronger $\lambda 1526$ absorption lines are 70-85% deep. Also, the S II $\lambda\lambda 1250, 1253$ lines (which differ in their $f\lambda$ values by a factor of 2) in the $z_{damp} = 2.8110$ system toward Q 0528–2505 yield consistent column densities despite the fact that the intrinsically stronger $\lambda 1253$ absorption is 85% deep. The most dramatic example is offered by the $z_{damp} = 2.8268$ system toward Q 1425+6039, where the Fe II $\lambda\lambda 1608, 1611$ absorption lines, which differ in their $f\lambda$ values by a factor of 62, yield $N(\text{Fe II})$ values differing by less than 0.1 dex, and the $\lambda 1608$ absorption line is 80% deep. Similar examples may be found for the more ionized species such as Al III, Si IV, and C IV, each having doublet absorption lines differing in their $f\lambda$ values by a factor of 2. In fact, we have yet to find an example where an absorption line with peak absorption depth $< 80\%$ shows convincing evidence of being saturated and unresolved. Thus, for ion species for which only a single absorption line is observed (i.e., for which we cannot check independently if there is any unresolved saturation in the absorption), we will assume that the column density derived from integrating its $N_a(v)$ profile is unbiased with respect to unresolved saturation if its peak absorption depth is less than 80%. In reality, most of the single absorption lines studied here are $< 50\%$ deep, corresponding to a peak optical depth of 0.7 if the lines are resolved. The only single absorption lines with peak absorption depth between 50 to 80% for which we have adopted their $N_a(v)$ -integrated column density as real measurements (rather than lower limits) are the Si II $\lambda 1808$ lines at $z_{damp} = 2.8110$ toward Q 0528–2505 and at $z_{damp} = 4.0803$ toward Q 2237–0608, the Fe II $\lambda 1608$ line at $z_{damp} = 2.8268$ toward Q 1425+6039, and Al II $\lambda 1670$ lines at $z_{damp} = 2.8443$ toward Q 1946+7658 and at $z_{damp} = 4.0803$ toward Q 2237–0608 (see §3 for details).

We emphasize that, for unsaturated or mildly saturated lines, the apparent optical depth method will yield column density measurements in agreement with the profile fitting technique. For heavily saturated lines, neither method will yield very reliable column densities in practice. For this reason, the analyses in this paper will concentrate on column density measurements made from unsaturated lines. Column density *limits* from saturated lines may be used occasionally in the discussion. For lines that are undetected or detected at significance level less than 4σ , we will use the 4σ upper limits of the equivalent width to estimate the upper limits of the column density assuming linear part of the curve of growth.

Atomic data, including rest-frame vacuum wavelength, oscillator strength (f -value), and radiation damping constant, are taken from Morton (1991) except for those which have revised f -values as given in the compilation of Tripp, Lu, & Savage (1996; see Savage & Sembach 1996 for additional information).

3. DISCUSSION OF INDIVIDUAL SYSTEMS

In this section, we derive column densities and elemental abundances for each individual damped Ly α system studied here. In general, absorption lines occurring in the Ly α forest will not be discussed unless the line is relatively clean of contamination from forest absorption. It will be assumed that the ionization state of the absorbing gas is dominated by species appropriate for H I gas (e.g., O I, N I, C II, Si II, Fe II, etc.) so that abundance corrections for unobserved ionization stages are negligible. This is believed to be a good assumption given the large H I column density of the systems (see Viegas 1995).

Two damped Ly α systems not covered by the spectra listed in Table 1 will also be discussed. These are the $z_{damp} = 1.1743$ system toward Q 0450–1312, and the $z_{damp} = 0.8598$ system toward Q 0454+0356. Keck HIRES observations of these two quasars were made by Drs. Christopher Churchill and Steven Vogt, who have kindly made their spectra available to us. Details of the observations and reductions for these two objects are discussed in Churchill & Vogt (1997).

3.1. Q 0000–2620 $z_{damp} = 3.3901$ Damped System

This damped Ly α system has been known ever since the quasar was first discovered by C. Hazard (unpublished; but see Webb et al. 1988). It is one of the four damped Ly α galaxies at $z > 3$ for which abundance information has been obtained. The HIRES spectrum used here for this object was already published by Lu et al. (1996b). We estimate $N(\text{H I}) = (2.6 \pm 0.5) \times 10^{21} \text{ cm}^{-2}$ from fitting the Ly α damping profile (figure 1), which agrees quite well with other determinations (Webb et al. 1988; Sargent, Steidel, & Boksenberg 1989; Savaglio, D’Odorico, & Moller 1994). Absorption lines detected redward of the Ly α emission are listed in Table 2; the absorption profiles are shown in figure 2. Several other lines (Si II $\lambda\lambda 1190, 1193, 1260, 1304$, Si III $\lambda 1206$, O I $\lambda 1302$, C II $\lambda 1334$, Si IV $\lambda\lambda 1393, 1402$) are clearly detected in the Ly α forest but are blended with Ly α forest absorption (see the spectrum in Lu et al. 1996b). These lines will not be discussed here.

Except for the line tentatively identified as S II $\lambda 1253$, all the low ion lines shown in figure 2 are clearly saturated, so only lower limits to their column densities are given in Table 2, along with the abundance limits. Similarly, only a lower limit to the C IV column density is given. For Fe II, we give both the lower and upper limits to the column density determined from the saturated Fe II $\lambda 1608$ absorption and from the absence of the Fe II $\lambda 1611$ absorption.

In Lu et al. (1996b) we tentatively identified a weak absorption feature in the Ly α forest as the S II $\lambda 1253$ line associated with this damped Ly α system. This weak feature is also shown in figure 2, and it shows excellent redshift agreement with the other low ion lines. The corresponding S II $\lambda\lambda 1250, 1259$ lines are badly blended with Ly α forest absorption. If our identification of this S II line is correct, then the estimated column density, $\log N(\text{S II}) = 14.70 \pm 0.03$ (Lu et al. 1996b), would imply an abundance of $[\text{S}/\text{H}] = -1.98$. This is consistent with the limits obtained

for the other elements. We note that Pettini et al. (1995b) estimated $[Zn/H] \leq -1.76$ (3σ) and $[Cr/H] = -2.46$.

3.2. Q 0216+0803 $z_{damp} = 2.2931$ System

This damped Ly α system was discovered by Lanzetta et al. (1991) and confirmed by Lu & Wolfe (1994), who estimated $\log N(H\text{ I}) = 20.45 \pm 0.16$ for the system. Our Keck spectrum does not cover the wavelength region containing the damped Ly α absorption. We will therefore adopt the $N(H\text{ I})$ value from Lu & Wolfe (1994). The absorption lines detected redward of the Ly α emission are listed in Table 3, and the absorption line profiles are shown in figure 3. Lines detected in the Ly α forest, which will not be used in the analysis, include C II $\lambda 1334$, O I $\lambda 1302$, Si II $\lambda 1304$, and Si IV $\lambda\lambda 1393, 1402$.

The Zn II $\lambda 2026$ and Cr II $\lambda 2056$ absorption lines are detected at the 2.3σ and 2.6σ levels, respectively; we will only use their 4σ upper limits in the subsequent analyses. The Fe II $\lambda 1608$ absorption is probably saturated and we conservatively give a lower limit of $\log N(\text{Fe II}) > 14.81$. The much weaker Fe II $\lambda 2260$ absorption is detected at the 2.6σ level, and the corresponding 4σ upper limit is $\log N(\text{Fe II}) < 14.97$. We will therefore adopt $\log N(\text{Fe II}) = 14.89 \pm 0.08$.

3.3. Q 0216+0803 $z_{damp} = 1.7688$ System

This system was identified as a candidate damped Ly α absorption by Lanzetta et al. (1991) based on a low resolution spectrum. No higher-resolution confirmation of the damped Ly α absorption is available. However, the fact that we detect intrinsically weak absorption lines like Fe II $\lambda 2260$, Mn II $\lambda 2576$, and Ni II $\lambda 1751$ suggests that most likely this is a damped Ly α system. For example, even for solar metallicity, the observed Fe II column density would imply $N(H\text{ I}) \sim 10^{19} \text{ cm}^{-2}$. The Ly α line equivalent given by Lanzetta et al. (1991) implies $\log N(H\text{ I}) = 20$. We tentatively adopt $\log N(H\text{ I}) = 20 \pm 0.18$, assuming a 50% uncertainty. The absorption lines redward of Ly α emission for this system are listed in Table 4, and the profiles are shown in figure 4. Note that none of the Zn II and Cr II absorption lines is detected at over 4σ significance level so only upper limits to their column densities are listed in Table 4. Metal lines detected in the Ly α forest include C IV $\lambda\lambda 1548, 1550$, Fe II $\lambda 1608$, and Al II $\lambda 1670$.

3.4. Q 0449–1326 $z_{damp} = 1.2667$ System

The redshift of this system is too low to see the corresponding Ly α absorption line ($\lambda_{obs} = 2755 \text{ \AA}$) from the ground. The damped Ly α nature of the system is inferred from the detection of the intrinsically weak Mn II triplet lines and the Fe II $\lambda\lambda 2249, 2260$ lines (see Table 5), which even for

solar abundances, implies a $N(\text{H I}) \sim 4 \times 10^{19} \text{ cm}^{-2}$. The metal lines detected in this system are listed in Table 5. Figure 5 shows the absorption line profiles.

The derivation of the Mn II column density deserves some discussion. The estimated values of $N(\text{Mn II})$ obtained by integrating $N_a(v)$ increases systematically with decreasing $f\lambda$ value of the lines (Table 5). This seems to indicate that all three Mn II lines are moderately saturated. However, we argue that this is most likely not the case. The Mn II lines are weaker than or comparable to the Fe II $\lambda 2260$ absorption in the system. The good agreement in the estimated $N(\text{Fe II})$ from the Fe II $\lambda 2260$ absorption and the weaker Fe II $\lambda 2249$ absorption indicates that the Fe II $\lambda 2260$ absorption is not saturated. Thus it is difficult to understand why the Mn II lines should be saturated. The S/N near Mn II $\lambda 2576$ is twice as good as the region near Mn II $\lambda 2594$, and three times as good as the region near Mn II $\lambda 2606$. The values of $N(\text{Mn II})$ from the $\lambda 2576$ and $\lambda 2594$ lines agree well within 1σ . It is only the $N(\text{Mn II})$ from the $\lambda 2606$ line that differs significantly. A careful look at the actual apparent column density profiles (figure 6) of the three Mn II lines confirms that it is the Mn II $\lambda 2606$ absorption that shows significant deviation from the other two lines. It is likely that the Mn II $\lambda 2606$ absorption is contaminated by an unidentified weak absorption line from another redshift system. We will therefore adopt the Mn II column density determined from the $\lambda 2576$ and $\lambda 2594$ lines.

Since we do not have the $N(\text{H I})$ information, it is not possible to derive absolute abundances for the system. However, it may be interesting to get a crude idea of what the abundances might be for reasonable guess of the $N(\text{H I})$. For $N(\text{H I}) = 2 \times 10^{20} \text{ cm}^{-2}$, the column densities given in Table 5 implies: $[\text{Fe}/\text{H}] = -0.68$, $[\text{Mn}/\text{H}] = -0.96$, and $[\text{Mg}/\text{H}] > -1.78$. As we will see later in §4, the overabundance of Fe relative to Mn in this system, $[\text{Fe}/\text{Mn}] = +0.28$, is quite representative of damped Ly α systems in general and has important implications for the nucleosynthetic history of the absorbing galaxies.

3.5. Q 0450–1312 $z_{damp} = 1.1743$ System

The HIRES spectrum of this object came from Churchill & Vogt (1997). Figure 7 shows the metal line profiles, where the intrinsically weak Fe II $\lambda\lambda 2249, 2260$, Mn II $\lambda\lambda 2576, 2594, 2606$, and Cr II $\lambda 2056$ lines are clearly detected. The equivalent widths and column densities of the lines are given in Table 6. The $N(\text{H I})$ of the system is unknown so it is not possible to derive absolute metal abundances. However, the Fe II column density implies $N(\text{H I}) = 4 \times 10^{19} \text{ cm}^{-2}$ even for solar metallicity. Hence we believe that this is a damped Ly α system.

3.6. Q 0454+0356 $z_{damp} = 0.8598$ System

Abundances of Fe, Zn, and Cr for this damped Ly α system have been determined by Steidel et al. (1995) using a medium-resolution spectrum; they found $[\text{Fe}/\text{H}] = -1.04$, $[\text{Zn}/\text{H}] = -1.08$, and

$[\text{Cr}/\text{H}] = -1.07$ (note that these values have been corrected for the f -values of Tripp et al. 1996). Steidel et al. also estimated a $N(\text{H I}) = (5.7 \pm 0.3) \times 10^{20} \text{ cm}^{-2}$ from the damped Ly α absorption in a HST FOS spectrum of the quasar. The Keck HIRES spectrum used in this study came from Churchill & Vogt (1997). Figure 8 shows the metal lines, while Table 7 gives the measurements. The stronger Zn II $\lambda 2026$ line is not covered by the HIRES spectrum. In any case, the S/N of the spectrum near the Zn II and Cr II lines is very low, and none of the Zn II or Cr II lines is detected at $\geq 4\sigma$ significance level. The upper limits on $[\text{Zn}/\text{H}]$ and $[\text{Cr}/\text{H}]$ (Table 7) are consistent with the Steidel et al. (1995) measurements. The $[\text{Fe}/\text{H}]$ estimated from the HIRES spectrum also agrees with the Steidel et al. estimate. The only additional information obtained for this system is the Mn abundance.

3.7. Q 0528–2505 $z_{damp} = 2.8110$ System

We detect over 30 metal lines from 15 different species in this system, partially because the damped Ly α system has a redshift slightly higher than the emission redshift of the quasar ($z_{em} = 2.779$), so more metal lines than usual are shifted out of the Ly α forest. Even though our spectrum covers most of the damped Ly α absorption line, the coverage to the blue side of the damped Ly α absorption is too short to reliably assess the continuum level before the damped Ly α absorption. We therefore adopt $\log N(\text{H I}) = 21.2 \pm 0.1$ from Morton et al. (1980) and Foltz, Chaffee, & Black (1988). The metal lines are presented in Table 8 and figure 9. We also derive upper limits to the abundance of several other elements, including P, Cl, Ti, Co, Cu, Ga, and Ge, in order to compare with the results of Songaila & Cowie (1996). Note that our abundance upper limits are 4σ values. The corresponding 2σ limits should be 0.3 dex lower than those given in the table.

This system is unique in several ways. First, the redshift of the damped Ly α absorption is higher than that of the quasar, suggesting that the absorbing galaxy may be physically associated with the quasar in a group or cluster. The presumed close proximity of the background quasar, which is an intense source of ionizing photons, may have significant effect on the physical state of the absorbing gas in the damped Ly α galaxy. Secondly, this is the only damped Ly α system for which molecular hydrogen absorption has been detected (Foltz et al. 1988; Songaila & Cowie 1996). Thirdly, the metal absorption lines are unusually wide and complex, spreading over 600 km s^{-1} in the strongest low ion lines and 500 km s^{-1} in the high ion lines. It appears that the absorption consists of two groups of components at above and below 140 km s^{-1} , respectively (figure 9). The complexity of the metal line absorption may be caused by two galaxies in superposition.

The Si II $\lambda 1808$ absorption is relatively strong (about 70% deep) and might be somewhat saturated. However, the comparably strong S II $\lambda 1253$ absorption does not appear to show any unresolved saturation based on a comparison of the $N(\text{S II})$ column densities derived from this line and from the weaker $\lambda 1250$ line (Table 8). We will therefore assume that the $N(\text{Si II})$ derived

from the $\lambda 1808$ absorption is correct.

Of particular interest is the C II* $\lambda 1335$ absorption. The ratio of $N(\text{C II}^*)/N(\text{C II})$ is a density indicator (§5). The ratio can also be used to estimate the temperature of the cosmic microwave background radiation at the redshift of the absorption system (§6). The C II* absorption in this system is clearly detected but is partially blended with the C II $\lambda 1334$ absorption line (figure 9). However, we note that the part of the C II* absorption at $v > 140 \text{ km s}^{-1}$ is free of any obvious blending. Hence it is possible to estimate $N(\text{C II}^*)$ for this part of the absorption (see last section of Table 8).

Another ion of special interest is N I since the abundance ratio of N/O can be used to infer the origin of the heavy elements (§4). We have clearly detected N I absorption from the triplet near 1200 \AA , but they are all blended with each other (figure 9). However, the part of the absorption at $v > 150 \text{ km s}^{-1}$ for the weakest N I line $\lambda 1200.710$ appears to be free of blending. Thus we have attempted to derive $N(\text{N I})$ for this part of the absorption, and also for a few other elements (see last section of Table 8) in order to examine the relative abundances. A direct integration of the apparent column density profile of the N I $\lambda 1200.710$ line between $v = [+140, +300] \text{ km s}^{-1}$ yields $\log N(\text{N I}) = 14.86 \pm 0.02$. It is possible that the N I $\lambda 1200.710$ absorption in this velocity interval is somewhat saturated. In order to be conservative, we use the Fe II lines to estimate the maximum possible degree of saturation in the N I absorption. The Fe II $\lambda\lambda 1608, 2260$ lines yield $\log N(\text{Fe II}) = 14.65 \pm 0.02$ and $\log N(\text{Fe II}) < 15.12$ (4σ) respectively, over the interval $v = [+140, +300] \text{ km s}^{-1}$ (Table 8). The Fe II $\lambda 1608$ absorption might be saturated in this velocity interval, but the column density from the $\lambda 2260$ line indicates that the value of $\log N(\text{Fe II}) = 14.65$ may underestimate the true $N(\text{Fe II})$ by at most 0.47 dex. Since the N I $\lambda 1200.710$ absorption has similar optical depth as the Fe II $\lambda 1608$ absorption over the velocity interval $[+140, +300] \text{ km s}^{-1}$, it may be reasonable to assume that the true $\log N(\text{N I})$ over this velocity interval should be no more than $14.86 + 0.47 = 15.33$. Thus we find conservatively $\log 14.65 < N(\text{N I}) < 15.33$, and $[\text{N}/\text{O}] < +0.65$ or $-1.21 < [\text{N}/\text{Si}] < -0.53$ for the absorption complex at $v > 140 \text{ km s}^{-1}$.

3.8. Q 0528–2505 $z_{damp} = 2.1410$ System

Morton et al. (1980) estimated $N(\text{H I}) = 5 \times 10^{20} \text{ cm}^{-2}$ for this system, which we will adopt and assume a 20% uncertainty. Figure 10 shows the metal absorption lines detected in this system. The measurements are given in Table 9. The Zn II $\lambda 2026$ absorption is probably detected but unfortunately blended with the Al II $\lambda 1670$ line at $z_{damp} = 2.8110$, and we only have an upper limit to $N(\text{Zn II})$ from the weaker Zn II $\lambda 2062$ line. The Fe II $\lambda\lambda 2249, 2260$ lines, which normally provide the best measure of $N(\text{Fe II})$ owing to their weak but detectable strength, are unfortunately blended with the Al III $\lambda 1854$ and $\lambda 1862$ lines in the $z_{damp} = 2.8110$ damped system, so no measurements are possible. We can only derive a lower limit to $N(\text{Fe II})$ from the moderately saturated Fe II $\lambda 1608$ line. An upper limit of $\log N(\text{Fe II}) < 15.21$ can be obtained from the absence of Fe II $\lambda 1611$ absorption. We thus adopt $\log N(\text{Fe II}) = 14.94 \pm 0.26$ in the

analysis.

3.9. Q 1425+6039 $z_{damp} = 2.8268$ System

This bright high redshift quasar ($z_{em} = 3.2$, $V=16.5$) was discovered by Stepanian et al. (1991). Our Keck spectrum for this object is of exceptionally high quality, with typical S/N reaching 120 per resolution element redward of Ly α emission. The damped Ly α absorption line in the Keck spectrum is shown in figure 11. The metal absorption lines are shown in figure 13. A number of lines are detected in the Ly α forest, including Si II $\lambda\lambda 1190, 1193, 1260, 1304$, Si III $\lambda 1206$, O I $\lambda 1302$, and several Fe II lines. These will not be used in the analysis.

The metal absorption lines in this damped system contain two groups of components, one between $[-100, +100]$ km s $^{-1}$, and another one between $[+200, +300]$ km s $^{-1}$ (figure 13). The low ion absorption lines clearly indicate that the bulk of neutral gas occurs at zero velocity ($z = 2.82680$). However, damping profiles fitted to the Ly α and Ly β absorption lines, with the redshift fixed at 2.82680, yield satisfactory fits to the blue sides of the profiles for $N(\text{H I})=2 \times 10^{20}$ cm $^{-2}$ and $b = 10$ km s $^{-1}$, but leave a big chunk of absorption unaccounted for at the red side of the line profiles (figure 11). The “extra” absorption is clearly due to the group of components occurring between $+200$ and $+300$ km s $^{-1}$. Figure 12 shows the same as figure 11, but with another component added at $z_{abs} = 2.83058$, corresponds to $v = 300$ km s $^{-1}$ in figure 13. The extra component has $N(\text{H I})=1.0 \times 10^{19}$ cm $^{-2}$ and $b = 10$ km s $^{-1}$, which fits the Ly α profile well, but not that of Ly β . This is because the red side of the Ly α profile is dominated by the damping wing of the component at $v = 300$ km s $^{-1}$ (i.e., independent of the velocity dispersion of the gas), while the Ly β line, saturated but not damped, depends on the relative distribution of the gas in the group of components between $[+200, +300]$ km s $^{-1}$ and on the velocity dispersion of each component. Figure 12 suggests that the total $N(\text{H I})$ of the group of components between $[+200, +300]$ km s $^{-1}$ is roughly 10^{19} cm $^{-2}$. Experiments indicate that the total $N(\text{H I})$ of this group is definitely no higher than 2×10^{19} cm $^{-2}$. Because of this relatively low $N(\text{H I})$, one might worry about ionization corrections. For this reason, we will confine the analysis of this system to the components at $v < 120$ km s $^{-1}$, and adopt a $\log N(\text{H I}) = 20.3 \pm 0.03$. Table 10 lists the metal lines and the measurements.

The N I triplet near 1200 Å is clearly detected (see figure 13), although the N I $\lambda 1200.710$ line (not shown) is contaminated by Ly α forest absorption. We are only able to derive a lower limit to $N(\text{N I})$. The O I $\lambda 1302$ absorption occurs in the Ly α forest and is strongly saturated. Thus even deriving a limit to the N/O ratio is not possible. Our spectrum does not extend red enough to cover the weak Si II $\lambda 1808$ absorption line. The Si II $\lambda 1526$ absorption is saturated, and the component near -90 km s $^{-1}$ is blended with the C IV $\lambda 1548$ absorption at $z_{abs} = 2.7727$. We are only able to derive a lower limit to $N(\text{Si II})$ from the Si II $\lambda 1526$ absorption at $v > -50$ km s $^{-1}$. The Fe II $\lambda 1608$ absorption is relatively strong and might be somewhat saturated. We estimate $\log N(\text{Fe II}) = 14.44$ from integrating its $N_a(v)$ profile. The much weaker Fe II $\lambda 1611$ absorption is

detected with $w_r = 0.007 \pm 0.002 \text{ \AA}$ (3.5σ detection), with a column density of $\log N(\text{Fe II})=14.48$. This suggests that the Fe II $\lambda 1608$ absorption is unsaturated or nearly unsaturated. However, in order to be self-consistent, we adopt $\log N(\text{Fe II}) < 14.52$ (4σ) for Fe II $\lambda 1611$, and adopt $\log N(\text{Fe II}) = 14.48 \pm 0.04$ as the final column density. The S II lines are apparently blended with strong Ly α absorption lines so no measurements are possible. Most (perhaps all) of the absorption in the C II* $\lambda 1335$ panel is from the C II $\lambda 1334$ line. The contamination made it impossible to estimate the $N(\text{C II}^*)$ or its upper limit.

3.10. Q 1946+7658 $z_{damp} = 2.8443$ System

This damped Ly α system and another one at $z_{damp} = 1.7382$ in the same spectrum (see §3.11) have been studied in some detail by Lu et al. (1995b; see also Fan & Tytler 1994). The Keck spectrum obtained here is of higher quality than those used in previous studies and extends further into the blue. Thus it is worthwhile to repeat the analysis, particularly in light of the N I lines which are covered by the Keck spectrum. The $N(\text{H I})$ of the system is estimated to be $\log N(\text{H I}) = 20.3 \pm 0.1$ by Lu et al., which agrees well with the new determination based on the Keck spectrum: $\log N(\text{H I}) = 20.27 \pm 0.06$ (see figure 14).

The metal lines in this systems are shown in figure 15. The Si II $\lambda 1190, 1193$ and Si III $\lambda 1206$ lines are detected in the Ly α forest. The comparison between the C II $\lambda 1334$ absorption and the O I $\lambda 1302$ absorption is very informative. While the O I absorption has only one obvious component centered at zero velocity, the C II absorption shows at least two extra components at -70 and $+80 \text{ km s}^{-1}$. This difference is almost certainly not due to the relative strength of the O I and C II absorption since the much weaker Al II $\lambda 1670$ absorption (and possibly the Si II $\lambda 1526$ absorption) also shows the two extra components as seen in C II. The difference is most likely due to ionization effects. The O I ion may be considered the best tracer of neutral gas (other than H I itself) since it has an ionization potential (13.61 eV) nearly identical to that of H I. On the other hand, ions like C II, Al II, Si II, etc. can exist in partially ionized regions because of their higher ionization potentials. Thus essentially all of the neutral hydrogen in the system is associated with the component at zero velocity. We will hence restrict the column density measurements of the low ion lines to the component at zero velocity (which is reflected in the v_- and v_+ values used to estimate the equivalent width and column density). This distinction makes an appreciable difference only for Al II. The results are given in Table 11.

The C II* $\lambda 1335$ absorption is clearly absent, and the upper limit obtained here is twice as good as that given by Lu et al. (1995b). By chance, all three N I lines occur in clean regions of the Ly α forest (figure 15; for space considerations the weakest N I line is not shown); however, none is detected at $\geq 4\sigma$ significance level. The upper limit on $N(\text{N I})$ and the lower limit on $N(\text{O I})$ from the saturated O I $\lambda 1302$ absorption yields a firm upper limit of $[\text{N/O}] < -0.76$ dex. We are also able to put a not-very-informative upper limit on $[\text{S/H}]$ from the absence of the S II $\lambda 1250$ absorption, which happens to occur in a clean region of the forest. The two stronger S II lines are

blended with Ly α absorption. The absorption in the N V λ 1242 panel is most likely due to Ly α forest lines.

3.11. Q 1946+7658 $z_{damp} = 1.7382$ System

The Ly α line at this redshift occurs at a wavelength blueward of the Lyman limit absorption from the $z_{damp} = 2.8443$ damped system in the same quasar spectrum and is thus not observable. The damped Ly α nature of the system is inferred from the detection of the intrinsically weak Si II λ 1808, Fe II $\lambda\lambda$ 2249,2260 and the Cr II lines (figure 16), which implies $N(\text{H I}) = 1.6 \times 10^{19} \text{ cm}^{-2}$ even for solar abundances. The metal lines detected in the system are shown in figure 16 and listed in Table 12. The Cr II λ 2066 absorption is blended with the C IV λ 1548 absorption at $z_{abs} = 2.6541$. The C IV absorption lines in this damped system occur in the Ly α forest and is probably somewhat contaminated.

The column densities for Al III obtained from the Al III $\lambda\lambda$ 1854,1862 absorption seem to indicate unresolved saturation in the Al III lines as the difference between the two estimates, 0.12 dex, is significantly larger than the 1σ errors. This is surprising given the relative weakness of the absorption lines. However, most of the difference occurs near $v = 20 \text{ km s}^{-1}$, where the intrinsically weaker Al III λ 1862 absorption is even deeper than the intrinsically stronger λ 1854 absorption. We believe the Al III λ 1862 absorption is probably contaminated by an unidentified metal absorption line. We will assume this is the case and adopt the $N(\text{Al III})$ from the λ 1854 line.

The lack of $N(\text{H I})$ information prevents an estimate of the absolute abundances in this system. For reference, if $\log N(\text{H I}) = 20.3$, then the following abundances would be obtained: $[\text{Si}/\text{H}] = -1.09$, $[\text{Fe}/\text{H}] = -1.35$, $[\text{Zn}/\text{H}] < -1.12$, $[\text{Cr}/\text{H}] = -1.20$, and $[\text{Mn}/\text{H}] = -1.71$ (adopting $\log N(\text{Mn II}) = 12.12$ from Lu et al. 1995b).

3.12. Q 2212–1626 $z_{damp} = 3.6617$ System

This is the third highest redshift damped Ly α system for which detailed analysis has been carried out. Only the $z_{damp} = 4.0803$ damped system toward Q 2237–0608 (§3.14) and the $z_{damp} = 4.3829$ damped system toward BR 1202–07 (Lu et al. 1996a) are at higher redshifts. From our Keck spectrum (see figure 17), we estimate $\log N(\text{H I}) = 20.20 \pm 0.08$. The metal lines are shown in figure 18 and listed in Table 13. A number of other metal lines (e.g., Si III λ 1206, Si II $\lambda\lambda$ 1190,1193,1260) appear to be present in the Ly α forest but are badly blended with forest absorption.

One peculiarity about this system is that the O I λ 1302 absorption clearly does not reach zero flux in its line center, which is unusual for this normally-strong absorption line. The O I

absorption occurs on top of the strong Ly α emission line of this quasar. Since heavily saturated Ly α absorption lines to the blue of the O I absorption clearly goes to zero flux in their line centers, the residual flux in the O I absorption line center is not an artifact of the data reduction procedure. Indeed, visual inspections of the raw images clearly confirm that the flux in the O I absorption line center is not zero. We consider two possible causes of this residual flux: resolution smearing and ionization effects.

If the O I absorption consists of many extremely narrow components that are not resolvable at our resolution (FWHM=6.6 km s⁻¹), smearing of the components due to the inadequate resolution could lift the flux in the absorption line center above the zero level even if the absorption components are intrinsically saturated. This requires the components to have $b < 4$ km s⁻¹ or temperature $T < 1.5 \times 10^4$ K. Experiments show that, indeed, one can explain the residual flux in the O I absorption line center if it contains several appropriately spaced components narrower than $b = 4$ km s⁻¹.

Another possible explanation of the residual flux in the O I absorption is that it is *real*, namely, the O I absorption line is unsaturated. This is unusual but not impossible. If this is the case, then the $N(\text{O I})$ from integrating the $N_a(v)$ profile (see table 13) should be an actual measurement rather than lower limit. This in turn implies $[\text{O}/\text{H}] = -2.37$ for this system. This O abundance is nearly 0.5 dex below the Si abundance ($[\text{Si}/\text{H}] = -1.90$) in the same system, which is inconsistent with nucleosynthesis considerations (see §4.3). One can reconcile this difference if the Si abundance in this system has been overestimated because some of the Si II ions come from partially ionized gas rather than from neutral gas³. If this is the case, it would mean substantial ionization corrections for this system. However, we consider this explanation unlikely for the following reasons. Firstly, when there are significant ionization corrections, usually there are notable differences in the absorption profiles between O I and other ions that can exist in H II regions (e.g., C II, Si II, etc.; see the $z_{damp} = 2.8443$ system toward Q 1946+7658 in §3.10). In contrast, the O I absorption in the Q 2212–2616 system has identical velocity structure to the C II and Si II absorption in the system. Secondly, the upper limit on the temperature of the microwave background radiation at the redshift of this absorption system as derived from the C II*/CII ratio (§6) is extremely close to the Big Bang prediction, indicating that collisional excitation of the C II atoms by free electrons is negligible in the absorbing gas. This is in contradiction with the large electron density expected in this system if the absorbing gas is substantially ionized. These considerations suggest that the resolution-smearing interpretation given in the preceding paragraph is likely the correct explanation. In fact, the implied low electron density in this system from the C II*/CII ratio (§6) suggests that this system may be *less* ionized than typical damped Ly α systems, which in turn may imply a lower temperature and hence narrower line widths (see the preceding paragraph).

³Recall that it takes 16.3 eV to turn Si II into Si III, so Si II ions can exist in H II regions. In contrast, the ionization potential of O I is 13.61 eV, making it the best tracer of neutral gas other than H I itself.

3.13. Q 2231–0015 $z_{damp} = 2.0662$ System

Our Keck spectrum does not cover the damped Ly α line. Lu & Wolfe (1994) estimated $\log N(\text{H I})=20.56 \pm 0.10$ for this system, which we adopt. The metal lines are shown in figure 19 and listed in Table 14. Metal lines detected in the Ly α forest include Si II $\lambda 1526$, C II $\lambda 1334$, Si IV $\lambda\lambda 1393, 1402$, and C IV $\lambda\lambda 1548, 1550$, but they all appear to be contaminated by forest absorption. The Fe II $\lambda 1608$ absorption yields a $\log N(\text{Fe II})= 14.72 \pm 0.01$ from integrating the apparent optical depth profile. Given its strength, it is probably saturated. Thus we take the above value as lower limit. The absence of the Fe II $\lambda 1611$ absorption yields an 4σ upper limit of $\log N(\text{Fe II}) < 15.08$. Hence we conservatively adopt $\log N(\text{Fe II})= 14.90 \pm 0.18$. The Cr II absorption is below the 4σ significance level.

3.14. Q 2237–0608 $z_{damp} = 4.0803$ System

This is the second highest redshift damped Ly α galaxy studied in detail. The damped Ly α absorption line in the Keck spectrum is shown in figure 20. We estimate a $N(\text{H I})=3 \times 10^{20} \text{ cm}^{-2}$ with about 30% uncertainty. This $N(\text{H I})$ estimate is more uncertain than the estimates for the other damped systems based on Keck spectra because both wings of the damped Ly α line are affected by strong, dense Ly α forest absorption due to its very high redshift. The $N(\text{H I})$ may have been slightly underestimated judging from the base of the damped Ly α absorption, although increasing $N(\text{H I})$ will overfit the wings farther away from the line center.

The metal lines in this system are shown in figure 21; the measurements are given in Table 15. The C II $\lambda 1334$ and C II* $\lambda 1335$ lines (and to some degree the Ni II $\lambda 1370$ line) happen to occur in the red wing of the strong Ly α emission line so the S/N are exceptionally good. The Si II $\lambda 1526$ and Al II $\lambda 1670$ absorption lines are about 80% and 70% deep, respectively. Based on the discussion in §2.2, they are likely to be unsaturated or nearly unsaturated. We will therefore adopt their column densities as measurements rather than lower limits.

Many metal lines in this system are expected in the Ly α forest, but trying to identify them is meaningless given the strong possibility of contamination from the extremely dense Ly α forest.

4. CHEMICAL EVOLUTION OF DAMPED LYMAN-ALPHA GALAXIES

In this section we combine the abundance information obtained for the sample of damped Ly α galaxies discussed in §3 with those from previous studies in order to carry out a statistical analysis of the chemical evolution of damped Ly α galaxies. In particular, we will examine the metallicity distribution of damped Ly α galaxies and compare that with those for the various components (disk, halo) in the Milky Way galaxy and with external galaxies. We will examine the age-metallicity relation of the damped Ly α galaxies and compare that with the similar relation

determined for the Milky Way. We will also examine the abundance ratios of various elements with different nucleosynthetic origin in order to gain more insight into the chemical enrichment processes in these damped Ly α galaxies. The effects of dust on the derived abundances through selective depletion will also be discussed.

4.1. Sample Construction

4.1.1. Damped Ly α Abundances

Elemental abundances have been measured for a number of damped Ly α galaxies in the literature with varying degrees of accuracy. In constructing the sample of damped Ly α galaxies for further statistical analysis, we will only consider those abundance measurements that we believe to be largely free of saturation effects. This means that, in general, measurements (but not lower limits) from heavily saturated lines will be discarded. Previous abundance estimates or upper limits that were based on lines with less than 4σ significance level will be converted where possible into 4σ *upper limits* to conform to the standard adopted in §3, or else they will be discarded. Where appropriate, we will also correct the published abundance measurements for the set of new oscillator strengths compiled by Tripp et al. (1996) so that all the measurements will be on the same footing. Following tradition, we will use Fe as the metallicity indicator. Hence, in general, only damped Ly α galaxies whose Fe abundance is available will be included in the sample. However, as we will see in §4.3, the Cr abundance tracks Fe abundance very well in damped Ly α galaxies, i.e., the Cr/Fe abundance ratios in damped Ly α galaxies (when both are measured) are consistent with their solar ratio. In order to increase the sample size, we will sometimes substitute [Cr/H] for [Fe/H] when the Fe abundance is not available (this happens in only 4 of the 23 systems listed in Table 16). Hence damped Ly α galaxies without [Fe/H] measurement, but with [Cr/H] measurement, will be included in the sample. The final sample of damped Ly α galaxies, including those discussed in §3 and those from previous studies that satisfy the above selection criteria, is given in Table 16.

4.1.2. Galactic Disk and Halo Star Abundances

The intrinsic chemical compositions of Galactic disk and halo stars of different age reflect the conditions of the local interstellar medium in the Galaxy when the stars were formed, which depend on the cumulative effects of the rate of star formation, the stellar initial mass function, stellar yields, gas infall/outflow, etc. prior to that epoch. The chemical compositions of Galactic stars not only allow us to study the past history of chemical evolution of the Milky Way, but also provide a fundamental reference of what might be expected of the chemical compositions of interstellar gas at different stages of a galaxy’s enrichment history. In §4.3 we will compare the relative abundances of various elements found in damped Ly α galaxies to those found in Galactic

stars in order to gain some insight into the chemical enrichment processes occurring in damped Ly α galaxies. In constructing the sample of stellar abundances, the following sources are used: Gratton & Sneden 1988, 1991 (Fe, Si, Cr, Ni), Edvardsson et al. 1993 (Fe, Si, Ni), Clegg, Lambert, & Tomkin 1981 (Fe, S), Francois 1987, 1988 (Fe, S). Gratton 1989 (Fe, Mn), Beynon 1978 (Fe, Mn), Sneden & Crocker 1988 (Fe, Zn), Sneden, Gratton, Crocker 1991 (Fe, Zn), and Magain 1989 (Fe, Cr).

We note that stellar abundances of sulphur are rarely studied mainly because the most useful S I lines occur in the near-infrared (~ 8700 Å) and are weak and blended. Of the three references for sulphur that we can find, Clegg et al. (1981) studied 20 stars mostly with $[\text{Fe}/\text{H}] > -0.5$, while Francois (1987, 1988) contain 26 stars mostly with $-1.5 < [\text{Fe}/\text{H}] < -0.5$. Although the Francois sample stars are more useful for comparison with the damped Ly α galaxies from the metallicity point of view, Lambert (1989) argued that the sulphur abundances of Francois for halo stars, $\langle [\text{S}/\text{Fe}] \rangle = 0.6$ dex, may be too high by 0.2 dex owing to the S I f -values used. Fortunately, this uncertainty does not affect any of the conclusions reached later.

4.1.3. Galactic ISM Cloud Abundances

It is well known that the relative abundances of elements in Galactic ISM clouds differ significantly from the solar composition and vary widely from sight line to sight line, i.e., from cloud to cloud. These deviations from solar relative abundances stem from the fact that some elements (refractory elements) are preferentially incorporated into solid forms or dust grains, while other elements are much less affected. Assuming that the intrinsic abundances of the elements in the ISM clouds are the same as the solar abundances, the measured gas-phase abundances of the elements in ISM clouds then allow one to infer the fractions of different elements that are locked up in grains, i.e., the amount of depletion. Thus the abundance ratios of elements measured in diffuse ISM clouds provide a fundamental reference to gauge the effects of dust depletion. With the understanding that the properties of dust grains in damped Ly α galaxies may be significantly different from those of Galactic dust⁴, we will compare in §4.3 the abundance ratios found in damped Ly α galaxies with those found in the ISM clouds in order to get a handle on the possible presence or absence of dust in damped Ly α galaxies.

Abundances of Si, S, Cr, Mn, Fe, Ni, and Zn measured for ISM clouds based on recent high quality HST GHRS data are compiled in Table 17. Only abundance measurements with relatively small uncertainties (typically less than 0.1 dex) that are judged to be free of significant saturation effects will be used. As with the damped Ly α abundances, we have corrected the GHRS measurements for the set of new f -values compiled by Tripp et al. (1996) where appropriate.

⁴Indeed, the extinction curves found for the LMC and the SMC are known to be different from each other and from that found in the Milky Way, indicating that the dust grains in all three galaxies are different. Similarly, the reddening law has been found to depend on radius in M31 (Iye & Richter 1985).

4.2. Age-metallicity Relation

Figure 22 shows the distribution of $[\text{Fe}/\text{H}]$ as a function of redshift for the damped Ly α galaxies in our sample (solid circles). This is equivalent to the age-metallicity relation commonly known in Galactic chemical evolution studies. We have used $[\text{Fe}/\text{H}]$ as the metallicity indicator, as is conventional. In a few cases, $[\text{Cr}/\text{H}]$ is used in place of $[\text{Fe}/\text{H}]$ when the latter is not available (see §4.3 for justification). Also displayed in figure 22 is the age-metallicity relation for the sample of Galactic disk stars (“+” symbols) studied by Edvardsson et al. (1993). The conversion between age (starting from the Big Bang) and redshift assumes $q_0 = 0.1$ and $H_0 = 50 \text{ km s}^{-1} \text{ Mpc}^{-1}$, which gives a current age of the universe of 16.6 Gyrs, consistent with the stellar age determinations.

As is clear from figure 22, the damped Ly α galaxies have Fe-metallicities in the range of 1/10 to 1/300 solar, or $[\text{Fe}/\text{H}]$ between -1.0 and -2.5 . Hence they represent a population of young galaxies that are still in the early stages of their chemical evolution. In fact, as we argue in §4.3, the star formation process in most of these galaxies probably started less than 1 billion years before the epoch corresponding to their redshift. The $N(\text{H I})$ -weighted mean metallicity of the damped Ly α galaxies between $2 < z < 3$ is $[\text{Fe}/\text{H}] = -1.56$, which may be regarded as the cosmic metallicity at $\langle z \rangle = 2.5$.

It is important to note that the true Fe abundances of damped Ly α systems could be systematically higher than those indicated in figure 22 if significant depletion of Fe onto dust grains has occurred. However, as we argue in §4.3, the amount of Fe depletion in the damped Ly α galaxies in our sample is probably negligible, and should be on average no more than 0.4 dex. Hence modest depletion of Fe will not change the qualitative picture presented in this work.

4.2.1. The Large Spread in $[\text{Fe}/\text{H}]$

As already noted by Pettini et al. (1994), the chemical enrichment processes in damped Ly α galaxies appear quite inhomogeneous. For example, the $[\text{Zn}/\text{H}]$ distribution in the sample of damped systems studied by Pettini et al. spans at least a factor of 20 or 1.3 dex. The $[\text{Fe}/\text{H}]$ in our sample at $z \sim 2 - 3$ spans roughly the same range. A metallicity gradient similar to those found in the Milky Way and in local spiral disks can only account for a factor of ~ 2 spread in the observed metallicities of damped Ly α galaxies (Pettini et al. 1994). If all galaxies in the sample formed at roughly the same time, then the large spread in $[\text{Fe}/\text{H}]$ may indicate widely different star formation histories in these galaxies. However, we consider it more likely that the large metallicity spread is due to the different formation epoch of the sample galaxies and/or that the sample contains a heterogeneous mix of galaxy types. Steidel (1995) found that galaxies responsible for the MgII absorption systems at $z < 1.6$ in quasar spectra come with a variety of morphological types, colors, and luminosities. This may explain the large metallicity spread in damped Ly α galaxies if they sample the same parent population of galaxies. We point out that varying amounts of Fe depletion due to dust grains are unlikely to account for the bulk of

metallicity spread since $[\text{Zn}/\text{H}]$ shows similar spread (Pettini et al. 1994), and Zn is not expected to be depleted heavily by dust grains (see discussion in §4.3).

4.2.2. Evidence for $z \geq 3$ as the Epoch of Galaxy Formation

There is evidence in figure 22 that the mean metallicity of the sample increases with time. This is perhaps not unexpected, but nonetheless reaffirms the notion that heavy metals gradually build up with time in galaxies through successive generations of star formation. There was a hint of such a trend in earlier studies (Pettini et al. 1995b), but the trend is made much clearer here by the addition of several new measurements at $z > 3$ and by the fact that most of our data points are actual measurements rather than upper limits (as is the case in Pettini et al. 1995). In particular, all four of the damped Ly α galaxies at $z > 3$ have $[\text{Fe}/\text{H}] < -1.7$ (or, $[\text{Fe}/\text{H}] < -2.0$ if we use the 2σ upper limit for the Q2212–1626 system). In comparison, many of the galaxies at $2 < z < 3$ have reached ten times higher metallicity. Thus the time around $z \sim 3$ could be the epoch of galaxy formation in the sense that it signifies the onset of significant star formation in galaxies. Several other lines of evidence appear to point to the same conclusion, as we discuss below.

The first such evidence comes from the space density distribution of quasars. It is found that the space density of quasars peaks at $2 < z < 3$ and starts to decline at $z > 3$ (Schmidt, Schneider, & Gunn 1995; Warren, Hewett, & Osmer 1994). By $z \sim 4.3$, the space density of quasars has dropped by a factor of 7 compared to their peak density at $z = 2 - 3$ (Kennefick, Djorgovski, & de Carvalho 1995). If this drop in quasar space density at $z > 3$ signifies the early phase of structure formation from the highest density peaks of the primordial fluctuation, it is perhaps “natural” to expect galaxy formation and subsequent star formation to occur at slightly lower redshifts. The second supporting evidence comes from studies of the neutral gas content in damped Ly α systems. Previous studies found that Ω_{damp} , the cosmological density contained in the H I gas in damped Ly α galaxies, decreases from $z \sim 3$ to $z = 0$, which was interpreted to indicate the transformation of gas into stars (Lanzetta et al. 1995; Wolfe et al. 1996; but also see Pei & Fall 1995). Recent extension of such studies to even higher redshift reveals that Ω_{damp} declines rapidly at $z > 3$ (Storrie-Lombardi & Wolfe 1996). This may indicate that damped Ly α galaxies are still forming at $z > 3$. The third supporting evidence comes from the morphology of high redshift galaxies. HST images of $z > 3$ galaxies identified from their redshifted Lyman continuum break (Steidel, Pettini, & Hamilton 1996a; Steidel et al. 1996b; Giavalisco, Steidel, & Macchetto 1996) reveal morphological structures that could be interpreted to indicate star formation in the spheroidal component of massive galaxies.

Even if none of these arguments is convincing by itself, taken together, they do consistently point to a picture that galaxies started forming at z around or slightly higher than 3.

Finally, it may be significant that the lowest Fe-metallicity we find for the sample of damped

$\text{Ly}\alpha$ galaxies is about -2.4 , which, coincidentally, also represents the lowest metallicity found for Galactic globular clusters. Recent observations of extremely low metallicity halo stars ($[\text{Fe}/\text{H}] < -2.5$) reveal that the Galaxy underwent a distinct phase of nucleosynthesis before reaching $[\text{Fe}/\text{H}] \sim -2.4$, characterized by some unusual elemental abundance ratios and large variations (McWilliams et al. 1995; Ryan, Norris, & Beers 1996). Possibly, this marks a time before which the chemical composition of the gas is only affected by a few Type II supernovae (Audouze & Silk 1995), namely, the epoch of formation of the first generation stars. More studies of $z > 3$ damped $\text{Ly}\alpha$ galaxies may eventually reveal such systems (i.e., $[\text{Fe}/\text{H}] < -2.5$), which would provide unambiguous evidence for the initial formation of galaxies.

4.2.3. *Comparison with the Milky Way Galaxy and Other Nearby Galaxies*

We note from figure 22 that the degree of chemical enrichment in the sample of damped $\text{Ly}\alpha$ galaxies is, on average, considerably lower than the Milky Way disk at any given time in the past. This may bear significantly on the nature of the damped $\text{Ly}\alpha$ galaxies. It was initially suggested (cf. Wolfe 1988) that the damped $\text{Ly}\alpha$ absorbers may trace disks or proto-disks of high-redshift spirals. But the low metallicities of the damped $\text{Ly}\alpha$ galaxies cast some doubts on this interpretation. A thick disk similar to that of our own Galaxy also appears to be inconsistent with the observed abundance distribution in damped $\text{Ly}\alpha$ galaxies, since the mean metallicity of stars in the thick disk is around $[\text{Fe}/\text{H}] = -0.6$ with a range of -1.4 to 0 (cf. Pardi, Ferrini, & Matteucci 1995). However, Beers & Sommer-Larsen (1995) suggested that the $[\text{Fe}/\text{H}]$ distribution of thick disk stars probably extends to as low as -2 . Since existing studies of thick-disk stars are still limited to within a few kpc of the disk, the known metallicity distribution may be biased toward higher values. Thus a thick-disk interpretation of the damped $\text{Ly}\alpha$ abundances remains viable, especially in light of the (somewhat preliminary) evidence that damped $\text{Ly}\alpha$ galaxies exhibit kinematics expected of rotating structures (Wolfe 1995). Detailed accounts of the properties of the thick disk of the Milky Way may be found in Majewski (1993).

On the other hand, the damped $\text{Ly}\alpha$ galaxies have metallicities resembling those found for Galactic halo stars and globular clusters. Coincidentally, the range of $[\text{Fe}/\text{H}]$ spanned by the damped $\text{Ly}\alpha$ galaxies at $z \sim 2 - 3$ is nearly identical to that spanned by Galactic globular clusters. This suggests the interesting possibility that damped $\text{Ly}\alpha$ absorbers may represent a phase when the spheroidal component of high-redshift galaxies is being formed. Such a possibility has, in fact, been suggested previously based on different arguments (Lanzetta et al. 1995; Wolfe 1995). The Fe-abundance distribution of damped systems is also consistent with that of old stellar populations in local group dwarf spheroidal galaxies (cf. Da Costa 1992). Dwarf spheroidals contain old to intermediate age stellar populations but with little gas, and the metallicity distributions of their stellar populations indicate episodic star formation in their history. Presumably, most or all of them contained interstellar gas in their remote past that would be sufficient to produce damped $\text{Ly}\alpha$ absorption lines. The more gas-rich dwarf irregular galaxies (e.g., LMC and SMC)

also appear to contain old and sometimes intermediate age stellar populations, in addition to young stellar populations indicating ongoing or recent star formation. The metallicities of the old stellar populations in these galaxies are also similar to those seen in damped Ly α galaxies. These considerations suggest that damped Ly α galaxies may represent gas-rich dwarf galaxies or sub-galactic fragments which are still collecting themselves to form more massive galaxies. More discussion about the nature of damped Ly α galaxies may be found in §5.

4.3. Abundance Ratios: Nucleosynthesis vs Dust Depletion

In figure 23 we show the abundance ratios of Si, S, Zn, Cr, Mn, and Ni to Fe plotted against [Fe/H]. Again, except for the [Cr/Fe] panel, the Cr abundance has been used in place of the Fe abundance when the latter is not available. This is justified because all the Ly α galaxies for which we have both Fe and Cr measurements indicate $[\text{Cr}/\text{H}] \sim [\text{Fe}/\text{H}]$: $\langle [\text{Cr}/\text{Fe}] \rangle = 0.04 \pm 0.10$. The dispersion in [Cr/Fe] is consistent with the typical measurement uncertainty of ~ 0.1 dex. Most of the abundance limits for C, N, O, and Al in Table 16 are not strong enough to constrain the origin of these elements, so they will only be considered in special cases.

In principle, elemental abundance ratios allow one to infer what kind of nucleosynthetic processes may be responsible for the enrichment of the interstellar medium. They are important for constraining models of stellar nucleosynthesis and the shape of the IMF. This is because different elements have different nucleosynthetic origins and different enrichment time scales. For example, essentially all the oxygen in the Galaxy and much of the observable α -process elements (including Si, S, Ca and Ti) are produced by massive stars ($M > 10M_{\odot}$) through explosive nuclear burning during Type II SN explosions (cf. Wheeler et al. 1989). The corresponding time scale is very short: $< 2 \times 10^7$ yrs. In contrast, most of the Fe-peak elements (including V, Cr, Mn, Fe, Co, Ni, and possibly the lighter elements Sc and Ti, and the heavier elements Cu and Zn) are believed to be produced by Type Ia SN⁵ (cf. Wheeler et al. 1989), which evolve from low to intermediate mass stars ($M_{\odot} < M < 8M_{\odot}$). Thus the time scale for producing the bulk of Fe-group elements should be at least as long as the lifetime of the progenitor stars of Type Ia SN, which is $> 10^8 - 10^9$ yrs, and is possibly much longer depending on the uncertain time scale between the formation of the white dwarf and the ignition of SN Ia explosion. For example, Yoshii, Tsujimoto, & Nomoto (1996) deduced an “effective” lifetime of ~ 1.5 Gyrs for Type Ia SN progenitors based on the analysis of Galactic stellar abundance data. The same low-to-intermediate mass stars also make much of the solar N (and possibly C) through mass losses on comparable time scales. Hence the production of C, N, and Fe-group elements is expected to lag behind that of O and α -group

⁵Using the Type II supernova models of Woosley & Weaver (1995) and a simple chemical evolution model, Timmes, Woosley, & Weaver (1995) found that only 1/3 of the solar Fe abundance comes from Type Ia supernovae. However, they also found that better agreement with most of the observed abundance data can be achieved if the Type II supernova yields of Woosley & Weaver are systematically reduced by a factor of 2.

elements following an episode of star formation.

However, in the case of elemental abundances derived from gas phase absorption, one also needs to worry about the additional effect of dust depletion if a significant amount of dust exists in these damped Ly α galaxies. Refractory elements such as Si, Mn, Fe, Cr, Ni, etc. are preferentially incorporated into dust grains, which depletes their abundances in the gas phase. That different elements deplete in different amounts significantly modifies the relative abundances of these elements in the gas phase.

In order to distinguish between the effects of nucleosynthetic processes and dust depletion, we compare the abundance ratios observed in damped Ly α galaxies with those seen in Galactic disk and halo stars, and with those determined for diffuse Galactic ISM clouds. The former serves to illustrate the effects of nucleosynthesis at different stages of chemical evolution of the Milky Way, while the latter illustrates the effects of dust depletion. Granted, there is no guarantee that any of the damped Ly α galaxies would have the same chemical enrichment history as the Milky Way, or that the dust grains in these high-redshift galaxies would have properties similar to Galactic dust, but these comparisons should nevertheless be useful in providing some general guidance.

4.3.1. *Can Dust Depletion Explain the Observed Abundance Ratios?*

Figure 24 shows the abundance ratios in diffuse ISM clouds in both the Galactic disk and halo from Table 17. Reviews of this subject may be found in Jenkins (1987) and Savage & Sembach (1996). Since it is believed that the intrinsic elemental abundances of the local interstellar medium are solar, the spread in [Fe/H] (the horizontal axis in figure 24) represents different levels of dust depletion in the clouds rather than variations in the intrinsic metallicity of the clouds (as is the case for figure 23). The departure of the observed elemental abundances in ISM clouds from the solar mixture is generally considered to be caused by condensation of refractory elements into solid forms (grains). In the diffuse Galactic ISM, Fe, Cr, and Ni are among the most heavily depleted elements; Si and Mn are somewhat less depleted; while Zn, S and C, N, O are nearly unaffected by dust depletion (Jenkins 1987). These depletion characteristics show up clearly in figure 24. Comparing figure 23 and figure 24, one finds good agreement in the [Cr/Fe] and [Ni/Fe] ratios. The [Si/Fe], [S/Fe] and [Zn/Fe] ratios in damped Ly α galaxies are consistent with the effects of dust depletion (figure 24) in the *direction* of the deviations from the solar ratios, but the *amounts* of deviations are much less in the damped Ly α galaxies. This may be explained if the dust-to-gas ratio in damped Ly α galaxies is lower than the Galactic value or the mean gas density in damped Ly α galaxies is lower; the latter follows from the fact that the degree of elemental depletion is observed to correlate with the mean gas density along the line of sight in the Milky Way (see the review in Jenkins 1987). However, the Mn/Fe ratio found for damped Ly α galaxies is completely opposite to what is expected from the dust depletion effect. Another strong piece of evidence against a dust depletion interpretation of the observed abundance ratios in damped Ly α galaxies is their N/O ratio (see below).

The N I $\lambda\lambda 1199.55, 1200.22, 1200.71$ triplet occurs in the Ly α forest so it is generally not possible to make reliable measurements of their column densities. However, in two damped Ly α systems (see Table 16), the clear absence of N I absorption and the presence of saturated O I absorption provide firm upper limits on their [N/O] ratio of < -0.76 and < -0.31 dex, respectively. Stronger limits can be found for [N/Si]: < -1.31 and < 1.05 , respectively. In addition, we found $-1.21 < [N/Si] < -0.53$ for several components in the $z_{damp} = 2.8110$ system toward Q 0528–2505 (see §3.7). Since both Si and O are believed to come from massive stars, and indeed, are observed to have solar abundance ratio in Galactic halo stars (cf. Wheeler et al. 1989) and in metal-poor dwarf galaxies (Thuan, Izotov, & Lipovetsky 1995), it is probably safe to assume that [Si/O]=0 in damped Ly α galaxies. We then find N/O at least a factor of 3.3 to 20 times *lower* than the solar ratio in these damped Ly α galaxies.

The abundances of N and O in ISM clouds have been measured toward many sightlines using the *Copernicus* satellite by York et al. (1983), whose data were reanalyzed by Hibbert, Dufton, & Keenan (1985) and by Keenan, Hibbert, & Dufton (1985) using improved f -values. Similar determinations have been made for a few clouds using the GHRS on board the HST (Cardelli, Savage, & Ebbets 1991). Since these measurements were made using the extremely weak intersystem transition lines of N I] $\lambda 1160$ and O I] $\lambda 1335$ rather than the strongly saturated N I $\lambda 1200$ triplet and O I $\lambda 1302$ transition, they do not suffer significantly from the usual saturation problem associated with the strong lines. Their results indicate that the depletion of N and O in diffuse ISM clouds is almost always less than 0.3 dex, and in addition, N is usually less depleted than O. Hence, it is extremely difficult to explain the observed N/O ratios in damped Ly α galaxies with dust depletion if the intrinsic N/O ratio is solar.

Thus we conclude from the above discussion that dust depletion alone cannot explain the abundance ratios observed in damped Ly α galaxies.

4.3.2. Can Nucleosynthesis Explain the Observed Abundance Ratios?

Figure 25 shows the abundance ratios found in Galactic disk and halo stars (see §4.1.2 for references). The overabundance of Si to Fe relative to the solar ratio in halo stars ($[Fe/H] < -1$), $[Si/Fe] \sim 0.3 - 0.4$, is now well established, and is thought to reflect the yield of these elements from Type II supernovae. A similar overabundance is seen for S (figure 25) and other α -elements (cf. Wheeler et al. 1989). All the other elements displayed in figure 25 (Cr, Mn, Fe, Ni, Zn) are Fe-peak elements. The fact that the Fe-peak elements are believed to be formed under nuclear statistical equilibrium and thus share a common origin may explain why their abundance ratios in the halo stars are so similar to the solar values. The only exception is Mn, with $\langle [Mn/Fe] \rangle \sim -0.3$ for halo stars. This “odd-even” effect, namely, the relative underabundance of odd- Z elements (where Z is the atomic number) compared to the abundances of even- Z elements of the same nucleosynthetic origin, is fairly well established observationally. One theory of why this occurs is that the production of odd- Z elements depends on the neutron excess in the nuclear fuel, which

in turn depends on the initial metallicity of the stellar composition (Truran & Arnett 1971). Calculations of explosive nucleosynthesis in metal poor stars by Truran & Arnett indicate that the yield of both odd-Z nuclei and the neutron-rich isotopes of even-Z nuclei are significantly reduced relative to more metal-rich stars.

We find remarkable agreement in the Si/Fe, S/Fe, Cr/Fe, and Mn/Cr ratios between damped Ly α galaxies and those seen in Galactic stars in the same metallicity range. The difference in Ni/Fe between figures 23 and 25 may not be real and may have to do with the uncertain f -values of the Ni II transitions (cf. Morton 1991). Since the stellar abundances are not determined from the same Ni II lines (the stellar abundances are from Ni I lines) as for the damped Ly α galaxies, a systematic error in the Ni II f -values could explain the nearly constant offset of [Ni/Fe] from the zero point in damped Ly α galaxies. This may also explain why the Ni/Fe ratios in damped Ly α galaxies more closely resemble those seen in diffuse ISM clouds (figure 24) as in both cases the abundances of Ni are derived from the same Ni II transitions with the same f -values. We consider the Ni/Fe ratio unsuitable for the purpose of discriminating a nucleosynthetic origin of the damped Ly α abundances from a dust depletion origin. More reliable determinations of the Ni II f -values in the future would make the Ni measurements more useful. We also note that, although in most damped Ly α systems the Al II λ 1670 absorption lines are saturated, the Al II absorption in the $z_{damp} = 2.8443$ system toward Q 1946+7658 and in the $z_{damp} = 4.0803$ system toward Q 2237–0608 appears weak enough that the estimated $N(\text{Al II})$'s probably do not suffer from significant saturation effects. The ratios, [Al/Si]= -0.30 and -0.35 (Tables 11 and 15), are consistent with observations of Galactic halo stars (cf. Wheeler et al. 1989). Incidentally, Al and Si are both produced during hydrostatic carbon and neon burning in massive stars, but Al is an odd Z element. Accordingly, the underabundance of Al relative to Si is consistent with the odd-even effect.

The only significant difference between figure 23 and figure 25 is in the Zn/Fe ratio. A Zn/Cr overabundance, or equivalently, a Zn/Fe overabundance (since [Cr/Fe] \sim 0 in damped Ly α galaxies) was known since the first studies of damped Ly α abundances (Meyer, Welty, & York 1989; Pettini, Boksenberg, & Hunstead 1990), and was interpreted to indicate that some Cr (and Fe) is depleted by dust grains from the gas phase. We will have more discussion of this in §4.3.3.

In general, we consider the good agreement in the Si/Fe, S/Fe, Cr/Fe, and Mn/Fe ratios between damped Ly α galaxies and Galactic halo stars strong evidence for a Type II SN enrichment origin of these elements without significant modifications by dust grains. In particular, the observed Mn/Fe ratios *require* a Type II SN-enrichment explanation since they cannot be explained otherwise. Another strong argument for SN II enrichment in damped Ly α galaxies is the N/O ratios (see below).

In §4.3.1, we argued that the observed low N/O ratios in several damped Ly α galaxies are inconsistent with the interpretation of dust depletion. On the other hand, these low N/O ratios are very similar to those found in Galactic halo stars. There was some debate about whether

[N/Fe] in halo stars is more close to zero or less than zero (see discussion in Wheeler et al. 1989). But since [O/Fe] is known to be about +0.4 dex in halo stars, it is safe to say that [N/O] < -0.4 dex at [Fe/H] < -1. Similarly, observations of metal-poor ([O/H] < -1) external galaxies indicate [N/O] < -0.6 (Pagel et al. 1992; Skillman & Kennicutt 1993; Thuan et al. 1995). Such low N/O ratios are commonly interpreted in terms of the different nucleosynthetic origin of these elements. While O is almost exclusively produced by short-lived massive stars, N is thought to have two sources. For pristine gas or gas with very low metallicity, primary N production is made by intermediate mass stars ($3M_{\odot} < M < 8M_{\odot}$) during the third dredge-up episodes, which bring carbon-rich material from the He-burning shell into the hydrogen-burning shell (Renzini & Voli 1981). The N produced this way is primary because it does not depend on the initial metal content of the gas. The long evolution time scale of the intermediate mass stars necessarily means that there should be a time delay of several hundreds of million years between the injection of O into the ISM and that of primary N. Secondary production of N can occur in stars of any mass during main-sequence burning, when the initial metallicity in the star is high enough to provide the seed C and O nuclei. Although the above popular interpretation is challenged by some recent observational results (cf. Thuan et al. 1995), which suggest that significant amounts of *primary* N may be produced by massive stars, it remains true that the *observed* N/O ratio in halo stars and in metal-poor external galaxies is low and comparable to that observed in damped Ly α galaxies. We thus believe that the low N/O ratios (and the low Mn/Fe ratios) found for damped Ly α galaxies are indications that massive stars are the primary pollutants of the ISM in these galaxies. This probably happens because star formation in these galaxies has occurred shortly before they were observed, so that only massive stars have had time to evolve to Type II SN. Given this time scale, we expect to see α -elements overabundance relative to Fe-peak elements. This is clearly seen in figure 23. In fact, the observed overabundances of Si to Fe and S to Fe, and the underabundance of Al to Si and Mn to Fe can be entirely explained away with the above nucleosynthesis argument. The only remaining question is: is there a need for dust depletion on top of the nucleosynthesis pattern?

4.3.3. Dust Depletions On Top of Nucleosynthesis Pattern?

The preceding discussion demonstrates that dust depletion alone cannot explain the observed elemental abundances in damped Ly α galaxies. Rather, with the exception of Zn, all the observed abundances are nicely explained if Type II supernovae are the only significant sources of pollution in these galaxies. Could the Zn/Fe ratios, then, be suggesting that there is some dust depletion effect on top of the nucleosynthesis pattern?

In Galactic stars the Zn/Fe ratio is found to be solar at all metallicities (see figure 25). On the other hand, the observed Zn/Fe ratios in damped Ly α galaxies are essentially all above the solar ratio. Since Zn is almost unaffected by dust in warm diffuse ISM clouds, while Fe is among the most heavily depleted elements, a modest amount of Fe depletion would explain the observed

Zn/Fe ratios in damped Ly α systems. This was indeed the argument that was put forward previously to explain the observed Zn/Cr (equivalent to Zn/Fe) ratios (cf. Pettini et al. 1994). However, this interpretation does not appear to be consistent with the other observed ratios. For the damped Ly α systems in which both Zn and Fe abundances are measured, $\langle[\text{Zn}/\text{Fe}]\rangle = +0.39$. In other words, if the above dust-depletion explanation for the observed Zn/Fe ratios is correct, the gas phase Fe abundance in damped Ly α galaxies must have been on average depleted by about 0.4 dex (or more if Zn is also depleted). To explain the other ratios shown in figure 23, this requires Si, S, Cr, Mn being depleted by the same amount in order to maintain the expected Si/Fe, S/Fe, Cr/Fe, and Mn/Fe ratios from halo star observations and from theories of Type II SN enrichment (recall that the observed Mn/Fe and N/O ratios in damped Ly α galaxies *require* that the enrichment process be dominated by SN II). This is quite difficult to understand given the observed depletion patterns in Galactic ISM clouds. As discussed in Sembach & Savage (1996), even in warm diffuse halo clouds for which elemental depletion is the least, there is a differential depletion factor of 0.44 dex between Si and Fe (i.e., Fe is more depleted than Si by 0.44 dex). The difference in the Si and Fe depletion widens for cooler, denser clouds. The problem is especially acute for S since in diffuse ISM clouds S is essentially undepleted (see Table 17). Given that Fe is among the most heavily depleted elements in the Galactic ISM, it is difficult to understand how S and Fe could have the same depletion, unless the depletion property of dust in the damped Ly α galaxies is drastically different from Galactic dust. However, if the latter is true, then the basis for interpreting the Zn/Fe ratio to indicate dust depletion may no longer be valid.

The degree to which an element is depleted by dust grains in the Galactic ISM is known to roughly anticorrelate with its condensation temperature (Field 1974; Jenkins 1987), which is the temperature at which half of the atoms condenses into solid forms of some sort under thermal equilibrium conditions. To further look into the issue of dust depletion, we plot the abundances of the elements found in damped Ly α galaxies as a function of their condensation temperature using the data given in Table 16. Rather than plotting the abundance of individual elements for each damped Ly α galaxy, which would make the figure incomprehensible because of the large scatter, we chose to plot the elemental abundances relative to the Fe abundance in the damped Ly α galaxies in order to see the mean trend. The result, shown in figure 26, is both quantitatively and qualitatively different from the same relation seen in ISM clouds (cf. Jenkins 1987; Savage & Sembach 1996). The most notable difference is in the behaviour of Mn and N. The implication is that there is no significant evidence for dust depletion to be the origin of the observed abundance patterns in damped Ly α galaxies. This is in agreement with similar findings for two individual damped Ly α galaxies previously studied by Wolfe (1995) and by Prochaska & Wolfe (1996).

Another way to look for the effect of dust depletion is to examine the variations of elemental abundance ratios among the different velocity components in a given system. It is well established that the degree of dust depletion in ISM clouds generally varies with their locations (environment) in the Galaxy, with cool, diffuse disk clouds showing much larger depletion than the warm, diffuse halo clouds (cf. Sembach & Savage 1996). Such a dependence of depletion on environment

probably has to do with the modification or destruction of dust grains by supernova shocks. If the damped Ly α galaxies contain dust grains that are affected by similar energetic processes, then one might expect to see large variations in the elemental abundance ratios from one absorbing cloud to another. The best elements for this test are probably (S, Zn) and (Cr, Fe, Ni) since the two groups of elements are at the two extremes of dust depletion and because they are generally measurable in damped Ly α systems. In practice, however, such a test is difficult to carry out since one must rely on the weak lines to derive accurate column densities, which require high resolution, high S/N measurements. Prochaska & Wolfe (1996) examined the relative abundances of Si, Fe, Ni, Cr, and Zn in several components of the $z_{damp} = 2.462$ damped Ly α absorption system toward Q 0201+3634 and concluded that there is little dust present in the absorbing gas. Among all the damped Ly α systems studied in §3, we consider the $z_{damp} = 2.8110$ system toward Q 0528–2505 the best suited for this purpose since the S II $\lambda 1250, 1253$ lines are well measured and we have good measurements for six Ni II lines (see Table 8). Equally important is the fact that these ions are well measured across a $\sim 300 \text{ km s}^{-1}$ interval encompassing many components. The three panels to the left in figure 27 show the profiles of $N_a(v)$, the column density per unit velocity interval, for S II and Ni II derived from the average of two S II lines and of six Ni II lines in the system. The profile for Si II $\lambda 1808$ is also shown for comparison. The three panels to the right in figure 27 shows the $N_a(v)$ ratios of these ions. Amazingly, the S II/Si II, S II/Ni II, and Si II/Ni II ratios are nearly constant over the $\Delta v \sim 300 \text{ km/s}$ interval where these ratios are relatively well measured. Given that these ratios can be affected by many factors, including intrinsic relative abundance variations, ionization effects, as well as dust depletion, we find the relative constancy of these ratios quite remarkable. In comparison, the S II/Ni II ratio varies from ~ 6 in warm diffuse halo clouds to > 200 in cool disk clouds in the Milky Way (see Sembach & Savage 1996). The above result becomes even more remarkable in light of the fact that the $z_{damp} = 2.8110$ system toward Q 0528–2505 is the only damped Ly α system known to contain molecular hydrogen (Foltz et al. 1988; Songaila & Cowie 1996), which makes it more likely to contain dust. However, in this damped Ly α system the fraction of molecular hydrogen relative to neutral hydrogen is well below the Galactic value for sightlines with similar values of $N(\text{H I})$.

In conclusion, we find it difficult to interpret the observed Zn/Fe ratios (or Zn/Cr ratios) in damped Ly α galaxies as being a consequence of dust depletion.

4.3.4. Concluding Remarks

To summarize the preceding discussion, we favor the interpretation that the abundance ratios in damped Ly α galaxies are mostly or entirely a consequence of Type II SN nucleosynthesis without significant modification by dust depletion. The evidence for this conclusion is the much-lower-than-solar N/O ratio, the α -element overabundance relative to Fe peak elements, and the underabundance of Mn relative to Fe and Al relative to Si (odd-even effect). Such abundance patterns are, in some sense, expected in the early stages of galactic chemical evolution based on

what we know about the Milky Way (cf. Timmes, Lauroesch, & Truran 1995), and were indeed noted previously in individual damped Ly α systems (e.g., Lu et al. 1995b; Meyer, Lanzetta, & Wolfe 1995; Steidel et al. 1995; Wolfe 1995; Pettini et al. 1995a; Lu et al. 1996a; Prochaska & Wolfe 1996). The present study, however, puts the above conclusion on much firmer ground.

The Zn/Fe overabundance found for damped Ly α galaxies can be explained without invoking dust if there is an additional source of Zn (particularly ^{64}Zn , see figure 5 of Timmes et al. 1995) in SN II besides that synthesized under nuclear statistical equilibrium. Such an alternative production mechanism for Zn might occur in the neutrino-driven wind discussed by Hoffman et al. (1996). One difficulty with this interpretation is that a Zn/Fe overabundance is not observed during the early history of the Milky Way (figure 25). In that regard, it would be extremely valuable to obtain the Zn/Fe ratio for some metal-poor stars in external galaxies in order to see if Zn/Fe is universally solar. It is perhaps significant that we do not yet have a clear theoretical understanding of why Zn should track Fe so well in Galactic disk and halo stars. For example, using the Type II SN yield calculations of Woosley & Weaver (1995), both Timmes et al. (1995) and Malaney & Chaboyer (1996) found a much lower-than-solar Zn/Fe ratio (by a factor of 3-7) for plausible assumptions about the stellar initial mass function (see Arnett 1995 for a more in-depth discussion). If indeed the observed Zn/Fe ratios in damped systems are intrinsic to the nucleosynthetic processes, it will have significant implications for the theory of stellar nucleosynthesis. At this point, we consider Zn an anomalous element. It is important to note that, even if the observed Zn/Fe ratios are due to dust depletion (which we consider unlikely), the amount of Fe depletion should be no higher than 0.4 dex on average, assuming that Zn is undepleted. In other words, the amount of Fe locked up in grains should be less than 60% of the total. This is in contrast to the depletion of Fe in ISM clouds in which up to more than 99% of the Fe may be locked up in grains. It should also be noted that a 0.4 dex depletion of Fe would not explain all the differences between the metallicity distribution of damped Ly α galaxies and that of the Milky Way disk stars (figure 22).

Regardless of whether or not dust is present in the damped Ly α galaxies, the observed N/O ratios and Mn/Fe ratios strongly indicate a nucleosynthetic origin. This suggests that the chemical enrichment process in these damped Ly α galaxies must have occurred so recently prior to when they were observed that only Type II SN have made significant contributions to the pollution of their interstellar material; low to intermediate mass stars could not have had enough time to evolve and to make their presence known by dumping their nucleosynthetic products into the interstellar space. Hence the star formation process should not have proceeded more than several hundred million years from the time corresponding to their redshifts. One way to avoid this conclusion is if the stellar initial mass function in these young galaxies had a low mass cutoff so that there simply aren't that many low mass stars to make Type Ia SN, even if they had enough time to do so. Observations of elemental abundance ratios in lower redshift and more metal-rich damped Ly α galaxies should help to clarify this issue, since we expect SN Ia to catch up eventually.

4.4. Discussion

The issue of dust is critical for a complete and accurate understanding of damped Ly α galaxies. Fall and collaborators (Fall & Pei 1989; Fall, Pei, & McMahon 1989; Pei, Fall, & Bechtold 1991) found marginally significant evidence that quasars with known damped Ly α galaxies in the foreground are statistically redder than those without. This was taken as evidence for the presence of a modest amount of dust in damped Ly α galaxies. The dust-to-gas ratio inferred for the damped Ly α galaxies is roughly 1/10 of that in the Galaxy. However, the observational evidence for this reddening has been challenged recently (Foltz 1996, private communication; Storrie-Lombardi 1996, private communication). The only other independent evidence for the presence of dust in damped Ly α galaxies was thought to be the Zn/Cr or Zn/Fe ratios (cf. Pettini et al. 1994). But as we argued earlier, this interpretation has problems explaining many of the other observed abundance ratios.

Fall & Pei (1995; also Pei & Fall 1995) argued that most of the more dust-rich galaxies have been missed in existing surveys. This is because previous surveys for damped Ly α galaxies were based on quasars selected optically, hence quasars with dusty foreground galaxies would be preferentially missed owing to dust obscuration. Fall & Pei (1995) estimated that up to 70% of the bright quasars at $z \sim 3$ could be missing from optically selected samples. In principle, such a selection effect could occur even if there is no significant amount of dust in the *existing* sample of damped Ly α galaxies. If this is the case, then the damped Ly α galaxies studied here will not be representative of all high-redshift galaxies. In particular, the mean metallicity as given by [Fe/H] would be biased towards lower values, making them appearing (on average) more metal poor than they really are. The abundance ratios may also be affected. A critical test of this hypothesis is to conduct a new survey for damped Ly α galaxies using a sample of high redshift quasars selected from a *complete* sample of radio sources regardless of their optical brightness. Such a program is being pursued.

5. OTHER PROPERTIES AND THE NATURE OF DAMPED LYMAN-ALPHA GALAXIES

5.1. Electron Densities

The column density ratio of C II*/C II is a density indicator (Bahcall & Wolfe 1968). The lower level of the C II* $\lambda 1335$ transition is a fine structure level of the ground state of the C II atom. Under normal interstellar conditions, the population balance between the ground level and the fine structure level of the C II ground state is determined by collisional excitation with electrons and by spontaneous radiative decay. Table 18 summarizes the C II* and C II measurements in damped Ly α systems studied here and in Lu et al. (1996a). Upper limits on the electron density are derived using the formula and coefficients adopted in Tripp et al. (1996) by

assuming a temperature of 5000 K. The derived electron densities are upper limits because only lower limits to $N(\text{C II})$ are available in all systems considered, and because other mechanisms might also contribute significantly to the excitation (e.g., excitation by microwave background photons; see §6). These limits are consistent with the mean electron density of $\sim 0.07 \text{ cm}^{-3}$ estimated for the Galactic ISM (cf. Reynolds 1991; Spitzer & Fitzpatrick 1993). For reference, the derived upper limits are on average factors of 2-3 lower if we estimate $N(\text{C II})$ by assuming a solar C/Si ratio.

5.2. Ionization

The relative strength and velocity distribution of absorption from ion species with different ionization properties can provide insight into the ionization structure and the spatial distribution of the absorbing gas. Table 19 summarizes such information for some ions of interest based on data presented in this paper and other similar studies with Keck HIRES (see references in the table). We make the following comments:

(1) In all cases where such information is available, the Al III absorption profiles always have similar appearance as the low ionization lines. Additionally, the Al II lines are always much stronger than the Al III lines, indicating $N(\text{Al II}) \gg N(\text{Al III})$. These results suggest that Al III is likely to be produced in the same physical region as the low ion gas, and that most of the gas is neutral rather than ionized (as expected from the large H I column densities of the systems). This could happen if Al III comes from an ionized shell surrounding the neutral gas which produces the bulk of low ions.

(2) The Si IV and C IV absorption line profiles almost always resemble each other, and they usually have a very different appearance from the low ion absorption lines. This suggests that the bulk of the high ions are probably produced in physical regions distinct from that containing the low ions. The high ions could arise from low-density ionized gas (halo clouds?) surrounding the main structure which gives rise to the low ionization species.

The profile differences between low-ion and high-ion absorption lines have been noted previously in individual damped Ly α systems (eg. Wolfe et al. 1994; Lu et al. 1995b). The current discussion makes these trends much clearer. The results are reassuring in that, in general, the metal abundances derived from low ionization species without corrections for ionization effects should be substantially correct. This is consistent with theoretical expectations (Viegas 1995)

5.3. Kinematics

The profiles of metal absorption line in damped Ly α systems contain information about the kinematics of the gas. The total velocity spread of the absorption lines may allow one to estimate

the mass of the objects if they are caused by random motions of the absorbing clouds confined by gravitational potentials. In practice, the velocity spread may be affected by ordered motions (e.g., rotation, infall/outflow) and by energetic events such as supernova explosions. One needs also to take into account the fact that often the quasar sightlines do not probe the full gravitational potential of the absorbing objects, depending on the impact parameters. These considerations make it difficult to infer the mass of the absorbing galaxies.

On the other hand, analyses of the profiles of the metal absorption lines have yielded a potentially very exciting result. Wolfe (1995; see also Lanzetta & Bowen 1992) found preliminary evidence that the weak low-ionization metal absorption lines in damped Ly α systems often show an edge-leading asymmetry that is characteristic of absorption from rotating gaseous disks. It should be pointed out that only weak, unsaturated low-ionization absorption lines can be used to trace reliably the velocity structure of the neutral gas in galactic disks. Strong, saturated absorption lines are not appropriate for this purpose for two reasons: (1) one loses the information on the velocity structure of the absorption in the saturated part; (2) strong absorption lines are more sensitive to trace amounts of gas so they are more easily contaminated by diffuse clouds that are not associated with galactic disks (e.g., halo clouds). The implication of Wolfe’s finding is that damped Ly α galaxies may be high-redshift spiral disks. If this conclusion is confirmed with a much larger data set, it will not only provide strong evidence for the physical nature of the damped Ly α galaxies, but will also become one of the most significant constraints on cosmological models of structure formation in the early universe. Data contained in this paper are currently being analyzed by Wolfe and collaborators for the purpose discussed above.

5.4. Star Formation and Stellar Initial Mass Function

The rate and form of star formation and the initial mass function (IMF) of the stars formed are fundamental parameters for understanding galactic chemical evolution. The failure to detect Ly α emission from damped Ly α galaxies may suggest that damped Ly α galaxies generally do not have high star formation rates. For example, Lowenthal et al. (1995) surveyed seven quasar fields with known foreground damped Ly α absorbers and failed to detect any of the galaxies in Ly α emission down to quite stringent limits. The implied star formation rates are $< 1M_{\odot} \text{ yr}^{-1}$ for normal IMF, assuming negligible extinction by dust. Of course, if a significant amount of dust is present in these galaxies, the true star formation rate could be much higher. However, the Hu et al. (1993) observations of H α emission from three damped Ly α galaxies limit the star formation rates to less than $20M_{\odot} \text{ yr}^{-1}$ in those galaxies.

On the other hand, the lack of Ly α emission from a damped Ly α galaxy does not necessarily mean low star-formation activity, even if there is no significant extinction by dust. As demonstrated by Valls-Gabaud (1993), the equivalent width of Ly α emission from a galaxy is a strong function of the age of the stellar population. In the case of a star burst, the strength of the Ly α emission decreases rapidly after the burst, essentially because the massive stars (O and early B stars)

responsible for the Ly α emission are short-lived. His model calculations suggest that the Ly α photons disappear from the galaxy in $\sim 10^7$ years after the burst and the galaxy spectrum will even show stellar absorption in Ly α at later times. The case of continuous star formation is qualitatively different, with the galaxy showing relatively strong Ly α emission (equivalent width $> 100 \text{ \AA}$) at all times because O, B stars are continuously being formed. *If* the lack of strong Ly α emission in damped Ly α galaxies is indicative of the bursting nature of their star formation process, it may have significant implications for their nature. There is now strong evidence that normal spiral disks tend to have relatively constant star formation during their lifetimes while dwarf galaxies (dwarf irregulars and dwarf spheroidals) tend to have bursts of star formation (cf. Kennicutt 1995). A bursting nature of star formation for damped Ly α galaxies, *if established*, would favor them being dwarf galaxies or subgalactic structures.

The form of star formation in damped Ly α galaxies may also be inferred from the elemental abundance ratios. In particular, the relative abundance of O and α -process elements to those of the Fe-group elements is fairly sensitive to the intervals between episodes of star formation, essentially because of the ~ 1 Gyr delay between the almost-instantaneous enrichment from SN II and that from SN Ia. If some of the damped Ly α galaxies in our sample began with a strong burst of star formation which was followed by a long quiescent period, one would expect its Si/Fe ratio to drop below the SN II expectation (i.e., ~ 2 -3 times the solar value) after $\Delta t \gg 1$ Gyrs when Type Ia SN start to inject Fe into the ISM. Thus a uniform distribution of Si/Fe ratios may well indicate that the star formation process in these galaxies is relatively uniform. The existing data (figure 23) does show a fairly uniform Si/Fe ratio: $\langle [\text{Si}/\text{Fe}] \rangle = 0.36 \pm 0.11$ based on 12 measurements (note that the scatter of 0.11 dex is comparable to the typical measurement uncertainty of 0.1 dex). However, it is premature to make any firm conclusions because of the relatively small number of data points, and because we don't know when each galaxy was formed. The age span of the existing sample galaxies with Si/Fe measurements, ~ 3 Gyrs, is probably too small to even make a statistical inference about when these galaxies were formed. If the uniformity of the Si/Fe ratio persists to much lower redshifts in a much larger sample, then it may seriously constrain the history of star formation in these galaxies since at least some of the very low-redshift galaxies should have formed much longer than 1 Gyrs ago. A smooth star formation process would be more typical of disk galaxies than dwarfs. Alternatively, a constant Si/Fe ratio may be maintained by a top-heavy IMF. Dust depletion, which is expected to become significant at low enough redshift, may further complicate the issue.

The relative constancy in the Si/Fe ratio among the damped Ly α galaxies in the sample also suggests that the IMF integrated stellar yields of these elements are fairly uniform. If the relative yield of α -elements and Fe from Type II SN varies strongly with the progenitor mass, as was suggested in some theoretical calculations (e.g., Thielemann, Nomoto, & Hashimoto 1996), the scatter in the measured Si/Fe ratio may be used to put significant constraints on the variations of the stellar IMF in these galaxies over the range of 10-40 M_{\odot} (responsible for SN II). We did not attempt a quantitative calculation of the IMF constraint because all existing models of SN

II suffer from the uncertain nature of the explosion mechanism, which significantly affects the Fe yield.

5.5. Are Damped Ly α Galaxies Spirals?

There is direct evidence that at least some damped Ly α absorption systems may be associated with large, disk-like structures. Briggs et al. (1989) found that the 21-cm absorption from the $z_{damp} = 2.04$ damped Ly α galaxy toward PKS 0458–020 shows striking similarity in the measurements made with the Arecibo single dish and with the VLBI. This requires the absorbing galaxy to cover the entire radio source, which is an extended structure of about 10 kpc size in the absorber’s reference frame. Kinematic arguments further suggest that the actual size of the absorber may be several times bigger. More recently, Djorgovski et al. (1996) identified a galaxy at $z = 3.150$ responsible for a damped Ly α absorption system in the spectrum of a background quasar. The projected separation between the detected galaxy and the quasar then indicates that the absorbing galaxy must be at least as large as 17 kpc, comparable to the sizes of normal galaxy disks.

Another evidence for high-redshift damped Ly α galaxies to be spiral disks comes from the work of Wolfe (1995), who presented evidence that the absorption profiles of the metal absorption lines in damped Ly α galaxies generally show an edge-leading asymmetry that is characteristic of absorption from rotating gaseous disks. If this result is confirmed with more detailed modeling using a large sample, it will constitute the strongest evidence that damped Ly α galaxies are spiral disks or proto-disks.

Evidence regarding the nature of damped Ly α galaxies also comes from direct imaging identification of their low-redshift counterparts. Steidel et al. (1994) presented ground-based images of two quasar fields, 3C 286 (Q 1328+3045) and PKS 1229–021, containing foreground low-redshift ($z < 1$) damped Ly α absorbers, and identified *candidate* damped Ly α absorbing galaxies (i.e., no spectroscopic redshifts were obtained). The galaxy responsible for the damped Ly α absorption toward 3C 286 appears to be a low surface brightness galaxy, while the one responsible for the damped Ly α absorption toward PKS 1229–021 appears to be a normal galaxy somewhat fainter than L^* . In another study (Cohen et al. 1996), the damped Ly α absorber at $z_{damp} = 0.437$ toward the quasar 3C 196 was identified with a spiral galaxy of luminosity roughly L^* in an HST image, although no spectroscopic redshift confirmation was available.

More broadly, Steidel and collaborators (see Steidel 1995 and references therein; see also Bergeron and Boisse 1991) have been very successful in identifying galaxies responsible for the Mg II absorption systems seen in quasar spectra at $z_{abs} < 1.6$. The colors and luminosities of the identified galaxies are consistent with them being normal Hubble-sequence galaxies, spanning the range of E to Irr but mostly early to late type spirals. The implication is that normal galaxies are already in place by a redshift of 1.6 with properties not that different from the local population.

This is consistent with results from deep surveys of field galaxies (cf. Driver et al. 1995).

Direct searches for high-redshift galaxies are also starting to produce interesting results, some relevant to the nature of damped Ly α galaxies. Identifications of $z > 3$ galaxies in quasar fields based on the presence of a redshifted Lyman continuum break (Steidel et al. 1996a,b; Giavalisco et al. 1996) have produced a population of what appears to be the progenitors of normal, massive galaxies that are forming stars of their spheroidal component, although this interpretation is not unique. One such “Lyman break” galaxy is confirmed to be a damped Ly α galaxy (Steidel et al. 1996a; Djorgovski et al. 1996), and another is a candidate for a damped Ly α galaxy (Giavalisco et al. 1996).

These results suggest that it may not be unreasonable to think that damped Ly α galaxies are high-redshift spirals or their precursors. In fact, if one takes the age estimates of the disk stars in the sample of Edvardsson et al. (1993) literally⁶ (see figure 23), then it is clear that the Milky Way disk was already in place 10-15 Gyrs ago or at $z = 2 - 4$ for the cosmology adopted here ($q_0 = 0.1$, $H_0 = 50$). Unless our Milky Way is among the first galaxies formed in the universe, one may be forced to conclude that (some) spiral disks must exist by the redshift of 2-4 in some form. If we insert a sightline through such a galaxy, a damped Ly α absorption will clearly result. The key question is: what dominates the absorption cross-section at $N(\text{HI})=10^{20} - 10^{22} \text{ cm}^{-2}$ at the relevant redshifts, spirals or subgalactic structures?

If the damped Ly α galaxies in our sample are indeed disks or proto-disks, we must explain why their Fe metallicities are so much lower than the Milky Way disk in its past. One possibility is that this is a selection bias due to dust obscuration (Pei & Fall 1995; see discussion in §4.4). In principle, disks or proto-disk could be present at $z > 2$ without being included in our sample if the existing sample of damped Ly α galaxies is dominated by a large population of smaller structures. Such subgalactic structures could be the building blocks of large, normal galaxies that are still falling into each other, or they might survive to the present epoch. If the damped Ly α galaxies at $z = 2 - 4$ are predominantly sub-galactic structures, then the number density of damped Ly α galaxies, $dN/dz = 0.3$ at $z \sim 3$ (Lanzetta et al. 1991; Wolfe et al. 1996), requires a space density of $322h_{50}/R_0^2 \text{ Mpc}^{-3}$, where R_0 is the characteristic size (radius in units of kpc) of the subgalactic structures with $N(\text{H I}) > 2 \times 10^{20} \text{ cm}^{-2}$ for a spherical geometry. This may provide significant constraints on cosmological models of structure formation.

⁶Private communications with Dr. Edvardsson suggest that, due to observational uncertainties and uncertainties in stellar evolution models, the oldest disk stars in the Edvardsson et al. (1993) sample are not necessarily as old as were suggested in the study. Some of the oldest stars in the sample may also be halo stars that happen to have orbits very close to the Galactic plane. A detailed discussion of the age of the Galactic disk is beyond the scope of this paper. Interested readers are referred to the nice discussion by Majewski (1993).

6. TEMPERATURE OF THE COSMIC MICROWAVE BACKGROUND

Big Bang cosmology predicts that the temperature T_{CMB} of the cosmic microwave background (CMB) radiation should behave like $T_{CMB} \propto (1+z)$. As suggested by Bahcall & Wolf (1968), this relation is testable since one can estimate the CMB temperature from the relative populations of ground-state fine-structure levels of suitably selected atoms in high-redshift quasar absorption systems. This technique has previously been applied to the C I atom (Meyer et al. 1986; Songaila et al. 1994a) and to the C II ion (Songaila et al. 1994b; Lu et al. 1996a). In §3, we have estimated column densities (or limits) of C II and C II* for several damped Ly α absorption systems. Since in most cases we only have lower limits to $N(\text{C II})$ and/or upper limits to $N(\text{C II}^*)$, the resulting upper limits on $N(\text{C II}^*)/N(\text{C II})$ yield strict upper limits on the temperature of the CMB since other mechanisms may contribute significantly to the excitation of the C II ion (e.g., collisional excitations by electrons or hydrogen atoms, direct UV pumping, etc.).

Table 20 summarizes the available measurements of the temperature of the cosmic microwave background at high redshifts, including four based on measurements made in §3, one from Lu et al. (1996a), and three from Songaila et al. (1994a,b). In the case of Q 1331+1704 (Songaila et al. 1994a), both the C I and C I* absorption are detected so it was possible to actually measure the excitation temperature rather than providing upper limits. These results are displayed in figure 28, where the dotted line is the prediction of $T_{CMB} = 2.73(1+z)$ from Big Bang cosmology. All the existing measurements or upper limits are consistent with the Big Bang prediction.

We note that, other than the two measurements at $z = 1.776$ (which are based on C I*/C I), the two upper limits at $z > 4$ are particularly tight. This may be partially attributed to the good S/N of the data, but is also due to the fact that at $z > 4$, the peak of the microwave background radiation is shifted to a wavelength region very close to the energy separation (158 μm) between the fine structure levels of the C II ion ground state. Thus the C II ion is a particularly good probe of the microwave background temperature at very high redshifts. It is also significant that one of the measurements at $z = 1.7660$ and the upper limit at $z = 4.0803$ are very close to the Big Bang predictions, suggesting that contributions from other excitation mechanisms are negligible in these systems.

7. SUMMARY

We have obtained high quality spectra of quasars using the High Resolution Spectrometer (HIRES) on the 10m Keck telescope in order to study the elemental abundances in 14 high-redshift ($0.9 < z < 4.0$) damped Ly α galaxies. The HIRES spectra have a resolution of FWHM=6.6 km s $^{-1}$, with a typical S/N ~ 40 per resolution element. The chemical elements being studied include C, N, O, Al, Si, S, Cr, Mn, Fe, Ni, and Zn, although not every element listed is measured for every damped Ly α galaxy. In order to ensure accuracy, we measure column densities and abundances using only those absorption lines with $\geq 4\sigma$ detection significance that are believed

to be unsaturated. This allows us to circumvent the difficulty associated with measuring reliable column densities using saturated absorption lines. In all other cases, we derive abundance limits using either the 4σ upper limits (for weaker or undetected lines) or the lower limits (for saturated lines) on their column densities. We also use the improved oscillator strengths (f -values) for a number of important transitions as given in the compilation of Tripp et al. (1996). These new abundance measurements are combined with similar measurements in the literature that are believed to be largely free of biases resulting from line saturations in order to investigate the chemical evolution of damped Ly α galaxies. Where appropriate, we have corrected the earlier measurements with the set of improved f -values (Tripp et al. 1996) so that all the measurements will be on the same footing. The total sample contains 23 damped Ly α absorption systems in the redshift range $0.7 < z < 4.4$. Our main results are the following.

1. The damped Ly α galaxies have $[\text{Fe}/\text{H}]$ in the range of -2.5 to -1 , or (Fe/H) between $1/10$ to $1/300$ solar, clearly indicating that these are young galaxies in the early stages of chemical evolution. The $N(\text{H I})$ -weighted mean metallicity of the damped Ly α galaxies with $2 < z < 3$ is $[\text{Fe}/\text{H}] = -1.56$, which may be regarded as the cosmic metallicity at $\langle z \rangle = 2.5$. There is a large scatter (about a factor of 30) in (Fe/H) at $z < 3$, which we argue is real and which probably results from the different formation histories of the absorbing galaxies or a mix of galaxy types.

2. Comparisons of the distribution of $[\text{Fe}/\text{H}]$ vs redshift for the sample of damped Ly α galaxies with the similar relation for the Milky Way disk (i.e., the Galactic age-metallicity relation) as defined by the stars in the Edvardsson et al. (1993) sample indicate that the damped Ly α galaxies are much less metal-enriched than the Galactic disk in its past. Since there is evidence from our analyses that depletion of Fe by dust grains in the damped Ly α galaxies is unimportant, the difference in the enrichment level between the sample of damped Ly α galaxies and the Milky Way disk suggests that the damped Ly α galaxies are probably not high-redshift spiral disks in the traditional sense. Rather, they could represent a thick disk phase of galaxies, or more likely the spheroidal component of galaxies, or dwarf galaxies.

3. There is evidence that the mean metallicity in damped Ly α galaxies rises sharply at $z \leq 3$, possibly indicating the onset of significant star formation and chemical enrichment in early galaxies. Such an epoch may be identified as the epoch of galaxy formation in the sense that galaxies are beginning to form the bulk of their stars. This conclusion is consistent with the drop in the neutral baryon content of damped Ly α galaxies at $z > 3$ (Storrie-Lombardi & Wolfe 1996), with the sharp decrease in quasar space density at $z > 3$ (cf. Kenefick et al. 1995), and with the morphology of $z \geq 3$ galaxies identified from their Lyman continuum break (Steidel et al. 1996a,b; Giavalisco et al. 1996). It would be extremely important to confirm the above results using a much larger statistical sample.

4. The relative abundance patterns of the elements being studied here closely resemble those seen in Galactic halo stars. This provides (in our opinion) unambiguous evidence that the bulk of heavy elements in these high-redshift galaxies were produced by Type II supernovae, with little

contribution from stellar mass loss of low-to-intermediate mass stars or from Type Ia supernovae. The evidence for Type II supernova enrichment includes the overabundance of O relative to N, the overabundance of α -elements (Si, S) relative to the iron peak elements (Cr, Mn, Fe, Ni), and the underabundance of Mn relative to Fe and Al relative to Si (i.e., the odd-even effect).

5. In agreement with earlier studies, we find Zn to be overabundant relative to Cr or Fe by an average of ~ 0.4 dex compared to their solar values. Although earlier studies have attributed this effect to selective depletion of Cr and Fe by dust grains, such an interpretation is inconsistent with many of the other elemental abundance ratios seen in these galaxies, most notably N/O and Mn/Fe. We find no dependence of the measured elemental abundances on their condensation temperature in a way that would suggest the depletion by dust grains (cf. Jenkins 1987). The lack of significant variations in the S/Ni ratio across a large velocity interval (several hundreds of km s^{-1}) in one damped Ly α system also argues against the presence of dust in this galaxy. Therefore, we suggest that the overabundance of Zn relative to Cr in damped Ly α galaxies may be intrinsic to their stellar nucleosynthesis. If this interpretation is correct, it will provide important new information to the theory of stellar nucleosynthesis.

6. We discuss the physical conditions in damped Ly α galaxies. The upper limits on the electron density in the absorbing gas as inferred from the C II*/C II ratios are consistent with the value found in the Galactic ISM. It is found that the absorption profiles of Al III in damped Ly α galaxies always resemble those of the low-ionization lines. The profiles of Si IV and C IV absorption, while resembling each other in general, are almost always different from those of the low-ionization absorption lines. These results suggest that Al III is probably produced in the same physical region as the low-ionization species in the absorbing galaxies, while the high-ionization species (Si IV and C IV) mostly likely come from different physical regions.

7. We discuss possible ways to get information on the history of star formation (i.e., continuous or episodic) in damped Ly α galaxies, and on the shape of their stellar initial mass functions.

8. We review the evidence for and against the hypothesis that damped Ly α galaxies are disks or proto-disks at high redshifts (Wolfe et al. 1986), and discuss the implications.

9. We determine upper limits on the temperature of the cosmic microwave background radiation at several redshifts using absorption from the fine structure level of the C II ion (i.e., C II*). These upper limits are consistent with the predicted increase of T_{CMB} with redshift.

It is a great pleasure to acknowledge helpful discussions with Bengt Edvardsson, Max Pettini, Yongzhong Qian, Blair Savage, Chuck Steidel, David Valls-Gabaud, Art Wolfe, and Stan Woosley on various topics related to this work. We are very grateful to Steven Vogt and Chris Churchill for making available their Keck HIRES spectra of Q 0450–1312 and Q 0454+0356 in advance of publication. We thank Craig Foltz and Lisa Storrie-Lombardi for communicating their separate, unpublished results on reddening by dust, and Lisa Storrie-Lombardi and Art Wolfe for their

unpublished result on the evolution of Ω_{damp} . We also thank the referee, Frank Timmes, for many helpful comments and suggestions, which led to significant improvement in the presentation of the results and discussion. The W. M. Keck Observatory is operated as a scientific partnership between the California Institute of Technology and the University of California; it was made possible by the generous financial support of the W. M. Keck Foundation. We especially thank Steven Vogt and the HIRES team for building a superb spectrograph, and the observatory staff for assisting with the observations. Support for this work was provided by NASA through grant number HF1062.01-94A (LL) from the Space Telescope Science Institute, which is operated by the Association of Universities for Research in Astronomy, Inc., for NASA under contract NAS5-26555. WWS acknowledges support from NSF grant AST92-21365.

REFERENCES

- Anders, E., & Grevesse, N. 1989, *Geochim. cosmochim. Acta*, 53, 197
- Arnett, D. 1995, *ARA&A*, 115
- Audouze, J., & Silk, J. 1995, *ApJ*, 451, L49
- Bahcall, J.N., & Wolf, R.A. 1968, *ApJ*, 152, 701
- Beers, T.C., & Sommer-Larsen, J. 1995, *ApJS*, 96, 175
- Bergeron, J., & Boisse, P. 1991, *A&A*, 243, 344
- Beynon, T.G.R. 1978, *A&A*, 64, 145
- Briggs, F.H., Wolfe, A.M., Liszt, H.S., Davis, M.M., & Turner, K.C 1989, *ApJ*, 341, 650
- Cardelli, J.A., Savage, B.D., & Ebbets, D.C. 1991a, *ApJ*, 383, L23
- Cardelli, J.A., Savage, B.D., Bruhweiler, F.C., Smith, A.M., Ebbets, D.C., Sembach, K.R., & Sofia, U.J. 1991b, *ApJ*, 377, L57
- Cardelli, J.A., Sembach, K.R., & Savage, B.D. 1994, *ApJ*, 440, 241
- Churchill, C.W., & Vogt, S. 1997, in preparation
- Clegg, R.E., Lambert, D.L., & Tomkin, J. 1981, *ApJ*, 250, 262
- Cohen, R.D., Beaver, E.A., Diplas, A., Junkkarinen, V.T., Barlow, T.A., & Lyons, R.W. 1996, *ApJ*, 456, 132
- Da Costa, G.S. 1992, in *The Stellar Populations of Galaxies*, eds. B. Barbuy & A. Renzini (Kluwer Academic Publishers), 191
- Djorgovski, S.G., Pahre, M.A., Bechtold, J., & Elston, R. 1996, *Nature*, submitted
- Driver, S.P., Windhorst, R.A., Ostrander, E.J., Keel, W.C., Griffiths, R.E., Ratnatunga, K.U. 1995, *ApJ*, 449, L23

- Edvardsson, B., Andersen, J., Gustafsson, B., Lambert, D.L., Nissen, P.E., & Tomkin, J. 1993, *A&A*, 275, 101
- Fall, S.M., & Pei, Y.C. 1989, *ApJ*, 337, 7
- Fall, S.M., & Pei, Y.C. 1995, in *QSO Absorption Lines*, ed. G.Meylan (Springer-Verlag), 23
- Fall, S.M., Pei, Y.C., & McMahon, R.G. 1989, *ApJ*, 341, L5
- Fan, X-M., & Tytler, D. 1994, *ApJS*, 94, 17
- Field, G. 1974, *ApJ*, 187, 453
- Fitzpatrick, E., & Spitzer, L. Jr. 1994, *ApJ*, 427, 232
- Foltz, C.B., Chaffee, F.H., & Black, J.H. 1988, *ApJ*, 324, 267
- Francois, P. 1987, *A&A*, 176, 294
- Francois, P. 1988, *A&A*, 195, 226
- Giavalisco, M., Steidel, C.C., & Macchetto, F.D. 1996, *ApJ*, in press
- Gratton, R.G. 1989, *A&A*, 208, 171
- Gratton, R.G., & Sneden, C. 1988, *A&A*, 204, 193
- Gratton, R.G., & Sneden, C. 1991, *A&A*, 241, 501
- Hewitt, A., & Burbidge G. 1993, *ApJS*, 87, 451
- Hibbert, A., Dufton, P.L., & Keenan, F.P. 1985, *MNRAS*, 213, 721
- Hoffman, R.D. et al. 1996, *ApJ*, submitted
- Hu, E.M., Songaila, A., Cowie, L.L., & Hodapp, K.W. 1993, *ApJ*, 419, L13
- Iye, M., & Richter, O-G, 1985, *A&A*, 144, 171
- Jenkins, E.B. 1987, in *Interstellar Processes*, ed. D.J.Hollenbach & H.A. Thronson, Jr. (Dordrecht: Reidel), 533
- Keenan, H.D., Hibbert, A., & Dufton, P.L. 1985, *A&A*, 147, 89
- Kennefick, J.D., Djorgovski, S.G., & de Carvalho R.R. 1995, *AJ*, in press
- Kennicutt, R. 1995, in *The Interplay Between Massive Star Formation, the ISM, and Galaxy Evolution*, ed. D. Kunth, B. Guiderdoni, M. Heydari-Melayari, T.X. Thuan, and J.T.T. Van (Paris: Editions Frontieres), in press.
- Lambert, D.L. 1989, in *Cosmic Abundances of Matter*, ed. C.J. Waddington (New York: AIP), 168
- Lanzetta, K.M., & Bowen, D. 1992, *ApJ*, 391, 48
- Lanzetta, K.M., Wolfe, A.M., & Turnshek, D.A. 1995, *ApJS*, 440, 435
- Lanzetta, K.M., Wolfe, A.M., Turnshek, D.A., Lu, L., McMahon, R.G., & Hazard, C. 1991, *ApJS*, 77, 1

- Lowenthal, J.D., Hogan, C.J., Green, R.F., Woodgate, B., Caulet, A., Brown, L., Bechtold, J. 1995, ApJ, 451, 484
- Lu, L., Sargent, W.L.W., & Womble, D.S., & Barlow, T.A. 1996a, ApJ, 457, L1
- Lu, L., Sargent, W.L.W., & Womble, D.S., & Takada-Hidai, M. 1996b, ApJ, accepted
- Lu, L., Sargent, W.L.W., & Barlow, T.A. 1995a, in Cosmic Abundances, the proceedings of the 6th Annual October Astrophysical Conference in Maryland, in press
- Lu, L., Savage, B.D., Tripp, T.M., & Meyer, D. 1995b, ApJ, 447, 597
- Lu, L., & Wolfe, A.M. 1994, AJ, 108, 44
- Magain, P. 1989, A&A, 209, 211
- Majewski, S.R. 1993, ARA&A, 575
- Malaney, R., & Chaboyer, B. 1996, ApJ, 462, 57
- McWilliams, A., Preston, G.W., Sneden, C., & Searle, L. 1995, AJ, 109, 2757
- Meyer, D.M., Black, J.H., Chaffee, F.H., Foltz, C., & York, D.G. 1986, ApJ, 308, L37
- Meyer, D.M., Lanzetta, K.M., & Wolfe, A.M. 1995, ApJ, 451, L13
- Meyer, D.M., & Roth, K.C. 1990, ApJ, 363, 57
- Meyer, D.M., Welty, D.E., & York, D.G. 1989, ApJ, 343, L37
- Meyer, D.M., & York, D.G., 1992, ApJ, 399, L121
- Morton, D.C. 1991, ApJS, 77, 119
- Morton, D.C., Chen, J-S., Wright, A.E., & Peterson, B.A. 1980, MNRAS, 193, 399
- Pardi, M.C., Ferrini, F., & Matteucci, F. 1995, ApJ, 444, 207
- Pagel, B.E.J., Simonson, E.A., Terlevich, R.J., & Edmunds, M.G. 1992, MNRAS, 255, 325
- Pei, Y.C., Fall, S.M., & Bechtold, J. 1991, ApJ, 378, 6
- Pei, Y.C., & Fall, S.M. 1995, 454, 69
- Pettini, M., Boksenberg, A., & Hunstead, R.W. 1990, ApJ, 348, 48
- Pettini, M., King, D.L., Smith, L.J., & Hunstead, R.W. 1995b, in *QSO Absorption Lines*, ed. G. Meylan (Springer-Verlag), p71
- Pettini, M., Lipman, K., & Hunstead, R.W. 1995a, ApJ, 451, 100
- Pettini, M., Smith, L.J., Hunstead, R.W., & King, D.L. 1994, ApJ, 426, 79
- Prochaska, J.X., & Wolfe, A.M. 1996, ApJ, submitted
- Renzini, A., & Voli, M. 1981, A&A, 94, 175
- Reynolds, R. 1991, ApJ, 372, L17
- Ryan, S.G., Norris, J.E., & Beers, T.C. 1996, ApJ, in press

- Sargent, W.L.W., Steidel, C.C., & Boksenberg, A. 1989, ApJS, 69, 703
- Savage, B.D., Cardelli, J.A., & Sofia, U.J. 1992, ApJ, 401, 706
- Savage, B.D., Lu, L., Weymann, R.J., Morris, S.L., & Gilliland, R.L. 1993, ApJ, 404, 124
- Savage, B.D., & Sembach, K.R. 1991, ApJ, 379, 245
- Savage, B.D., & Sembach, K.R. 1996, ARA&A, 1996, in press
- Savaglio, S., D’Odorico, S., & Moller, P. 1994, A&A, 281, 331
- Schmidt, M., Schneider, D.P., & Gunn, J.E. 1995, AJ, 110, 68
- Sembach, K.R., & Savage, B.D. 1996, 457, 211
- Skillman, E.D., & Kennicutt, R.C. 1993, ApJ, 411, 655
- Snedden, C., & Crocker, D.A., 1988, ApJ, 335, 406
- Snedden, C., Gratton, R.G., & Crocker, D.A. 1991, A&A, 246, 354
- Sofia, U.J., Cardelli, J.A., & Savage, B.D. 1994, ApJ, 430, 650
- Sofia, U.J., Savage, B.D., & Cardelli, J.A. 1993, ApJ, 413, 251
- Songaila, A., & Cowie, L.L. 1996, AJ, submitted
- Songaila, A., Cowie, L.L., Hogan, C., & Rugers, M., 1994a, Nature, 368, 599
- Songaila, A., Cowie, L.L., Vogt, S., Keane, M., Wolfe, A.M., Hu, E.M., Oren, A.L., Tytler, D.R., & Lanzetta, K. M. 1995b, Nature, 371, 43
- Spitzer, L.Jr., & Fitzpatrick, E. 1993, ApJ, 409, 299
- Spitzer, L. Jr., & Fitzpatrick, E. 1995, ApJ, 445, 196
- Steidel, C.C. 1995, in QSO Absorption Lines, ed. G. Meylan (Springer-Verlag), 139
- Steidel, C.C., Bowen, D.V., Blades, J.C., & Dickinson, M. 1995, ApJ, 440, L45
- Steidel, C.C., Giavalisco, M., Pettini, M., Dickinson, M., & Adelberger, K.L. 1996b, ApJ, L17
- Steidel, C.C., Pettini, M., Dickinson, M., & Persson, S.E. 1994, AJ, 108, 2046
- Steidel, C.C., Pettini, M., & Hamilton, D. 1996a, preprint
- Stepanian, J. A., Lipovetski, V. A., Chavushian, V. O., Erastova, L. K., & Shapovalova, A. I., 1991, Astrophysics, 34, 163.
- Storrie-Lombardi, L., & Wolfe, A.M. 1996, in preparation
- Thielemann, F-K, Nomoto, K., & Hashimoto, M. 1996, ApJ, 460, 408
- Timmes, F.X., Lauroesch, J.T., & Truran, J.W. 1995, ApJ, 451, 468
- Timmes, F.X., Woosley, S.E., & Weaver, T.A. 1995, ApJS, 98, 617
- Thuan, T.X., Izotov, Y.I., & Lipovetsky, V.A. 1995, ApJ, 445, 108
- Tripp, T.M., Lu, L., & Savage, B.D. 1996, ApJS, 102, 239

- Truran, J.W. & Arnett, W.D. 1971, *Astrophys. Space Sci.*, 11, 430
- Valls-Gabaud, D. 1993, *ApJ*, 419, 7
- Viegas, S.M. 1995, *MNRAS*, 276, 268
- Warren, S.J., Hewett, P.C., & Osmer, P.S. 1994, *ApJ*, 421, 412
- Webb, J.K., Parnell, H.C., Carswell, R.F., McMahon, R., Irwin, M., Hazard, C., Ferlet, R., & Vidae-Madjar, A. 1988, *The Messenger*, No. 51, 15
- Wheeler, J.C., Sneden, C., & Truran, J.W. 1989, *ARA&A*, 27, 279
- Wolfe, A.M. 1988, in *QSO Absorption Lines: Probing the Universe*, eds. J.C. Blades, D.A. Turnshek, & C.A. Norman (Cambridge University Press), p297
- Wolfe, A.M. 1995, in *QSO Absorption Lines*, ed. G. Meylan (Springer-Verlag), 13
- Wolfe, A.M., Fan, X.-M., Tytler, D., Vogt, S.S., Keane, M.J., & Lanzetta, K.M. 1994, *ApJ*, 435, L101
- Wolfe, A.M., Lanzetta, K.M., Foltz, C.B., & Chaffee, F.H. 1996, *ApJ*, 454, 698
- Wolfe, A.M., Turnshek, D.A., Smith, H.E., & Cohen, R.D. 1986, *ApJS*, 61, 249
- Woosley, S.E., & Weaver, T.A. 1995, *ApJS*, 101, 181
- York, D.G., Spitzer, L., Bohlin, R.C., Hill, J., Jenkins, E.B., Savage, B.D., & Snow, T.P. 1983, *ApJ*, 266, L55
- Yoshii, Y., Tsujimoto, T., & Nomoto, K. 1996, *ApJ*, 462, 266

Table 1. JOURNAL OF OBSERVATIONS

Object	z_{em}^a	Date	Coverage	Exposure
Q 0000–2620	4.108	13 Nov 95	5107-7608	6000s
		13 Nov 95	5146-7660	6000s
Q 0216+0803	2.992	11 Oct 94	4203-6633	6000s
		27 Dec 94	4223-6662	6000s
		22 Aug 95	5153-7670	6600s
Q 0449–1325	3.097	26 Dec 94	4203-6632	8000s
		26 Dec 94	4224-6662	8000s
Q 0528–2505	2.779	27 Dec 94	4541-7044	6000s
		27 Dec 94	6274-8697	9000s
		23 Feb 95	4540-7042	6000s
		23 Feb 95	6386-8695	3000s
Q 1425+6039	3.173	18 May 95	4077-6540	6000s
		18 May 95	4059-6513	8400s
		18 May 95	3719-6179	2400s
		19 May 95	3719-6179	9000s
		19 May 95	3732-6199	9000s
Q 1946+7658	2.994	12 Jun 94	4013-6514	4700s
		12 Jun 94	4031-6541	4000s
		14 Nov 93	5107-7608	9000s
Q 2212–1626	3.992	15 Nov 93	5146-7660	9000s
		22 Aug 95	4468-6887	6000s
		22 Aug 95	4492-6920	6000s
		22 Aug 95	5341-7775	3000s
Q 2231–0015	3.018	16 Jun 94	4060-6515	7600s
		17 Jun 94	4032-6425	6000s
Q 2237–0608	4.559	10 Oct 94	6401-8713	12000s
		11 Oct 94	6473-8801	18000s
		20 Aug 95	4899-7455	12000s
		20 Aug 95	4933-7350	3000s
		21 Aug 95	4933-7350	9000s

^a Redshift of the quasar as estimated from the Ly α emission line in the Keck spectrum except for Q 0528–2505, which is from Hewitt & Burbidge (1993).

Table 2. Measurements for the $z_{damp} = 3.3901$ System Toward Q 0000–2620

Ion	λ^a	f^a	v_-^b	v_+^b	$w_r \pm \sigma^c$	$N_a(v) \pm \sigma^d$	N_{adopt}^e	$[Z/H]^f$
H I	1215.670	0.4164	21.41 ± 0.08	...
Al II	1670.787	1.833	–60	+100	0.286 ± 0.020	> 13.15	> 13.15	> -2.74
Si II	1526.707	0.11	–60	+100	0.327 ± 0.008	> 14.56	> 14.56	> -2.40
Fe II	1608.451	0.0619	–60	+40	0.178 ± 0.013	> 14.48	> 14.48	> -2.44
	1611.201	0.00102	–60	+40	0.003 ± 0.017	< 15.45	< 15.45	< -1.47
C IV	1548.195	0.1908	–170	+130	0.966 ± 0.020	> 14.73	> 14.73	...
	1550.770	0.09522	–170	+130	0.814 ± 0.022^g	$> 14.86^g$

^aFrom Morton 1991 unless revised values appear in the compilation of Tripp *et al.* 1996.

^bThe velocity region over which the equivalent width and column density are measured.

^cRest-frame equivalent width and associated error.

^dColumn density from integrating the $N_a(v)$ profile. Upper limits are 4σ .

^eFinal adopted column density.

^fAbundance relative to the solar value of Anders & Grevesse 1989.

^gThe measurement is somewhat contaminated due to blending with the Mg II $\lambda 2796$ absorption at $z_{abs} = 1.433$.

Table 3. Measurements for the $z_{damp} = 2.2931$ System Toward Q 0216+0803

Ion	λ^a	f^a	v_-^b	v_+^b	$w_r \pm \sigma^c$	$N_a(v) \pm \sigma^d$	N_{adopt}^e	$[Z/H]^f$
H I	1215.670	0.4164	20.45 ± 0.16	...
Si II	1526.707	0.11	-340	+140	0.920 ± 0.034	> 15.06	15.45 ± 0.04	-0.55 ± 0.16
	1808.013	0.00218	-40	+100	0.153 ± 0.012	15.45 ± 0.04
Zn II	2026.136	0.489	-40	+100	0.067 ± 0.029	< 12.81	< 12.81	< -0.29
	2062.664	0.256	-40	+100	0.036 ± 0.031	< 13.11
Cr II	2056.254	0.105	-40	+100	0.064 ± 0.024	< 13.39	< 13.39	< -0.74
	2062.234	0.078	-40	+100	0.055 ± 0.030	< 13.61
Fe II	1608.451	0.0619	-80	+140	0.482 ± 0.022	> 14.81	14.89 ± 0.08	-1.07 ± 0.18
	2249.877	0.00182	-40	+100	0.027 ± 0.028	< 15.14
	2260.781	0.00244	-40	+100	0.067 ± 0.026	< 14.97
Ni II	1709.600	0.0689	-40	+100	0.064 ± 0.024	< 13.73	13.60 ± 0.07	-1.10 ± 0.17
	1741.549	0.1035	-40	+100	0.101 ± 0.016	13.60 ± 0.07
	1751.910	0.06375	... ^g	... ^g	... ^g	... ^g
Al II	1670.787	1.833	-340	+140	1.091 ± 0.030	> 13.88	> 13.88	> -1.05
Al III	1854.716	0.5602	-340	+140	0.580 ± 0.052	13.75 ± 0.03	13.74 ± 0.02	...
	1862.790	0.2789	-340	+140	0.359 ± 0.033	13.73 ± 0.02
C IV	1548.195	0.1908	-380	+130	1.460 ± 0.032	> 14.93	> 15.06	...
	1550.770	0.09522	-380	+130	1.150 ± 0.040	> 15.06

^aFrom Morton 1991 unless revised values appear in the compilation of Tripp *et al.* 1996.

^bThe velocity region over which the equivalent width and column density are measured.

^cRest-frame equivalent width and associated error.

^dColumn density from integrating the $N_a(v)$ profile. Upper limits are 4σ .

^eFinal adopted column density.

^fAbundance relative to the solar value of Anders & Grevesse 1989. The uncertainty includes that from the $N(\text{H I})$.

^gBlended with the C IV $\lambda 1550$ absorption at $z_{abs} = 2.7205$.

Table 4. Measurements for the $z_{damp} = 1.7688$ System Toward Q 0216+0803

Ion	λ^a	f^a	v_-^b	v_+^b	$w_r \pm \sigma^c$	$N_a(v) \pm \sigma^d$	N_{adopt}^e	$[Z/H]^f$
H I	1215.670	0.4164	20.00 ± 0.18	...
Si II	1808.013	0.00218	-30	+40	0.044 ± 0.011	14.89 ± 0.11	14.89 ± 0.11	-0.66 ± 0.21
Ni II	1751.910	0.06375	-30	+40	0.020 ± 0.005	13.09 ± 0.10	13.09 ± 0.10	-1.16 ± 0.21
Mn II	2576.877	0.3508	-30	+40	0.059 ± 0.015	12.48 ± 0.11	12.48 ± 0.11	-1.05 ± 0.21
	2594.499	0.2710	-30	+40	0.052 ± 0.017	< 12.63
Zn II	2026.136	0.489	-30	+40	0.030 ± 0.010	< 12.34	< 12.34	< -0.31
	2062.664	0.256	... ^g	... ^g	... ^g	... ^g
Cr II	2056.254	0.105	-30	+40	0.012 ± 0.011	< 13.06	< 13.06	< -0.62
	2062.234	0.078	-30	+40	0.033 ± 0.014	< 13.29
	2066.161	0.0515	-30	+40	0.011 ± 0.020	< 13.62
Fe II	2249.877	0.00182	-30	+40	0.013 ± 0.010	< 14.68	14.53 ± 0.09	-0.98 ± 0.20
	2260.781	0.00244	-30	+40	0.035 ± 0.007	14.53 ± 0.09
	2344.214	0.1097	-110	+40	0.395 ± 0.013	> 14.34
	2374.461	0.0326	-40	+40	0.253 ± 0.011	> 14.45
	2382.765	0.3006	-110	+40	0.533 ± 0.011	> 14.02
	2586.650	0.0684	-110	+40	0.407 ± 0.024	> 14.46
	2600.173	0.2239	-110	+40	0.534 ± 0.028	> 14.03
Al III	1854.716	0.5602	-150	+40	0.225 ± 0.043	13.23 ± 0.08	13.20 ± 0.07	...
	1862.790	0.2789	-150	+40	0.102 ± 0.022	13.17 ± 0.12

^aFrom Morton 1991 unless revised values appear in the compilation of Tripp *et al.* 1996.

^bThe velocity region over which the equivalent width and column density are measured.

^cRest-frame equivalent width and associated error.

^dColumn density from integrating the $N_a(v)$ profile. Upper limits are 4σ .

^eFinal adopted column density.

^fAbundance relative to the solar value of Anders & Grevesse 1989. The uncertainty includes that from the $N(\text{H I})$.

^gBlended with an unidentified absorption feature.

Table 5. Measurements for the $z_{damp} = 1.2667$ System Toward Q 0449–1326

Ion	λ^a	f^a	v_-^b	v_+^b	$w_r \pm \sigma^c$	$N_a(v) \pm \sigma^d$	N_{adopt}^e	$[Z/H]^f$
Fe II	2249.877	0.00182	–20	+40	0.082 ± 0.005	15.11 ± 0.03	15.13 ± 0.02	...
	2260.781	0.00244	–20	+40	0.103 ± 0.009	15.14 ± 0.03
	2344.214	0.1097	–60	+50	0.420 ± 0.011	> 14.27
	2374.461	0.0326	–40	+50	0.299 ± 0.010	> 14.67
	2382.765	0.3006	–60	+140	0.597 ± 0.019	> 13.98
	2586.650	0.0684	–60	+50	0.388 ± 0.011	> 14.39
	2600.173	0.2239	–60	+50	0.606 ± 0.015	> 14.02
Mn II	2576.877	0.3508	–20	+40	0.112 ± 0.008	12.86 ± 0.03	12.87 ± 0.03	...
	2594.499	0.2710	–20	+40	0.097 ± 0.015	12.91 ± 0.06
	2606.462	0.1927	–20	+40	0.099 ± 0.021	13.07 ± 0.09
Mg II	2796.352	0.6123	–110	+140	1.080 ± 0.015	> 13.86	> 14.11	...
	2803.531	0.3054	–110	+140	0.979 ± 0.015	> 14.11
Mg I	2852.964	1.830	–40	+40	0.267 ± 0.009	> 12.62	> 12.62	...

^aFrom Morton 1991 unless revised values appear in the compilation of Tripp *et al.* 1996.

^bThe velocity region over which the equivalent width and column density are measured.

^cRest-frame equivalent width and associated error.

^dColumn density from integrating the $N_a(v)$ profile.

^eFinal adopted column density.

^fNo absolute abundance estimates are possible owing to the lack of $N(\text{H I})$ information.

Table 6. Measurements for the $z_{damp} = 1.1743$ System Toward Q 0450–1312

Ion	λ^a	f^a	v_-^b	v_+^b	$w_r \pm \sigma^c$	$N_a(v) \pm \sigma^d$	N_{adopt}^e	$[Z/H]^f$
Mg II	2796.352	0.6123	–50	+260	1.840 ± 0.038	> 14.10	> 14.10	...
	2803.531	0.3054	... ^g	... ^g	... ^g	... ^g
Cr II	2056.254	0.105	–20	+130	0.086 ± 0.022	13.44 ± 0.12	13.44 ± 0.12	...
	2062.234	0.078	–20	+130	0.103 ± 0.032	< 13.64
	2066.161	0.0515	–20	+130	0.044 ± 0.033	< 13.83
Mn II	2576.877	0.3508	–20	+130	0.159 ± 0.019	12.96 ± 0.08	12.92 ± 0.07	...
	2594.499	0.2710	–20	+130	0.100 ± 0.020	12.84 ± 0.11
	2606.462	0.1927	–20	+130	0.069 ± 0.019	< 13.02
Fe II	2249.877	0.00182	–20	+130	0.105 ± 0.018	15.06 ± 0.10	15.12 ± 0.07	...
	2260.781	0.00244	–20	+130	0.129 ± 0.023	15.17 ± 0.09
	2344.214	0.1097	–50	+240	0.785 ± 0.042	> 14.55
	2374.461	0.0326	–50	+240	0.494 ± 0.050	> 14.86
	2382.765	0.2006	–50	+240	1.113 ± 0.038	> 14.29
	2600.173	0.2239	–50	+240	1.114 ± 0.044	> 14.33
Zn II	2026.136	0.489	–20	+130	0.067 ± 0.028	< 12.80	< 12.80	...
	2062.664	0.256	–20	+130	0.043 ± 0.035	< 13.16

^aFrom Morton 1991 unless revised values appear in the compilation of Tripp *et al.* 1996.

^bThe velocity region over which the equivalent width and column density are measured.

^cRest-frame equivalent width and associated error.

^dColumn density from integrating the $N_a(v)$ profile. Upper limits are 4σ .

^eFinal adopted column density.

^fNo absolute abundance estimates are possible owing to the lack of $N(\text{H I})$ information.

^gOnly partially covered.

Table 7. Measurements for the $z_{damp} = 0.8598$ System Toward Q 0454+0356

Ion	λ^a	f^a	v_-^b	v_+^b	$w_r \pm \sigma^c$	$N_a(v) \pm \sigma^d$	N_{adopt}^e	$[Z/H]^f$
H I	1215.67	0.4164	20.76 ± 0.03	...
Mg II	2803.531	0.3054	-110	+100	1.450 ± 0.017	> 14.38	> 14.38	> -1.97
Mg I	2852.964	1.830	-90	+60	0.303 ± 0.027	12.44 ± 0.04	12.44 ± 0.04	...
Cr II	2056.254	0.105	-90	+40	0.093 ± 0.108	< 14.04	< 14.04	< -0.40
	2062.234	0.078	-90	+40	0.070 ± 0.098	< 14.13
	2066.161	0.0515	-90	+40	0.043 ± 0.106	< 14.34
Mn II	2576.877	0.3508	-90	+40	0.158 ± 0.031	12.96 ± 0.09	12.93 ± 0.06	-1.36 ± 0.07
	2594.499	0.2710	-90	+40	0.113 ± 0.025	12.90 ± 0.09
	2606.462	0.1927	-90	+40	0.079 ± 0.033	< 13.06
Fe II	2249.877	0.00182	-90	+40	0.074 ± 0.044	< 15.33	15.27 ± 0.09	-1.00 ± 0.09
	2260.781	0.00244	-90	+40	0.170 ± 0.034	15.27 ± 0.09
	2344.214	0.1097	-100	+80	0.977 ± 0.018	> 14.74
	2374.461	0.0326	-100	+80	0.718 ± 0.024	> 15.00
	2382.765	0.2006	-100	+80	1.141 ± 0.016	> 14.34
	2586.650	0.0684	-100	+80	1.014 ± 0.016	> 14.83
	2600.173	0.2239	-100	+80	1.228 ± 0.011	> 14.49
Zn II	2062.664	0.256	-90	+40	0.096 ± 0.095	< 13.60	< 13.60	$< +0.19$

^aFrom Morton 1991 unless revised values appear in the compilation of Tripp *et al.* 1996.

^bThe velocity region over which the equivalent width and column density are measured.

^cRest-frame equivalent width and associated error.

^dColumn density from integrating the $N_a(v)$ profile. Upper limits are 4σ .

^eFinal adopted column density.

^fAbundance relative to the solar value of Anders & Grevesse 1989.

Table 8. Measurements for the $z_{damp} = 2.8110$ System Toward Q 0528–2505

Ion	λ^a	f^a	v_-^b	v_+^b	$w_r \pm \sigma^c$	$N_a(v) \pm \sigma^d$	N_{adopt}^e	$[Z/H]^f$
H I	1215.670	0.4164	21.20 ± 0.10	...
C II	1334.532	0.1278	–260	+380	2.234 ± 0.014^g	$> 15.58^g$	> 15.58	> -2.18
C IV	1548.195	0.1908	... <i>h</i>	... <i>h</i>	... <i>h</i>	... <i>h</i>	> 15.00	...
	1550.770	0.09522	–180	+320	0.887 ± 0.033	> 15.00
N I	1199.550	0.1327	... <i>i</i>	... <i>i</i>	... <i>i</i>	... <i>i</i>
	1200.223	0.0885	... <i>i</i>	... <i>i</i>	... <i>i</i>	... <i>i</i>
	1200.710	0.0442	... <i>i</i>	... <i>i</i>	... <i>i</i>	... <i>i</i>
N V	1238.821	0.157	–60	+100	0.163 ± 0.015	14.00 ± 0.04	13.99 ± 0.04	...
	1242.804	0.07823	–60	+100	0.080 ± 0.014	13.94 ± 0.07
O I	1302.169	0.04887	–260	+380	1.945 ± 0.018^j	$> 15.94^j$	> 15.94	> -2.19
Mg II	1239.925	0.00125	–40	+300	0.080 ± 0.033	< 15.88	< 15.88	< -0.91
	1240.395	0.000625	–40	+300	0.040 ± 0.033	< 16.19		
Al II	1670.787	1.833	–260	+380	2.174 ± 0.018	> 14.20	> 14.20	> -1.48
Al III	1854.716	0.5602	–110	+320	0.966 ± 0.026	> 14.04	> 14.07	...
	1862.790	0.2789	–110	+320	0.649 ± 0.025	> 14.07
Si II	1260.422	1.007	–260	+380	2.276 ± 0.012^k	$> 14.70^k$	16.00 ± 0.04	-0.75 ± 0.11
	1304.370	0.086	–120	+380	1.526 ± 0.016	> 15.55
	1526.707	0.11	–260	+380	1.998 ± 0.022^l	$> 15.44^l$
	1808.013	0.00218	–80	+300	0.495 ± 0.027	16.00 ± 0.04
Si IV	1393.755	0.514	–180	+320	1.006 ± 0.023	> 14.41	> 14.52	...
	1402.770	0.2553	–180	+320	0.744 ± 0.031	> 14.52
S II	1250.584	0.005453	–80	+300	0.261 ± 0.028	15.60 ± 0.05	15.59 ± 0.03	-0.88 ± 0.10
	1253.811	0.01088	–80	+300	0.429 ± 0.030	15.58 ± 0.03
	1259.519	0.01624	... <i>m</i>	... <i>m</i>	... <i>m</i>	... <i>m</i>
Cr II	2056.254	0.105	–40	+300	0.159 ± 0.040	13.65 ± 0.12	13.65 ± 0.12	-1.23 ± 0.16
	2062.234	0.078	... <i>n</i>	... <i>n</i>	... <i>n</i>	... <i>n</i>
	2066.161	0.0515	–40	+300	0.066 ± 0.037	< 13.89
Fe II	1608.451	0.0619	–120	+300	1.264 ± 0.018	> 15.32	15.45 ± 0.11	-1.26 ± 0.15
	1611.201	0.00102	–40	+300	0.072 ± 0.026	< 15.64
	2249.877	0.00182	–40	+300	0.194 ± 0.091	< 15.65
	2260.781	0.00244	–40	+300	0.274 ± 0.066	15.45 ± 0.11
Ni II	1317.217	0.146	–40	+300	0.136 ± 0.025	13.83 ± 0.08	13.89 ± 0.03	-1.56 ± 0.10
	1370.132	0.131	–40	+300	0.159 ± 0.026	13.92 ± 0.07
	1454.842	0.0596	–40	+300	0.089 ± 0.029	< 14.02
	1709.600	0.0689	–40	+300	0.141 ± 0.023	13.94 ± 0.07
	1741.549	0.1035	–40	+300	0.182 ± 0.024	13.87 ± 0.06

Table 8—Continued

Ion	λ^a	f^a	v_-^b	v_+^b	$w_r \pm \sigma^c$	$N_a(v) \pm \sigma^d$	N_{adopt}^e	$[Z/H]^f$
	1751.910	0.06375	–40	+300	0.124 ± 0.025	13.88 ± 0.09
Zn II	2026.136	0.489	–40	+300	0.201 ± 0.030	13.09 ± 0.07	13.09 ± 0.07	-0.76 ± 0.12
	2062.664	0.256	... ^o	... ^o	... ^o	... ^o
Undetected Elements								
P II	1532.533	0.00761	–80	+300	0.012 ± 0.027	< 14.84	< 14.84	< +0.07
Cl II	1347.240	0.118	–80	+300	-0.012 ± 0.044	< 13.97	< 13.97	< –0.50
Ti II	1298.697	0.0952	–80	+300	0.015 ± 0.031	< 13.95	< 13.95	< –0.18
Co II	1466.203	0.140	–80	+300	0.022 ± 0.031	< 13.67	< 13.67	< –0.44
Cu II	1358.773	0.380	–80	+300	0.000 ± 0.030	< 13.29	< 13.29	< –0.18
Ga II	1414.402	1.801	–80	+300	0.009 ± 0.032	< 12.61	< 12.61	< +0.28
Ge II	1237.059	0.876 ^p	–80	+300	0.015 ± 0.040	< 13.13	< 13.13	< +0.30
For the absorption complex at $v > 140 \text{ km s}^{-1}$								
C II	1334.532	0.1278	+140	+380	0.904 ± 0.006	> 15.18	> 15.18	...
C II*	1335.708	0.1149	+140	+300	0.226 ± 0.010	14.22 ± 0.02	14.22 ± 0.02	...
N I	1200.710	0.0442	+150 ^q	+300	0.277 ± 0.009	> 14.86	< 15.33 ^r	...
O I	1302.169	0.04887	+140	+380	0.807 ± 0.007	> 15.56	> 15.56	...
Si II	1808.013	0.00218	+140	+300	0.129 ± 0.012	15.36 ± 0.06	15.36 ± 0.06	...
S II	1250.584	0.005453	+140	+300	0.089 ± 0.013	15.10 ± 0.07	15.04 ± 0.04	...
	1253.811	0.01088	+140	+300	0.129 ± 0.015	15.00 ± 0.05
Fe II	1608.451	0.0619	+140	+300	0.406 ± 0.008	> 14.65	> 14.65	...
	1611.201	0.00102	+140	+300	0.016 ± 0.014	< 15.37
	2260.781	0.00244	+140	+300	0.070 ± 0.036	< 15.12

Note to Table 8:

^aFrom Morton 1991 unless revised values appear in the compilation of Tripp et al. 1996.

^bThe velocity region over which the equivalent width and column density are measured.

^cRest-frame equivalent width and associated error.

^dColumn density from integrating the $N_a(v)$ profile. Upper limits are 4σ .

^eFinal adopted column density.

^fAbundance relative to the solar value of Anders & Grevesse 1989. The uncertainty includes that from the $N(\text{H I})$.

^gMay be slightly contaminated at the red edge by the C II* $\lambda 1335$ absorption. The effect on the column density limit should be negligible.

^hOnly partially covered by our spectrum.

ⁱThe three N I lines are blended with each other.

^jBlended with the Si IV $\lambda 1402$ absorption at $z_{abs} = 2.5381$, but the effect on the column density limit should be negligible.

^kContaminated at the blue edge by the S II $\lambda 1259$ absorption in the same system. The equivalent width is thus somewhat overestimated, but the effect on the column density limit should be negligible.

^lSlightly contaminated by the Al III $\lambda 1854$ absorption at $z_{abs} = 2.1410$, but the effects on the measured equivalent width and the column density limit should be negligible.

^mBlended with the Si II $\lambda 1260$ absorption in the same system.

ⁿBlended with the Zn II $\lambda 2062$ absorption in the same system.

^oBlended with the Cr II $\lambda 2062$ absorption in the same system.

^pThe f -value is from Cardelli et al. 1991a.

^qThe v_- is adjusted to avoid the contaminating absorption at the left end. This should not have any significant effect on the estimated column density.

^rsee text in §3.5.

Table 9. Measurements for the $z_{damp} = 2.1410$ System Toward Q 0528–2505

Ion	λ^a	f^a	v_-^b	v_+^b	$w_r \pm \sigma^c$	$N_a(v) \pm \sigma^d$	N_{adopt}^e	$[Z/H]^f$
H I	1215.670	0.4164	20.70 ± 0.08	...
C IV	1548.195	0.1908	–140	+60	0.619 ± 0.012	> 14.57	> 14.71	...
	1550.770	0.09522	–140	+60	0.499 ± 0.014	> 14.71
Al II	1670.787	1.833	–120	+120	0.612 ± 0.013	> 13.46	> 13.46	> -1.72
Al III	1854.716	0.5602	–50	+30	0.104 ± 0.007^g	12.85 ± 0.03^g	12.77 ± 0.08	...
	1862.790	0.2789	–40	+30	0.049 ± 0.009	12.77 ± 0.08
Si II	1526.707	0.11	–120	+120	0.596 ± 0.017	> 14.79	15.26 ± 0.04	-0.99 ± 0.09
	1808.013	0.00218	–60	+30	0.098 ± 0.008	15.26 ± 0.04
Cr II	2056.254	0.105	–30	+30	0.044 ± 0.005	13.09 ± 0.05	13.10 ± 0.04	-1.28 ± 0.09
	2062.234	0.078	–30	+30	0.035 ± 0.005	13.10 ± 0.06
	2066.161	0.0515	–30	+30	0.028 ± 0.007	13.16 ± 0.11
Mn II	2576.877	0.3508	–30	+30	0.045 ± 0.011	12.38 ± 0.10	12.38 ± 0.10	-1.85 ± 0.13
Fe II	1608.451	0.0619	–120	+120	0.320 ± 0.024	> 14.68	14.94 ± 0.26	-1.27 ± 0.27
	1611.201	0.00102	–30	+30	0.017 ± 0.010	< 15.21
	2249.877	0.00182	... ^h	... ^h	... ^h	... ^h
	2260.781	0.00244	... ^h	... ^h	... ^h	... ⁱ
	2344.214	0.1097	–120	+120	0.778 ± 0.019	> 14.56
Ni II	2382.765	0.2006	–120	+120	1.091 ± 0.024	> 14.27
	1709.600	0.0689	–30	+30	0.019 ± 0.009	< 13.31	13.22 ± 0.06	-1.73 ± 0.10
	1741.549	0.1035	–30	+30	0.040 ± 0.007	13.18 ± 0.08
Zn II	1751.910	0.06375	–30	+30	0.030 ± 0.007	13.27 ± 0.10
	2026.136	0.489	... ⁱ	... ⁱ	... ⁱ	... ⁱ	< 12.28	< -1.07
	2062.664	0.256	–30	+30	0.008 ± 0.005	< 12.28

^aFrom Morton 1991 unless revised values appear in the compilation of Tripp *et al.* 1996.

^bThe velocity region over which the equivalent width and column density are measured.

^cRest-frame equivalent width and associated error.

^dColumn density from integrating the $N_a(v)$ profile. Upper limits are 4σ .

^eFinal adopted column density.

^fAbundance relative to the solar value of Anders & Grevesse 1989. The uncertainty includes that from the $N(\text{H I})$.

^gThis line occurs in the red wing of the strong Si II $\lambda 1526$ line at $z_{abs} = 2.8110$ so it may be contaminated.

^hBlended with the Al III $\lambda\lambda 1854, 1962$ lines at $z_{abs} = 2.8110$, respectively.

ⁱBlended with the Al II $\lambda 1670$ line at $z_{abs} = 2.8110$.

Table 10. Measurements for the $z_{damp} = 2.8268$ System Toward Q 1425+6039

Ion	λ^a	f^a	v_-^b	v_+^b	$w_r \pm \sigma^c$	$N_a(v) \pm \sigma^d$	N_{adopt}^e	$[Z/H]^f$
H I	1215.670	0.4164	20.30 ± 0.04	...
C II	1334.532	0.1278	-160	+120	0.842 ± 0.001	> 15.19	> 15.19	> -1.67
C IV	1548.195	0.1908	-140	+120	0.545 ± 0.003	14.32 ± 0.01	14.32 ± 0.01	...
	1550.770	0.09522	-140	+120	0.322 ± 0.004	14.31 ± 0.01
N I	1199.550	0.1327	-120	+60	0.291 ± 0.004	> 14.62	> 14.62	> -1.73
	1200.223	0.0885	-120	+60	0.202 ± 0.004	> 14.54
	1200.710	0.0442	... ^g	... ^g	... ^g	... ^g
Al II	1670.787	1.833	-120	+100	0.634 ± 0.003	> 13.55	> 13.55	> -1.23
Si II	1526.707	0.11	-50^h	+100	$> 0.471^h$	$> 14.78^h$	> 14.78	> -1.07
Si IV	1393.755	0.514	-140	+120	0.288 ± 0.003	13.62 ± 0.01	13.62 ± 0.01	...
	1402.770	0.2553	-140	+120	0.164 ± 0.006	13.62 ± 0.01
Fe II	1608.451	0.0619	-120	+100	0.266 ± 0.004	14.44 ± 0.01	14.48 ± 0.04	-1.33 ± 0.06
	1611.201	0.00102	-40	+40	0.007 ± 0.002	< 14.52
Ni II	1370.132	0.131	-40	+40	0.017 ± 0.001	12.90 ± 0.03	12.90 ± 0.03	-1.65 ± 0.00
	1454.842	0.0596	-40	+40	0.009 ± 0.002	12.91 ± 0.07

^aFrom Morton 1991 unless revised values appear in the compilation of Tripp *et al.* 1996.

^bThe velocity region over which the equivalent width and column density are measured.

^cRest-frame equivalent width and associated error.

^dColumn density from integrating the $N_a(v)$ profile. Upper limits are 4σ .

^eFinal adopted column density.

^fAbundance relative to the solar value of Anders & Grevesse 1989. The uncertainty includes that from the $N(\text{H I})$.

^gContaminated by Ly α forest absorption.

^hThe component at $v \sim -90 \text{ km s}^{-1}$ is blended with the C IV $\lambda 1548$ absorption at $z_{abs} = 2.7727$. Thus we restrict the integration to $v > -50 \text{ km s}^{-1}$ to yield lower limits of the equivalent width and column density.

Table 11. Measurements for the $z_{damp} = 2.8443$ System Toward Q 1946+7658

Ion	λ^a	f^a	v_-^b	v_+^b	$w_r \pm \sigma^c$	$N_a(v) \pm \sigma^d$	N_{adopt}^e	$[Z/H]^f$
H I	1215.670	0.4164	20.27 ± 0.06	...
C II	1334.532	0.1278	-40	+20	0.119 ± 0.003	> 14.14	> 14.14	> -2.69
C II*	1335.708	0.1149	-20	+20	0.001 ± 0.003	< 12.76	< 12.76	...
C IV	1548.195	0.1908	-100	+110	0.482 ± 0.006	14.36 ± 0.01	14.36 ± 0.01	...
	1550.770	0.09522	-100	+110	0.319 ± 0.006	14.37 ± 0.01
N I	1199.550	0.1327	-20	+20	0.011 ± 0.003	< 12.82	< 12.82	< -3.50
	1200.223	0.0885	-20	+20	-0.002 ± 0.003	< 13.01
	1200.710	0.0442	-20	+20	0.008 ± 0.003	< 13.28		
O I	1302.169	0.04887	-20	+20	0.081 ± 0.002	> 14.46	> 14.46	> -2.74
Al II	1670.787	1.833	-40	+20	0.068 ± 0.005	12.26 ± 0.03	12.26 ± 0.03	-2.49 ± 0.07
Si II	1304.370	0.086	-20	+20	0.040 ± 0.002	13.64 ± 0.02	13.63 ± 0.02	-2.19 ± 0.06
	1526.707	0.11	-20	+20	0.061 ± 0.002	13.61 ± 0.02
Si IV	1393.755	0.514	-100	+110	0.374 ± 0.008	13.86 ± 0.01	13.86 ± 0.01	...
	1402.770	0.2553	-100	+110	0.241 ± 0.007	13.87 ± 0.01
S II	1250.584	0.005453	-20	+20	0.003 ± 0.002	< 14.00	< 14.00	< -1.54
Fe II	1608.451	0.0619	-20	+20	0.029 ± 0.003	13.38 ± 0.04	13.38 ± 0.04	-2.40 ± 0.07
Ni II	1370.132	0.131	-20	+20	0.003 ± 0.002	< 12.57	< 12.57	< -1.95

^aFrom Morton 1991 unless revised values appear in the compilation of Tripp *et al.* 1996.

^bThe velocity region over which the equivalent width and column density are measured.

^cRest-frame equivalent width and associated error.

^dColumn density from integrating the $N_a(v)$ profile. Upper limits are 4σ .

^eFinal adopted column density.

^fAbundance relative to the solar value of Anders & Grevesse 1989. The uncertainty includes that from the $N(\text{H I})$.

Table 12. Measurements for the $z_{damp} = 1.7382$ System Toward Q 1946+7658

Ion	λ^a	f^a	v_-^b	v_+^b	$w_r \pm \sigma^c$	$N_a(v) \pm \sigma^d$	N_{adopt}^e	$[Z/H]^f$
Al III	1854.716	0.5602	–20	+40	0.053 ± 0.004	12.58 ± 0.03	12.58 ± 0.03	...
	1862.790	0.2789	–20	+40	0.039 ± 0.004	12.70 ± 0.04
Si II	1808.013	0.00218	–20	+30	0.033 ± 0.003	14.76 ± 0.03	14.76 ± 0.03	...
Cr II	2056.254	0.105	–20	+20	0.025 ± 0.004	12.84 ± 0.07	12.78 ± 0.06	...
	2062.234	0.078	–20	+20	0.015 ± 0.003	12.72 ± 0.08
	2066.161	0.0515	... g	... g	... g	... g
Fe II	2249.877	0.00182	–20	+20	0.023 ± 0.003	14.49 ± 0.05	14.46 ± 0.04	...
	2260.781	0.00244	–20	+20	0.026 ± 0.005	14.41 ± 0.07
	2344.214	0.1097	–30	+40	0.254 ± 0.006	> 14.17
Zn II	2026.136	0.489	–20	+20	0.006 ± 0.003	< 11.83	< 11.83	...
	2062.664	0.256	–20	+20	0.004 ± 0.003	< 12.10

^aFrom Morton 1991 unless revised values appear in the compilation of Tripp *et al.* 1996.

^bThe velocity region over which the equivalent width and column density are measured.

^cRest-frame equivalent width and associated error.

^dColumn density from integrating the $N_a(v)$ profile. Upper limits are 4σ .

^eFinal adopted column density.

^fAbundance relative to the solar value of Anders & Grevesse 1989. The uncertainty includes that from the $N(\text{H I})$.

^gBlended with the C IV $\lambda 1548$ absorption at $z_{abs} = 2.6541$.

Table 13. Measurements for the $z_{damp} = 3.6617$ System Toward Q 2212–1626

Ion	λ^a	f^a	v_-^b	v_+^b	$w_r \pm \sigma^c$	$N_a(v) \pm \sigma^d$	N_{adopt}^e	$[Z/H]^f$
H I	1215.670	0.4164	20.20 ± 0.08	...
C II	1334.532	0.1278	–50	+50	0.276 ± 0.005	> 14.53	> 14.53	> -2.29
C II*	1335.708	0.1149	–50	+50	0.017 ± 0.007	< 13.20	< 13.20	...
C IV	1548.195	0.1908	–40	+50	0.140 ± 0.018	13.73 ± 0.06	13.78 ± 0.06	...
	1550.770	0.09522	–40	+50	0.101 ± 0.016	13.84 ± 0.07
O I	1302.169	0.04887	–50	+50	0.242 ± 0.001	> 14.82	> 14.82	> -2.37
Si II	1304.370	0.086	–50	+50	0.087 ± 0.003	13.91 ± 0.01	13.91 ± 0.01	-1.90 ± 0.08
	1526.707	0.11	–50	+50	0.139 ± 0.013	13.92 ± 0.04
Si IV	1393.755	0.514	... ^g	... ^g	... ^g	... ^g	13.56 ± 0.04	...
	1402.770	0.2553	–40	+50	0.111 ± 0.009	13.56 ± 0.04
Fe II	1608.451	0.0619	–50	+50	0.038 ± 0.034	< 13.99	< 13.99	< -1.78
Ni II	1370.132	0.131	–50	+50	-0.012 ± 0.012	< 12.48	< 12.48	< -2.01

^aFrom Morton 1991 unless revised values appear in the compilation of Tripp *et al.* 1996.

^bThe velocity region over which the equivalent width and column density are measured.

^cRest-frame equivalent width and associated error.

^dColumn density from integrating the $N_a(v)$ profile. Upper limits are 4σ .

^eFinal adopted column density.

^fAbundance relative to the solar value of Anders & Grevesse 1989. The uncertainty includes that from the $N(\text{H I})$.

^gBlended with the Mg II $\lambda 2796$ absorption line at $z_{abs} = 1.3234$.

Table 14. Measurements for the $z_{damp} = 2.0662$ System Toward Q 2231–0015

Ion	λ^a	f^a	v_-^b	v_+^b	$w_r \pm \sigma^c$	$N_a(v) \pm \sigma^d$	N_{adopt}^e	$[Z/H]^f$
H I	1215.67	0.4164	20.56 ± 0.10	...
Al II	1670.787	1.833	... <i>g</i>	... <i>g</i>	... <i>g</i>	... <i>g</i>
Al III	1854.716	0.5602	–160	+30	0.173 ± 0.012	13.07 ± 0.03	13.07 ± 0.03	...
	1862.790	0.2789	–160	+30	0.084 ± 0.017	13.03 ± 0.09
Si II	1808.013	0.00218	–110	+20	0.091 ± 0.012	15.23 ± 0.06	15.23 ± 0.06	-0.88 ± 0.12
Cr II	2056.254	0.105	... <i>h</i>	... <i>h</i>	... <i>h</i>	... <i>h</i>	< 13.26	< -0.98
	2062.234	0.078	–110	+20	0.028 ± 0.013	< 13.26
	2066.161	0.0515	–110	+20	0.021 ± 0.012	< 13.40
Fe II	1608.451	0.0619	–160	+30	0.422 ± 0.006	> 14.72	14.90 ± 0.18	-1.17 ± 0.20
	1611.201	0.00102	–110	+20	0.004 ± 0.007	< 15.08
Ni II	1709.600	0.0689	–110	+20	0.034 ± 0.007	13.30 ± 0.10	13.28 ± 0.07	-1.53 ± 0.12
	1741.549	0.1035	–110	+20	0.048 ± 0.009	13.26 ± 0.08
	1751.910	0.06375	–110	+20	0.023 ± 0.012	< 13.45
Zn II	2026.136	0.489	–110	+20	0.035 ± 0.008	12.33 ± 0.12	12.33 ± 0.12	-0.88 ± 0.16
	2062.664	0.256	–110	+20	0.029 ± 0.013	< 12.74

^aFrom Morton 1991 unless revised values appear in the compilation of Tripp *et al.* 1996.

^bThe velocity region over which the equivalent width and column density are measured.

^cRest-frame equivalent width and associated error.

^dColumn density from integrating the $N_a(v)$ profile. Upper limits are 4σ .

^eFinal adopted column density.

^fAbundance relative to the solar value of Anders & Grevesse 1989. The uncertainty includes that from the $N(\text{H I})$.

^gBlended with the Si IV $\lambda 1402$ absorption at $z_{abs} = 2.6523$.

^hBadly affected by a night sky line.

Table 15. Measurements for the $z_{damp} = 4.0803$ System Toward Q 2237–0608

Ion	λ^a	f^a	v_-^b	v_+^b	$w_r \pm \sigma^c$	$N_a(v) \pm \sigma^d$	N_{adopt}^e	$[Z/H]^f$
H I	1215.670	0.4164	20.52 ± 0.11	...
C II	1334.532	0.1278	–140	+80	0.579 ± 0.002	> 14.89	> 14.89	> -2.19
C II*	1335.708	0.1149	–130	+60	-0.001 ± 0.003	< 12.83
C IV	1548.195	0.1908	–120	+80	0.198 ± 0.019	13.81 ± 0.04	13.81 ± 0.04	...
	1550.770	0.09522	–120	+80	0.109 ± 0.019	13.81 ± 0.08
Al II	1670.787	1.833	–130	+60	0.243 ± 0.013	12.85 ± 0.02	12.85 ± 0.02	-2.15 ± 0.11
Si II	1526.707	0.11	–130	+60	0.291 ± 0.007	14.27 ± 0.02	14.27 ± 0.02	-1.80 ± 0.11
Si IV	1393.755	0.514	–120	+80	0.183 ± 0.010	13.41 ± 0.03	13.44 ± 0.03	...
	1402.770	0.2553	–120	+80	0.119 ± 0.006	13.47 ± 0.03
Fe II	1608.451	0.0619	–130	+60	0.087 ± 0.022	13.85 ± 0.11	13.85 ± 0.11	-2.18 ± 0.15
Ni II	1370.132	0.131	–100	+300	-0.003 ± 0.008	< 13.17	< 13.17	< -1.6

^aFrom Morton 1991 unless revised values appear in the compilation of Tripp *et al.* 1996.

^bThe velocity region over which the equivalent width and column density are measured.

^cRest-frame equivalent width and associated error.

^dColumn density from integrating the $N_a(v)$ profile. Upper limits are 4σ .

^eFinal adopted column density.

^fAbundance relative to the solar value of Anders & Grevesse 1989. The uncertainty includes that from the $N(\text{H I})$.

Table 18. Electron Densities

Object	z_{damp}	$N(\text{C II})$	$N(\text{C II}^*)^a$	$n_e \text{ (cm}^{-3}\text{)}$	reference
0528–2505	2.8110 ^b	> 15.18	14.22	< 1.6	1
1946+7658	2.8443	> 14.14	< 12.46	< 0.30	1
2212–1626	3.6617	> 14.53	< 12.90	< 0.34	1
2237–0608	4.0803	> 14.89	< 12.53	< 0.06	1
1202–0725	4.3829	> 14.96	< 13.06	< 0.18	2

References. — (1) this paper; (2) Lu *et al.* 1996a.

^a Upper limits are 2σ .

^b For the components at $v > 140 \text{ km s}^{-1}$.

Table 19. Comparisons of Different Ionization Species

Object	z_{damp}	Al II/Al III ^a	Low Ion vs Al III ^b	Si IV vs C IV ^b	Low Ion vs High Ion ^b	Ref
0000–2620	3.3901	different	1
0100+1300	2.3090	similar?	different	2
0201+3634	2.4620	>> 1	...	similar	different	3
0216+0803	2.2931	>> 1	similar	...	different?	1
	1.7688	...	similar	1
0528–2505	2.8110	>> 1	similar	similar	similar?	1
	2.1410	>> 1	similar	...	different	1
1202–0725	4.3829	similar	different	4
1331+1704	1.7764	different	5
1425+6039	2.8268	similar?	different	1
1946+7658	2.8443	similar	different	1
	1.7382	...	similar	1
2212–1626	3.6617	similar	different	1
2231–0015	2.0662	...	similar	1
2237–0608	4.0803	similar?	different	1

References. — (1) this paper; (2) Wolfe et al. 1994; (3) Prochaska & Wolfe 1996; (4) Lu et al. 1996a; (5) Wolfe 1995.

^aThis column compares the relative strength of the Al II λ 1670 absorption with that of the Al III λ 1854, 1862 absorption. A >> 1 means the Al II absorption is much stronger than the Al III absorption.

^bThese columns compare the absorption profiles of low ion lines with Al III, and with high ion lines (ie, Si IV and C IV). The entry “similar” means that the two ions being compared have similar absorption profiles in terms of the velocity distribution and relative strength of the components. The entry “similar?” means the two ions being compared are more similar than different. The entries “different” and “different?” should be interpreted in an analogous way.

Table 20. Measurements of Cosmic Microwave Background Temperature

Object	redshift	T_{ex}^a (K)	T_{CMB}^b (K)	reference
1331+1704	1.7760	10.4 ± 0.5	7.6	1
		7.4 ± 0.8	7.6	1
0528–2505	2.8110	$< 31.5^c$	10.4	2
1946+7658	2.8443	< 20.1	10.5	2
0636+6801	2.9090	$< 16.0^d$	10.7	3
2212–1626	3.6617	< 20.6	12.7	2
2237–0608	4.0803	< 14.9	13.9	2
1202–0725	4.3829	< 18.1	14.7	4

References. — (1) Songaila *et al.* 1994a; (2) this paper; (3) Songaila *et al.* 1994b; (4) Lu *et al.* 1996a.

^a Excitation temperature as derived either from $N(\text{C II}^*)/N(\text{C II})$ or from $N(\text{C I}^*)/N(\text{C I})$. Upper limits are 2σ .

^b Predicted temperature of the cosmic microwave background from $2.73(1+z)$.

^c For the absorption complex at $v > 140 \text{ km s}^{-1}$ (see Table 8).

^d Songaila *et al.* (1994b) quoted $T_{ex} < 13.5 \text{ K}$ using $N(\text{C II})=4.6 \times 10^{14} \text{ cm}^{-2}$ estimated from profile fitting. Given the heavy saturation of the C II $\lambda 1334$ absorption, we consider this $N(\text{C II})$ very uncertain, and prefer to use $N(\text{C II}) > 1.5 \times 10^{14} \text{ cm}^{-2}$ estimated from the observed equivalent width of the C II absorption.

Fig. 1.— Damped Ly α absorption in the $z_{damp} = 3.3901$ system toward Q 0000–2620. The solid curve represents the best-fit damping profile with $N(\text{H I}) = 2.6 \times 10^{21} \text{ cm}^{-2}$. The dotted curves are damping profiles with $N(\text{H I}) = (2.2, 3.1) \times 10^{21} \text{ cm}^{-2}$.

Fig. 2.— Velocity profiles of metal lines in the $z_{damp} = 3.3901$ damped Ly α system toward Q 0000–2620. The zero velocity is fixed at $z = 3.39005$. Absorption features marked with “+” signs are unrelated to the absorption line in question. Lines that occur in the Ly α forest or are blended with other absorption lines are indicated as such.

Fig. 3.— Velocity profiles of metal lines in the $z_{damp} = 2.2931$ damped Ly α system toward Q 0216+0803. The zero velocity is fixed at $z = 2.29310$. The absorption at $v > 130 \text{ km s}^{-1}$ in the C IV $\lambda 1548$ panel (marked with a “+” sign) is from C IV $\lambda 1550$, and that at $v < -380 \text{ km s}^{-1}$ in the C IV $\lambda 1550$ panel (marked with a “+” sign) is from C IV $\lambda 1548$.

Fig. 4.— Velocity profiles of metal lines in the $z_{damp} = 1.7688$ damped Ly α system toward Q 0216+0803. The zero velocity is fixed at $z = 1.76880$.

Fig. 5.— Velocity profiles of metal lines in the $z_{damp} = 1.2667$ damped Ly α system toward Q 0449–1326. The zero velocity is fixed at $z = 1.26666$. The strongly saturated Fe II $\lambda 2600$ line is not shown due to space considerations. Features marked with “+” signs are unrelated to the absorption line in question.

Fig. 6.— Profiles of apparent column densities, $N_a(v)$, for the Mn II lines in the $z_{damp} = 1.2667$ damped Ly α system toward Q 0449–1326.

Fig. 7.— Velocity profiles of metal lines in the $z_{damp} = 1.1743$ damped Ly α system toward Q 0450–1312. The zero velocity is fixed at $z = 1.17428$. The data are from Churchill & Vogt (1997).

Fig. 8.— Velocity profiles of metal lines in the $z_{damp} = 0.8598$ damped Ly α system toward Q 0453+0356. The zero velocity is fixed at $z = 0.85980$. The data are from Churchill & Vogt (1997).

Fig. 9.— Velocity profiles of metal lines in the $z_{damp} = 2.8110$ damped Ly α system toward Q 0528–2505. The zero velocity is fixed at $z = 2.81100$. Features marked with “+” signs are unrelated to the absorption in question. Lines that are blended with other absorption lines are indicated as such.

Fig. 10.— Velocity profiles of metal lines in the $z_{damp} = 2.1410$ damped Ly α system toward Q 0528–2505. The zero velocity is fixed at $z = 2.14100$. Absorption features marked with “+” signs are unrelated to the absorption line in question. The Ni II $\lambda 1709$ and Cr II $\lambda 2066$ lines, though detected, are not shown due to space considerations. Lines that are blended with other absorption lines are indicated as such.

Fig. 11.— Ly α and Ly β absorption line profiles in the $z_{damp} = 2.8268$ damped Ly α system toward

Q 1425+6039. The dotted curves show the damping profiles with $z_{abs} = 2.8268$, $N(\text{H I}) = 2 \times 10^{20} \text{ cm}^{-2}$, and Doppler $b = 10 \text{ km s}^{-1}$. Note the excess absorption at the red wing of the line profiles, which comes from the absorbing subcomplex near $z_{abs} = 2.83058$ ($v \sim 300 \text{ km s}^{-1}$ in figure 13).

Fig. 12.— Same as figure 11, but with one additional component added to the fit at $z_{abs} = 2.83058$ with $N(\text{H I}) = 1 \times 10^{19} \text{ cm}^{-2}$ and $b = 10 \text{ km s}^{-1}$.

Fig. 13.— Velocity profiles of metal lines in the $z_{damp} = 2.8268$ damped Ly α system toward Q 1425+6039. The zero velocity is fixed at $z = 2.82680$. Absorption features marked with “+” signs are unrelated to the absorption line in question. Lines occurring in the Ly α forest are indicated as such. Note the expanded vertical scales for some panels. Essentially all absorption displayed in the C II* $\lambda 1335$ panel is from the C II $\lambda 1334$ line. Only the components at $v < 120 \text{ km s}^{-1}$ will be considered as part of the damped Ly α system (see main text).

Fig. 14.— Damped Ly α absorption in the $z_{damp} = 2.8443$ system toward Q 1946+7658. The solid curve represents the best-fit damping profile with $N(\text{H I}) = 1.86 \times 10^{20} \text{ cm}^{-2}$. The dotted curves are damping profiles with $N(\text{H I}) = (1.62, 2.14) \times 10^{20} \text{ cm}^{-2}$.

Fig. 15.— Velocity profiles of metal lines in the $z_{damp} = 2.8443$ damped Ly α system toward Q 1946+7658. The zero velocity is fixed at $z = 2.84430$. Absorption features marked with “+” signs are unrelated to the absorption line in question. Lines occurring in the Ly α forest are indicated as such.

Fig. 16.— Velocity profiles of metal lines in the $z_{damp} = 1.7382$ damped Ly α system toward Q 1946+7658. The zero velocity is fixed at $z = 1.73820$. Absorption features marked with “+” signs are unrelated to the absorption line in question. Lines blended with other lines are indicated as such.

Fig. 17.— Damped Ly α absorption in the $z_{damp} = 3.6617$ system toward Q 2212–1626. The solid curve represents the best-fit damping profile with $N(\text{H I}) = 1.6 \times 10^{20} \text{ cm}^{-2}$. The dotted curves are damping profiles with $N(\text{H I}) = (1.3, 1.9) \times 10^{20} \text{ cm}^{-2}$.

Fig. 18.— Velocity profiles of metal lines in the $z_{damp} = 3.6617$ damped Ly α system toward Q 2212–1626. The zero velocity is fixed at $z = 3.66170$. Absorption features marked with “+” signs are unrelated to the absorption line in question. Lines blended with other absorption lines are indicated as such.

Fig. 19.— Velocity profiles of metal lines in the $z_{damp} = 2.0662$ damped Ly α system toward Q 2231–0015. The zero velocity is fixed at $z = 2.06615$. Absorption features marked with “+” signs are unrelated to the absorption line in question.

Fig. 20.— Damped Ly α absorption in the $z_{damp} = 4.0803$ system toward Q 2237–0608. The solid curve represent the best-fit damping profile with $N(\text{H I}) = 3.0 \times 10^{20} \text{ cm}^{-2}$. The dotted curves are damping profiles with $N(\text{H I}) = (2.3, 3.9) \times 10^{20} \text{ cm}^{-2}$.

Fig. 21.— Velocity profiles of metal lines in the $z_{damp} = 4.0803$ damped Ly α system toward Q 2237–0608. The zero velocity is fixed at $z = 4.08026$. Absorption features marked with “+” signs are unrelated to the absorption line in question.

Fig. 22.— Age-metallicity relations. The conversion between age of the universe and redshift is for the cosmological parameters indicated in the figure. The solid circles are for damped Ly α galaxies in Table 16. The “+”s are for Galactic disk stars in the sample of Edvardsson et al. (1993).

Fig. 23.— Abundance ratios of selected elements against [Fe/H] for the sample of damped Ly α galaxies given in Table 16. In a few cases, except for the [Cr/Fe] vs [Fe/H] panel, Cr abundance has been used in place of Fe abundance when the latter is not available.

Fig. 24.— Similar to fig. 23, but for diffuse ISM clouds in the Galactic disk and halo as given in Table 17. Note that the spread in [Fe/H] in the horizontal axis reflects the different levels of Fe depletion in the ISM clouds rather than intrinsic differences in the clouds’ metallicity.

Fig. 25.— Similar to fig. 23, but for Milky Way disk and halo stars. These ratios reflect the chemical enrichment processes during the past history of the Milky Way. Sources of the data are given in §4.2.

Fig. 26.— Elemental abundances as a function of condensation temperature for damped Ly α galaxies. Note that the abundances are plotted relative to the Fe abundance (or Cr abundance, in case Fe measurement is not available) in the same system. For Al, Si, S, Cr, Mn, Fe, Ni, and Zn, the average values of the actual measurements (i.e., excluding upper and lower limits) are plotted (solid dots), with the vertical bars indicating the range of the measured values. For C, N, and O, individual limits are plotted since no actual measurements are available. Lower limits are indicated by open triangles, and upper limits are indicated by inverted solid triangles.

Fig. 27.— The three left panels show the profiles of apparent column density per unit velocity, $N_a(v)$, for S II, Si II, and Ni II in the $z_{damp} = 2.8110$ damped Ly α system toward Q 0528–2505, based on the average of two S II lines, the Si II $\lambda 1808$ line, and the average of six Ni II lines. The three panels to the right give the $N_a(v)$ ratios for S II/Si II, S II/Ni II, and Si II/Ni II.

Fig. 28.— Temperature of the cosmic microwave background as inferred from observations of high-redshift quasar absorption systems. The dotted line is the predicted relation of $T_{CMB} = 2.73(1+z)$ from Big Bang cosmology.

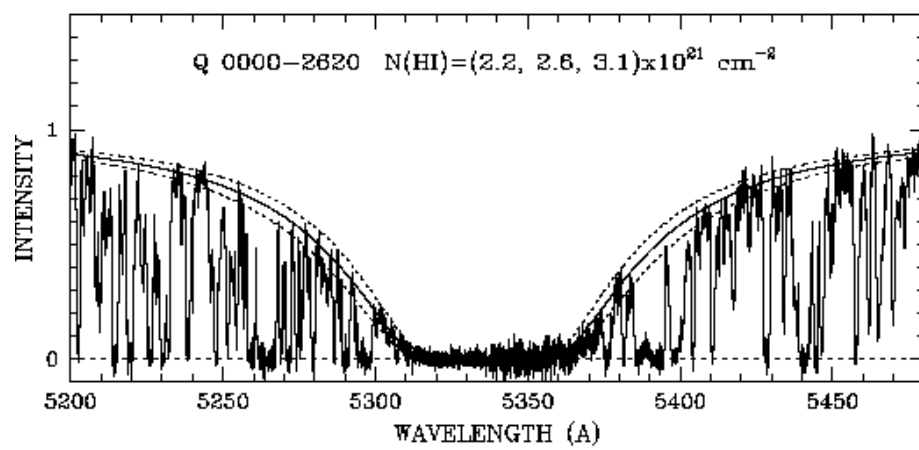


figure 1

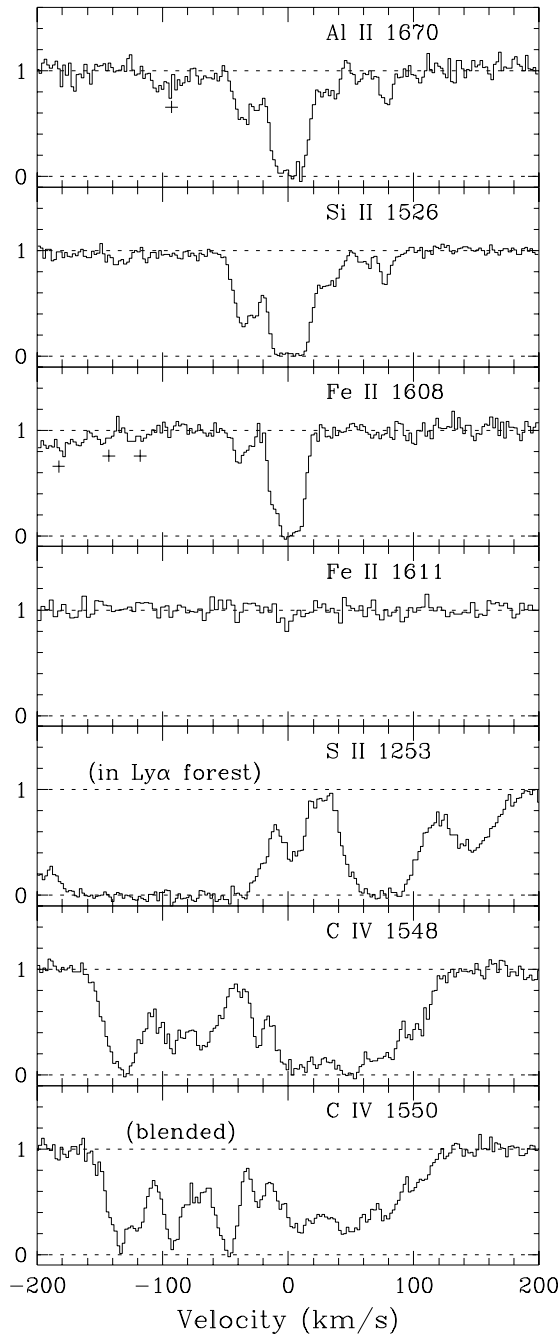


figure 2

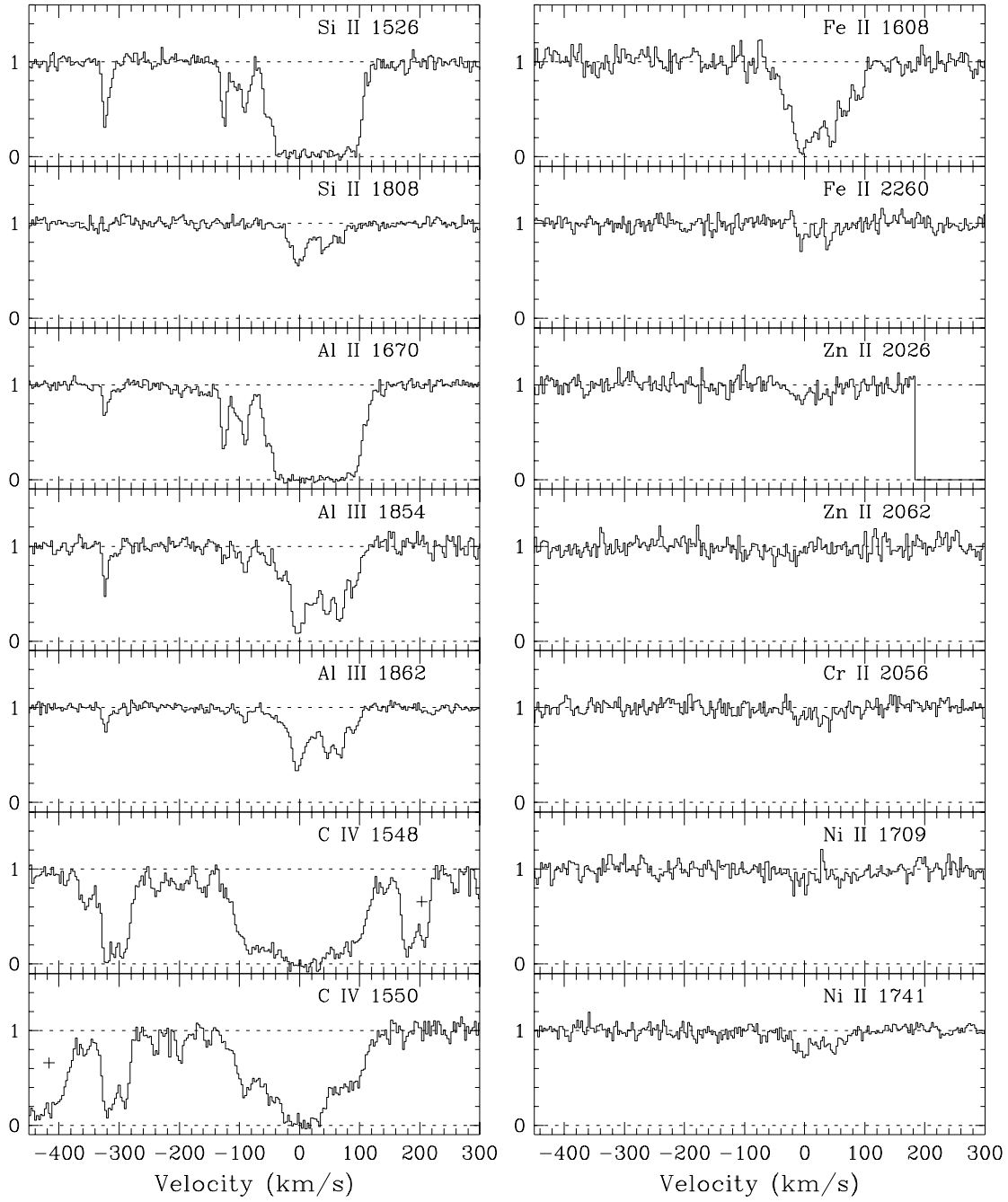


figure 3

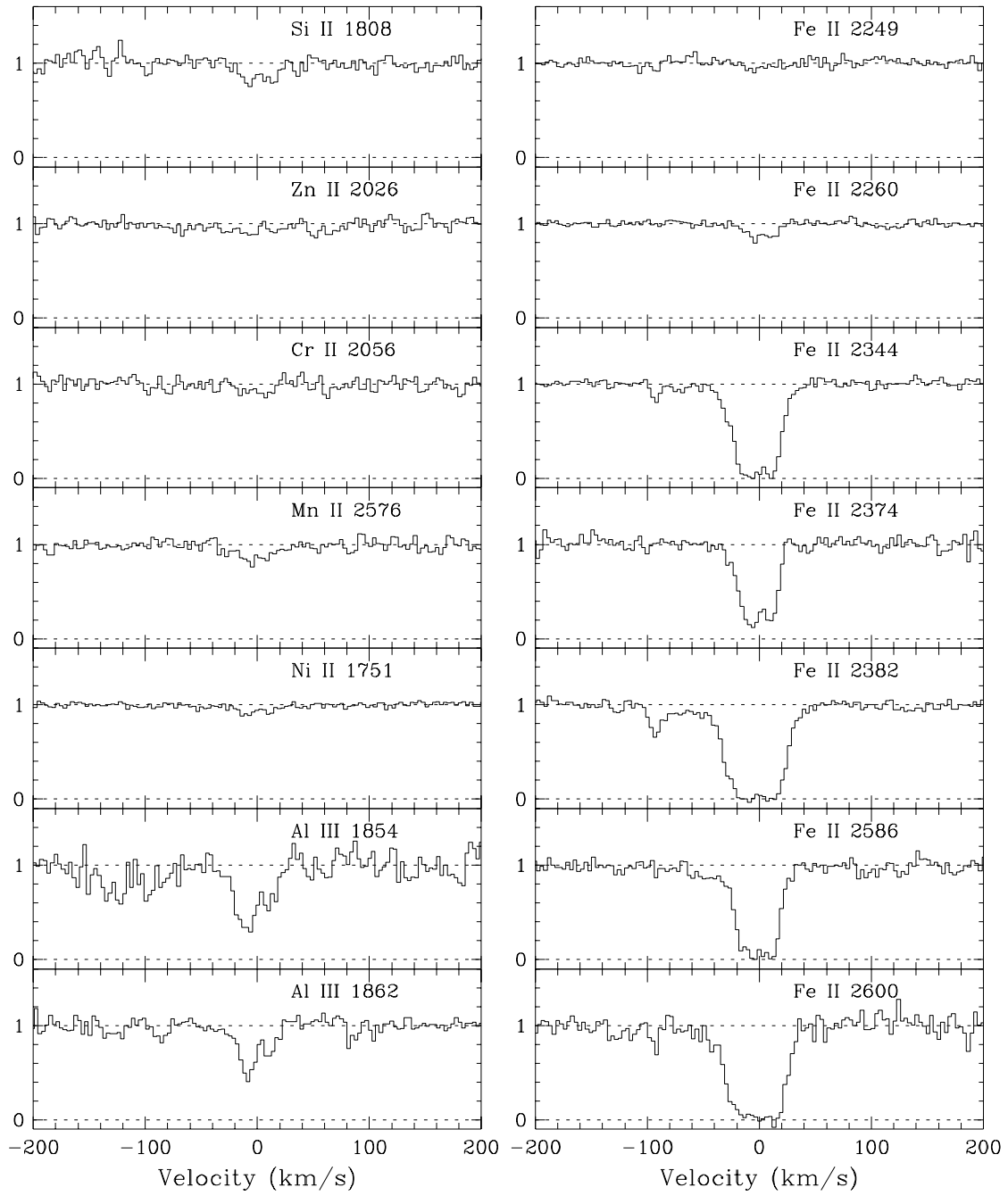


figure 4

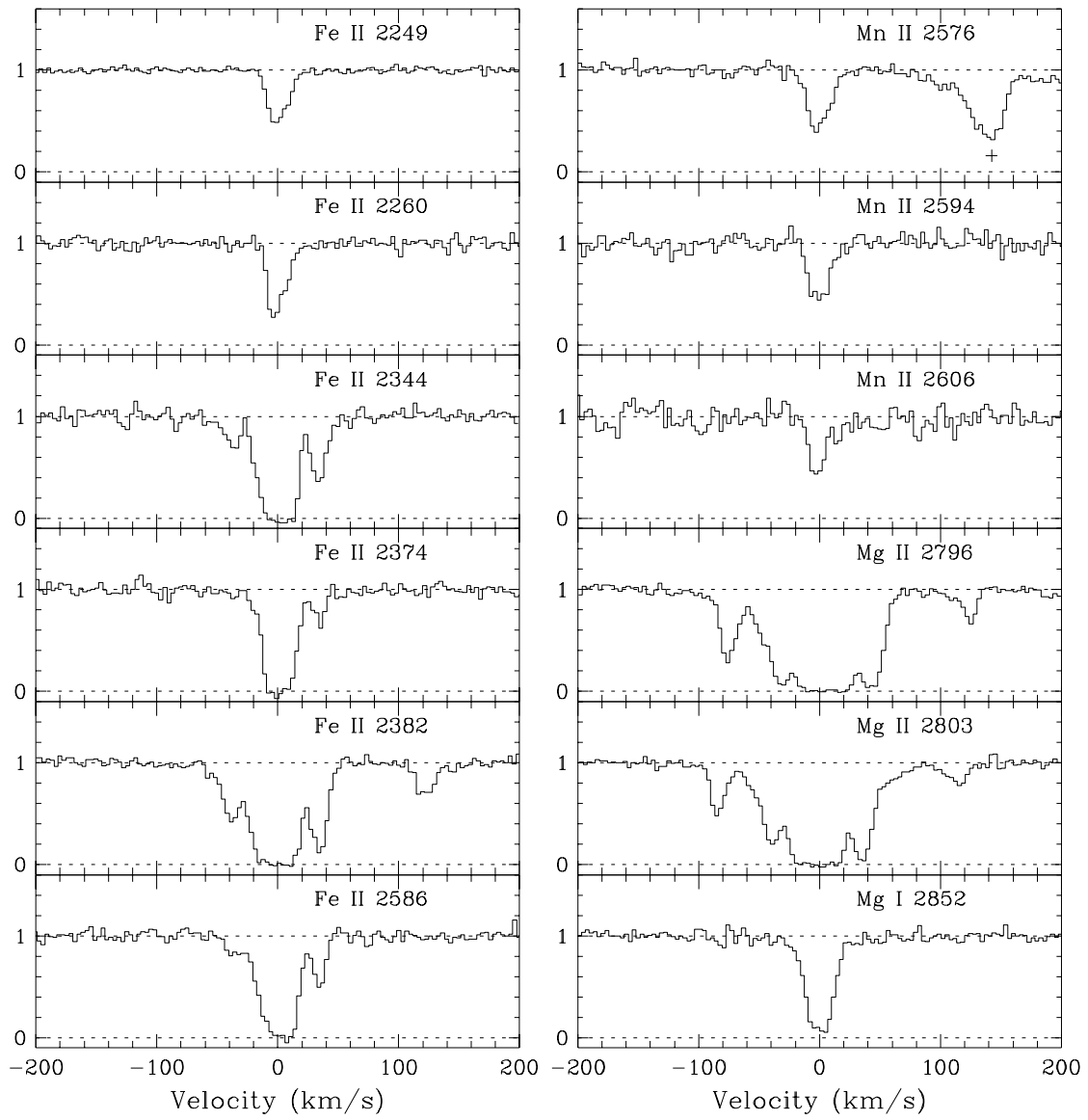


figure 5

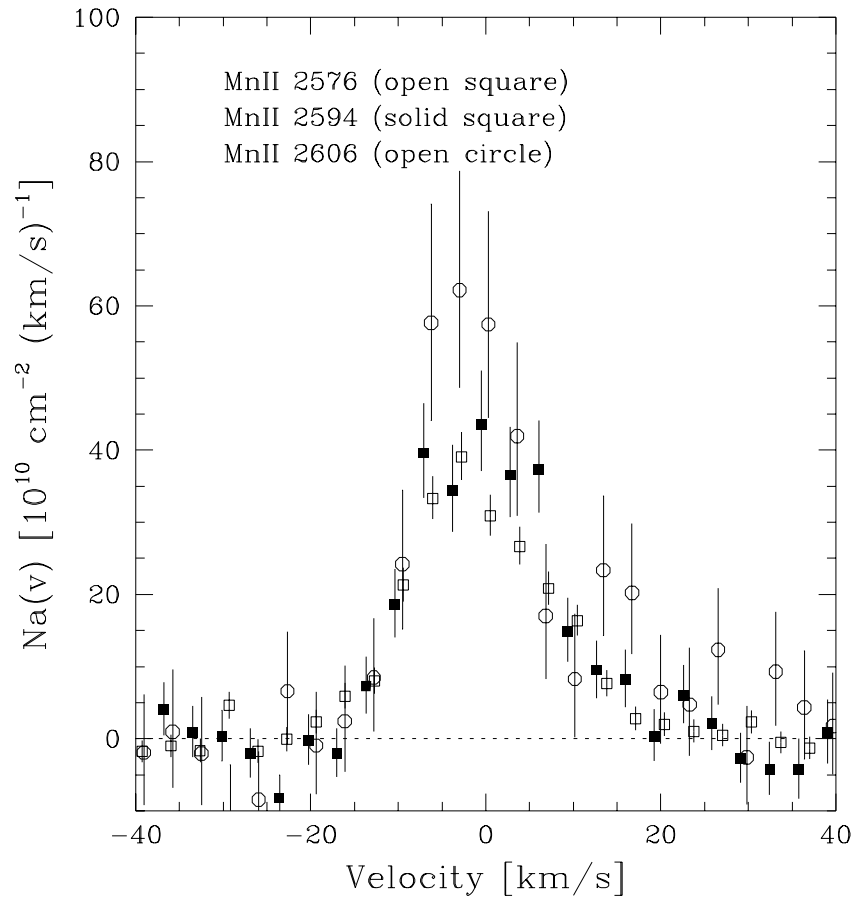


figure 6

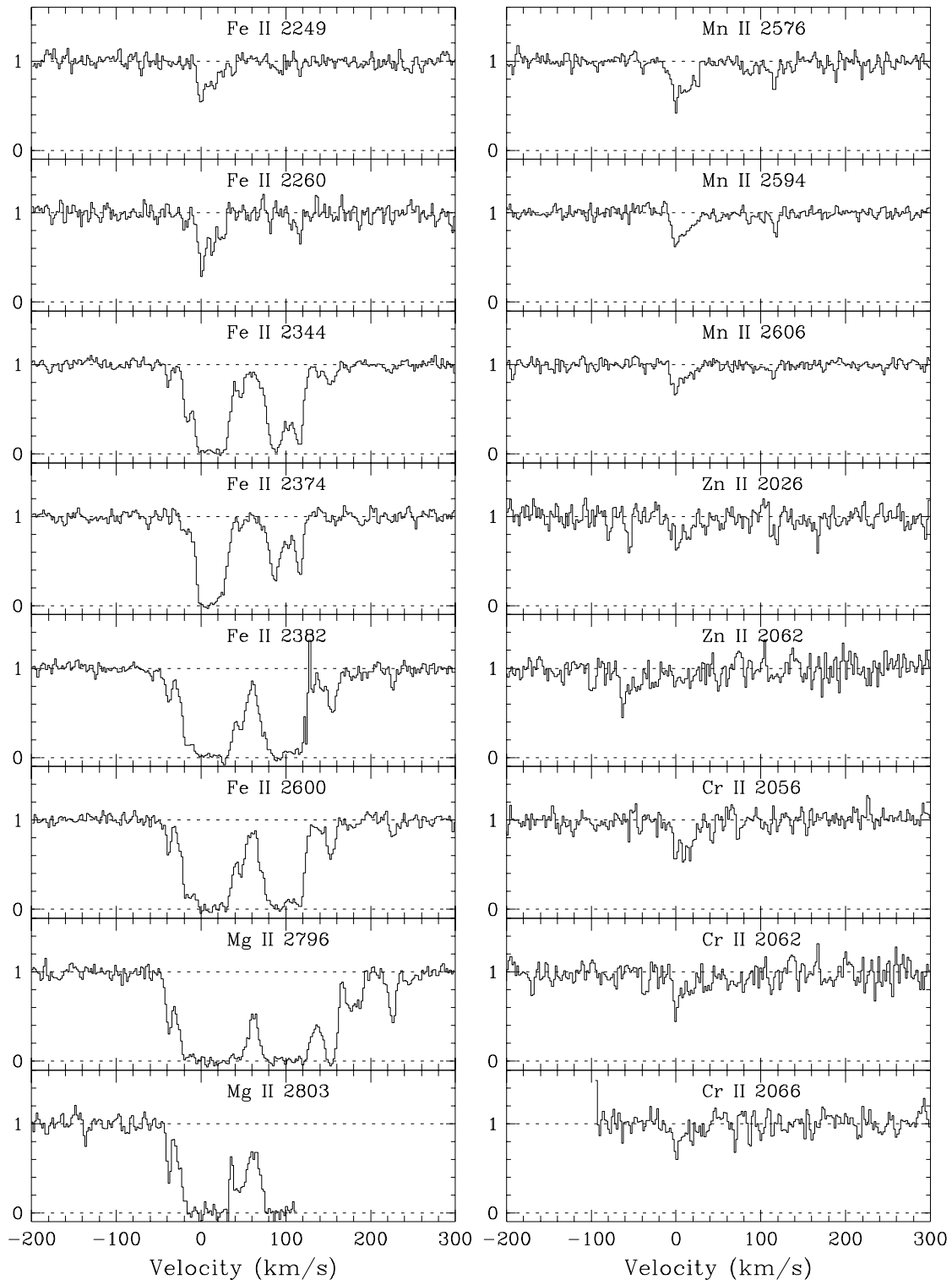


figure 7

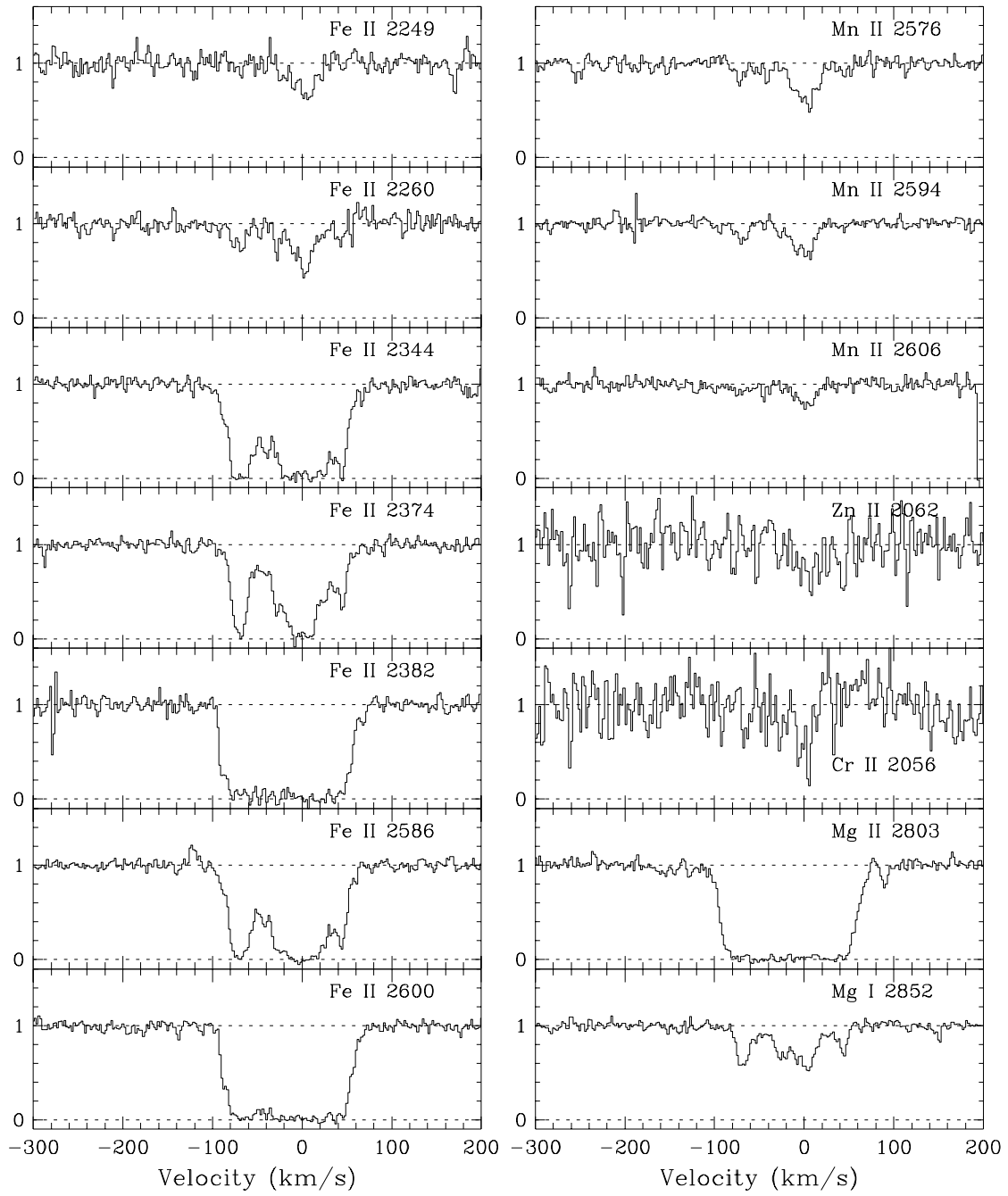


figure 8

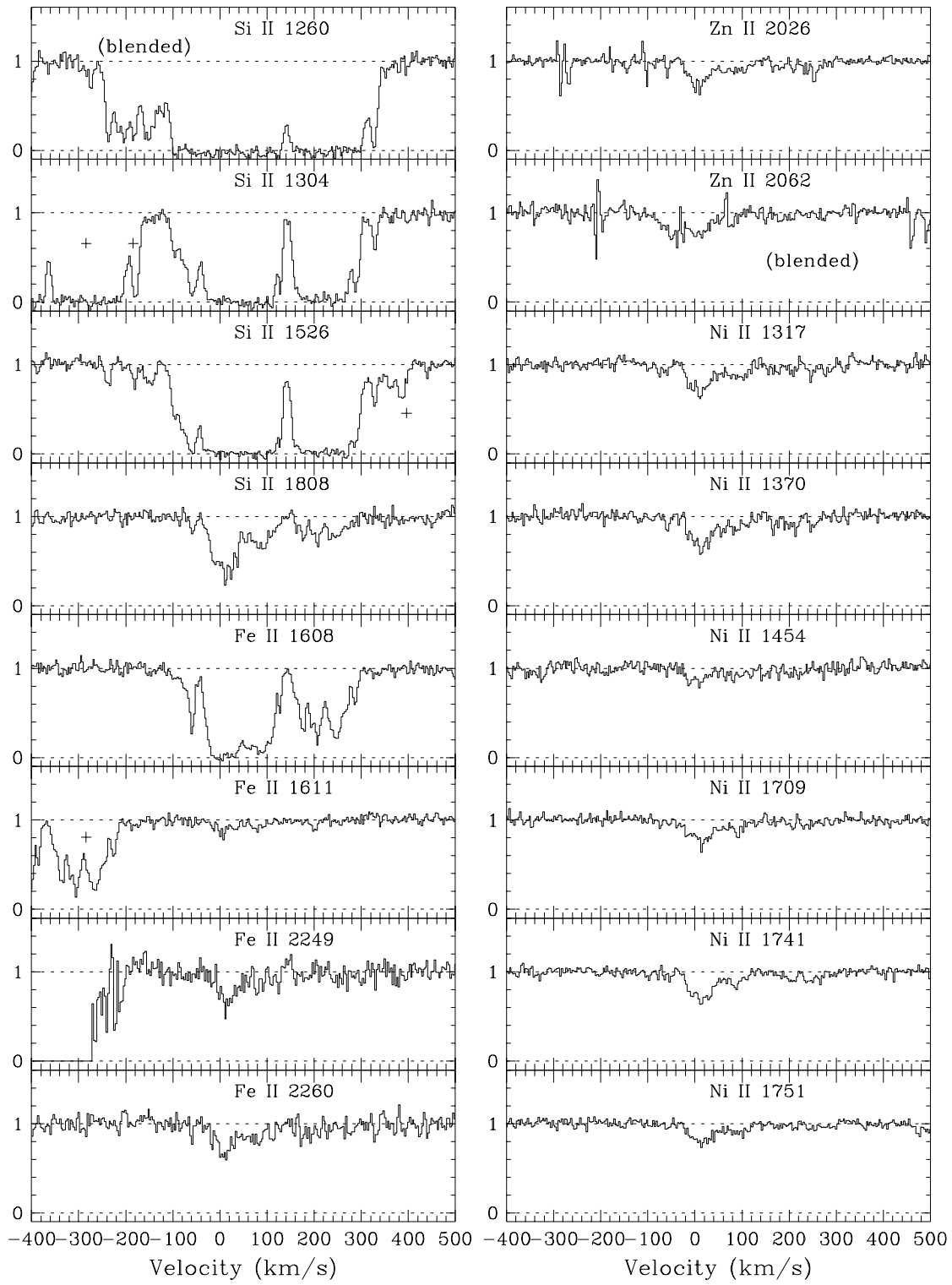


figure 9a

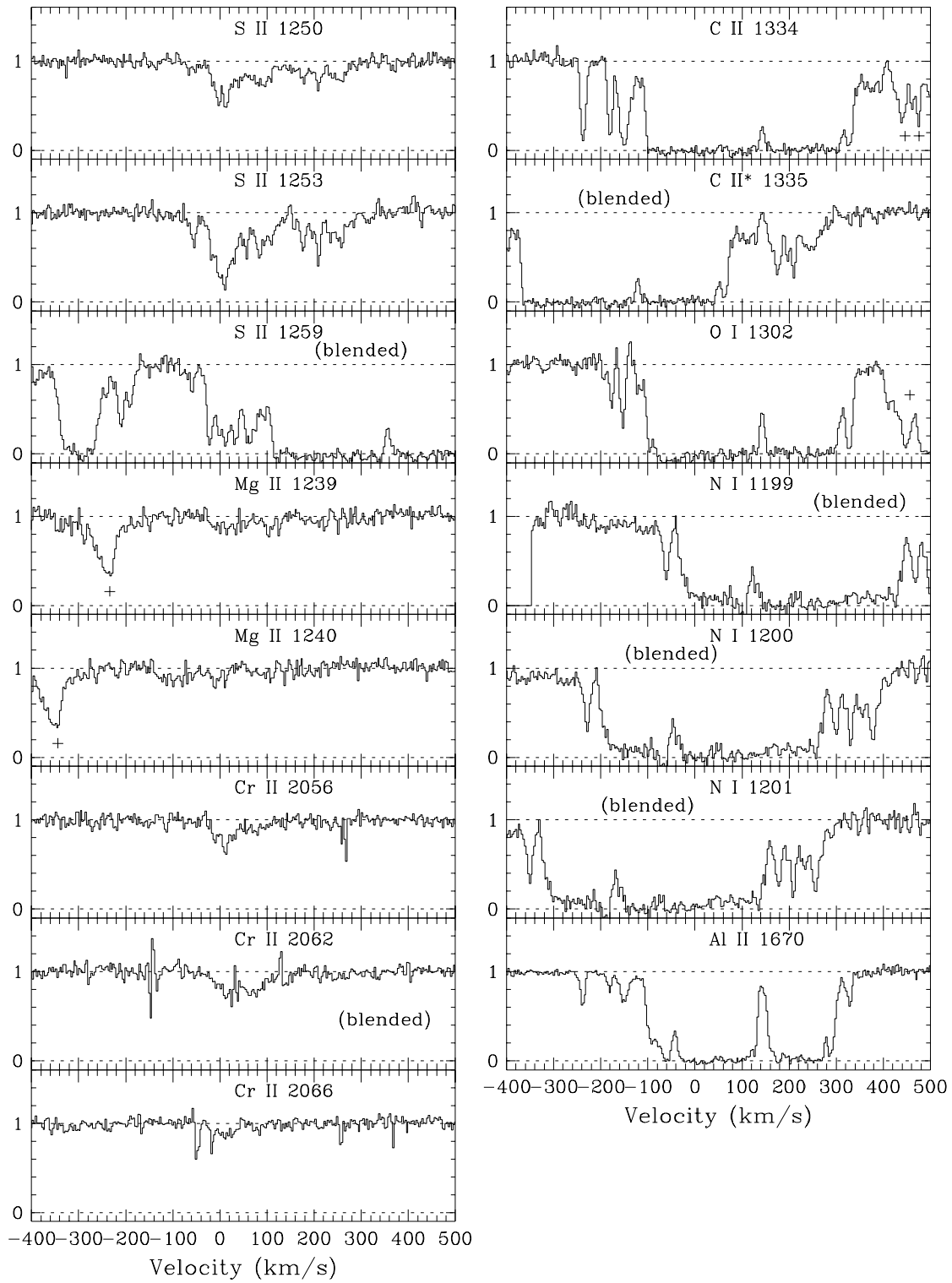


figure 9b

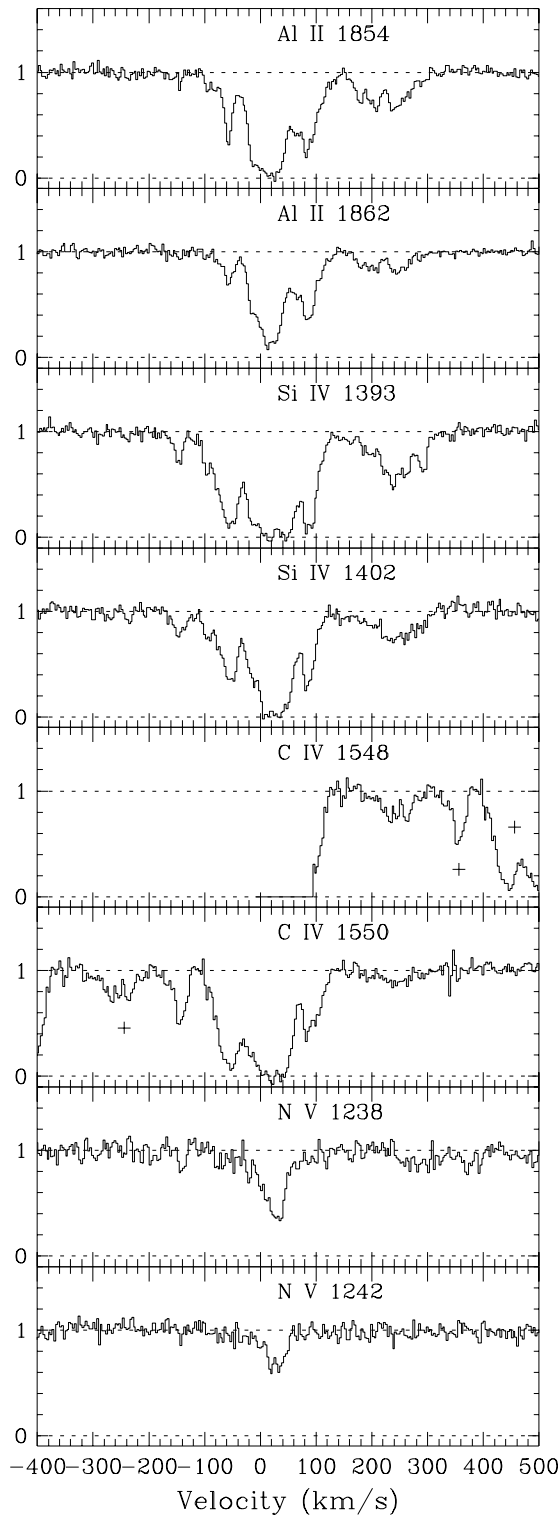


figure 9c

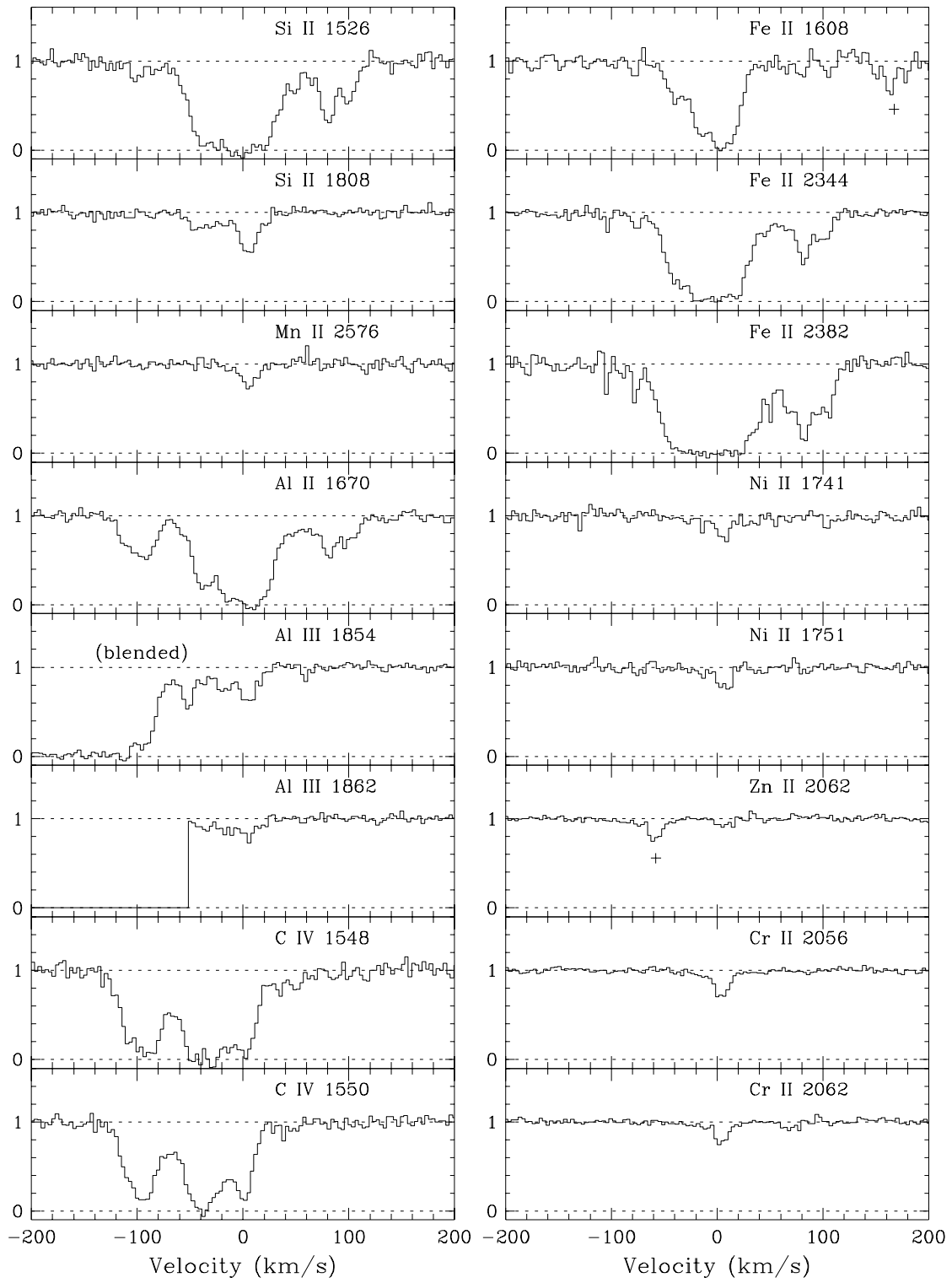


figure 10

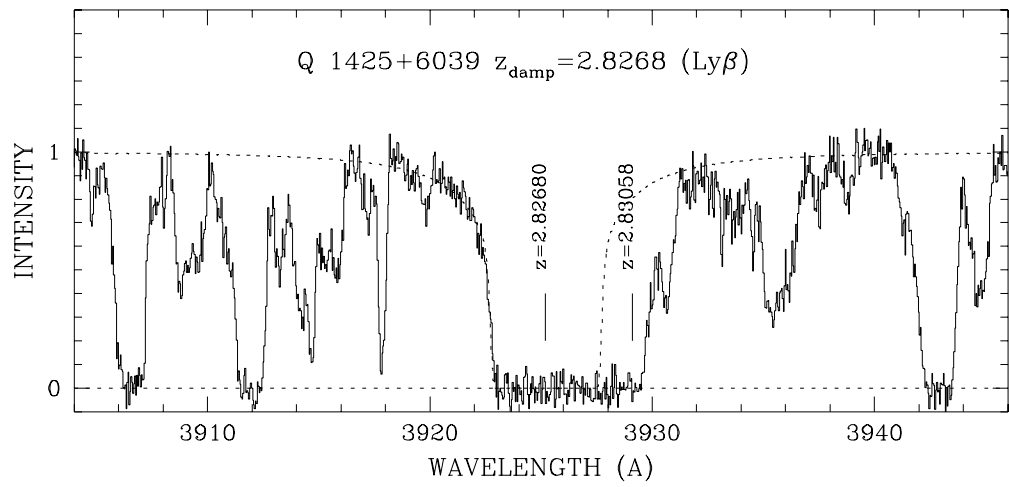
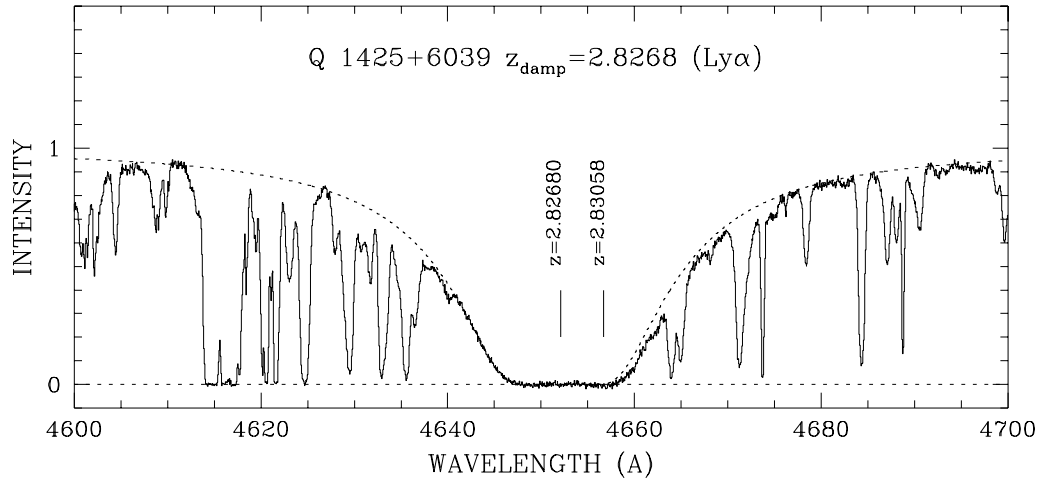


figure 11

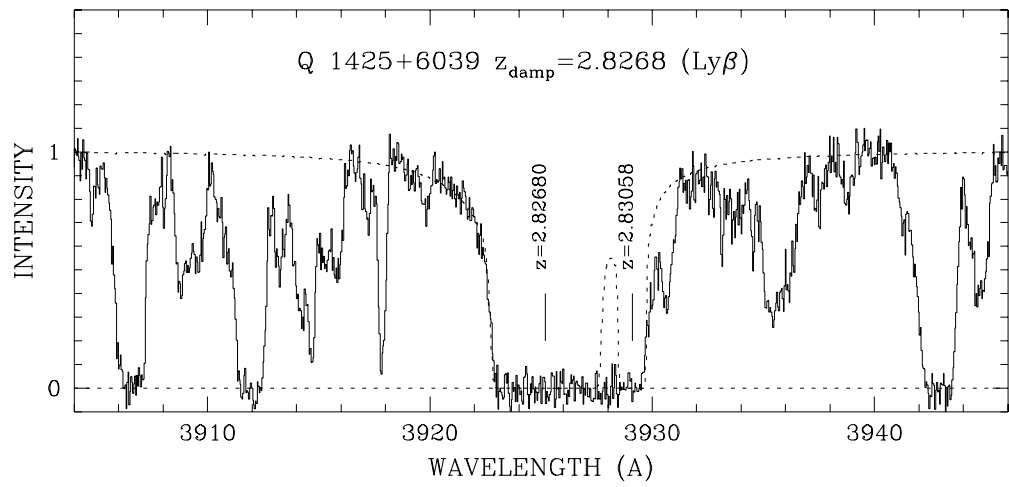
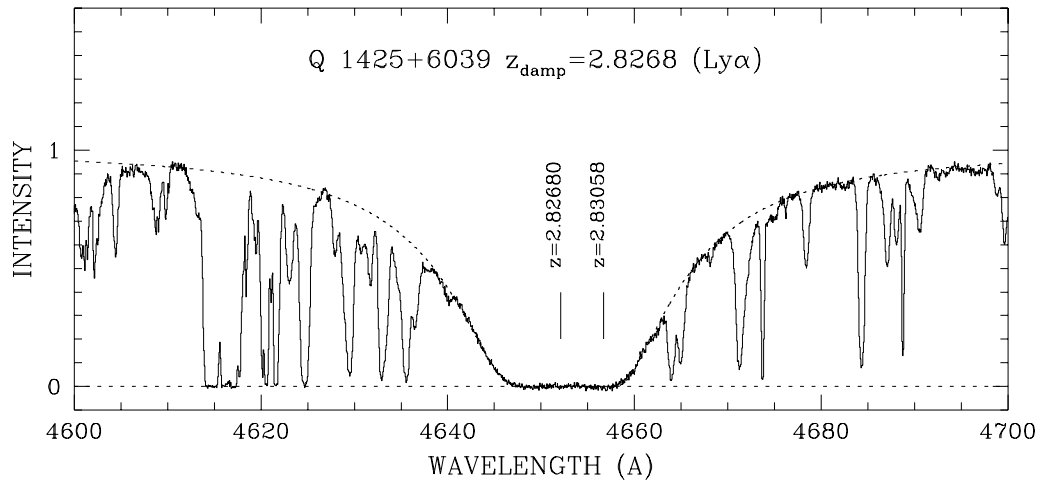


figure 12

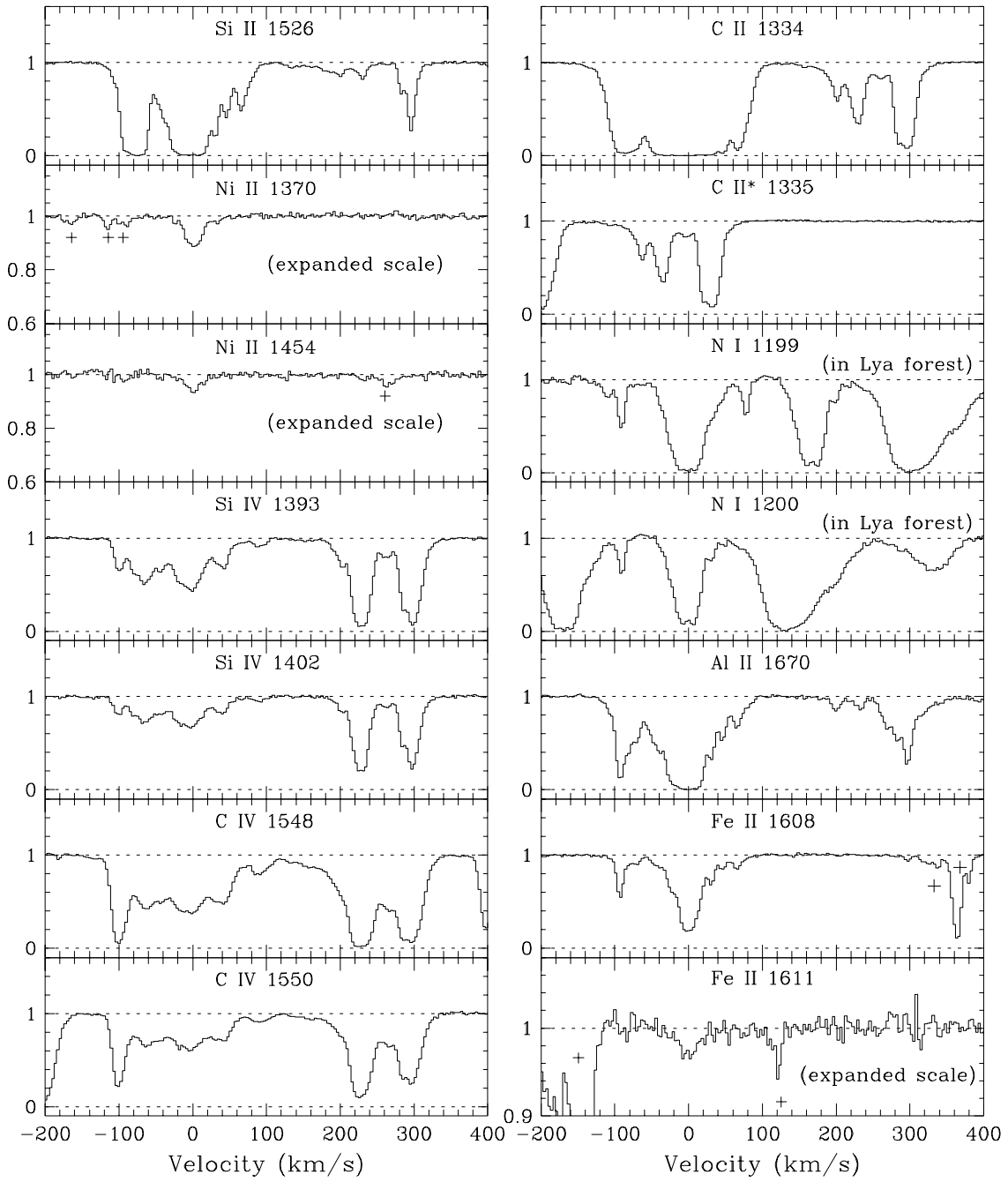


figure 13

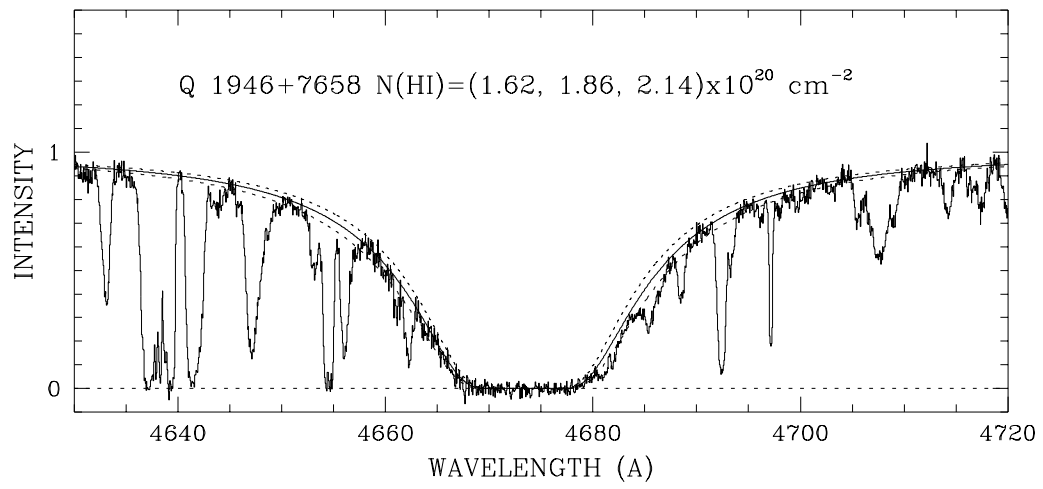


figure 14

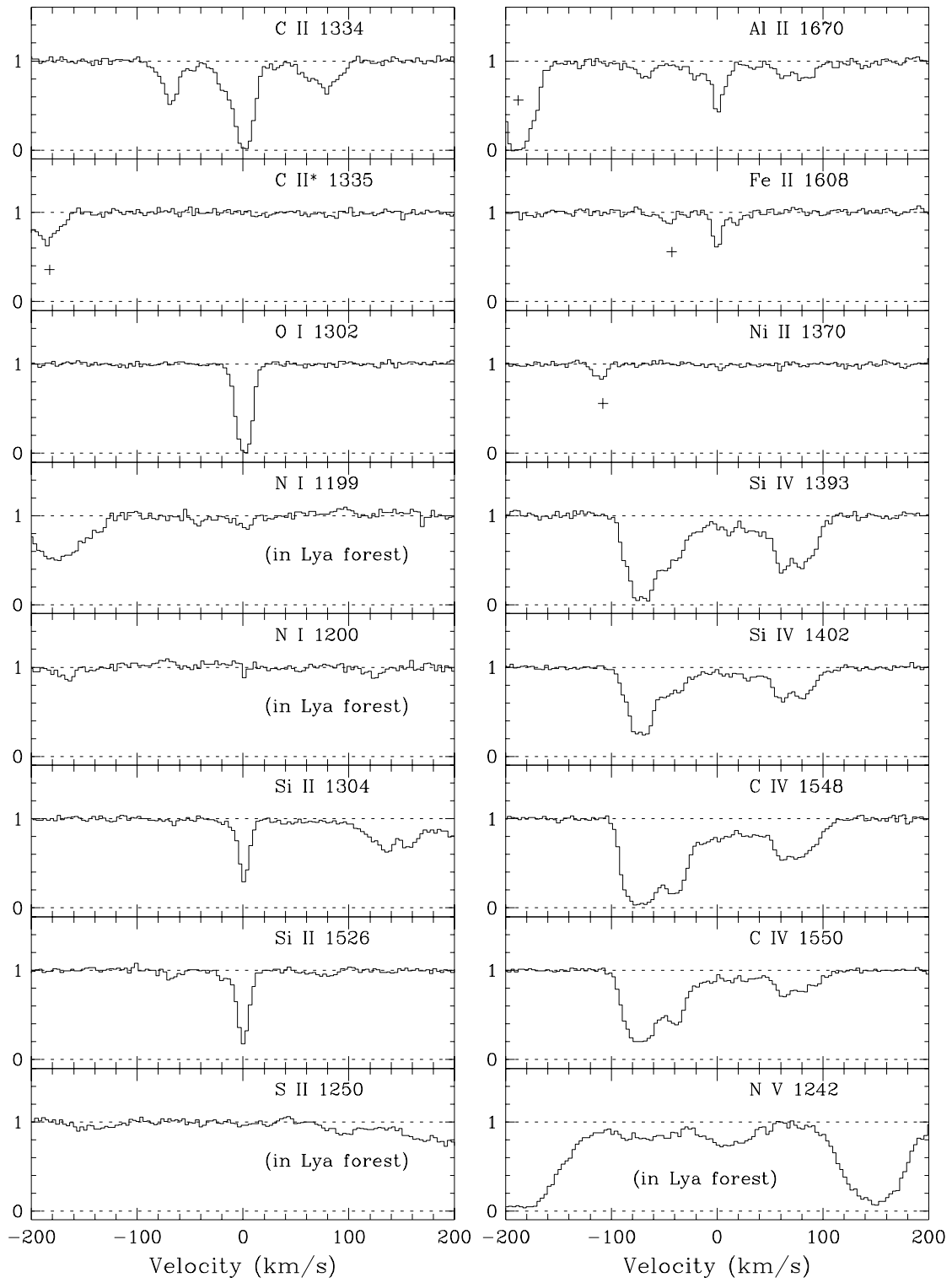


figure 15

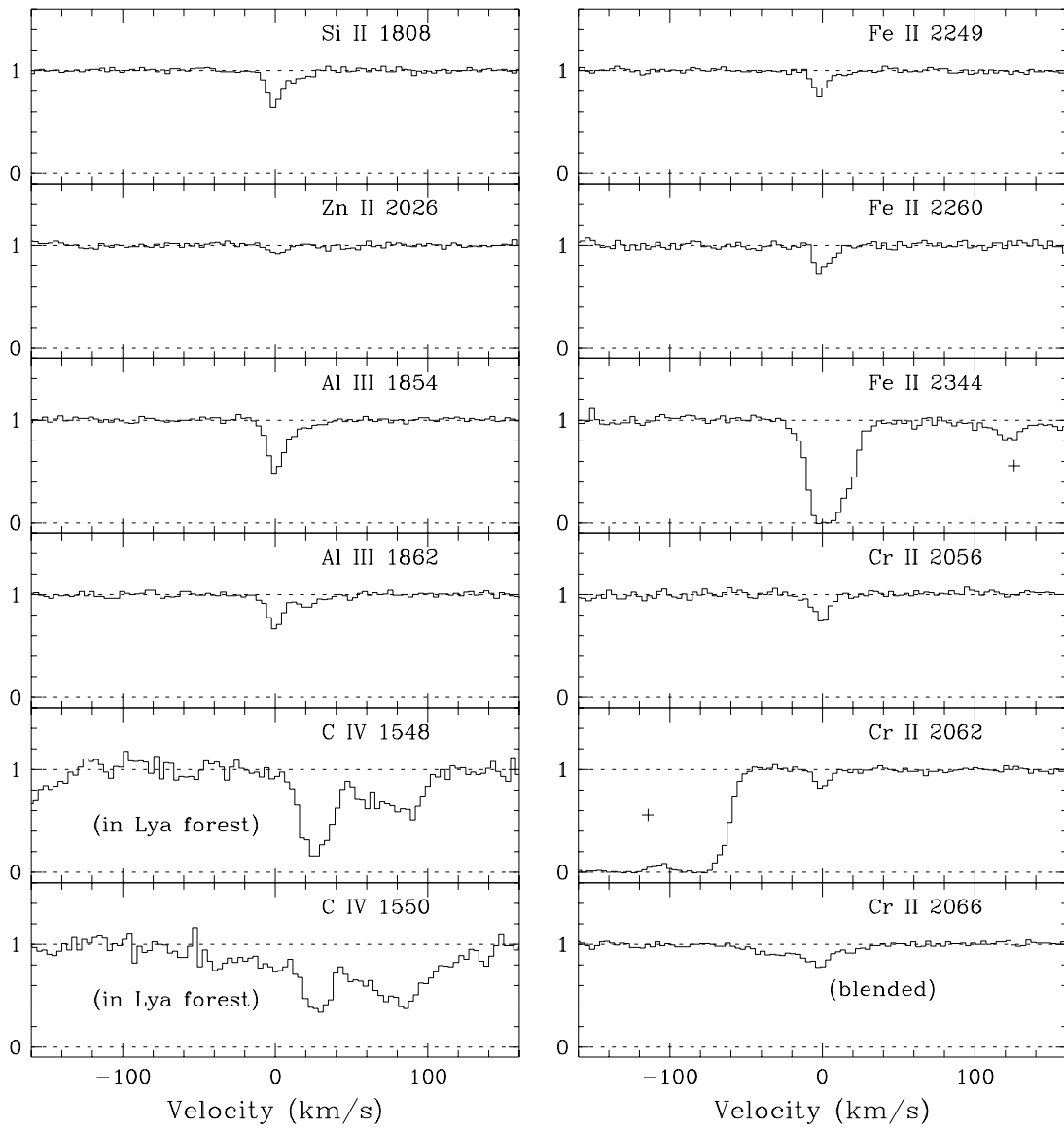


figure 16

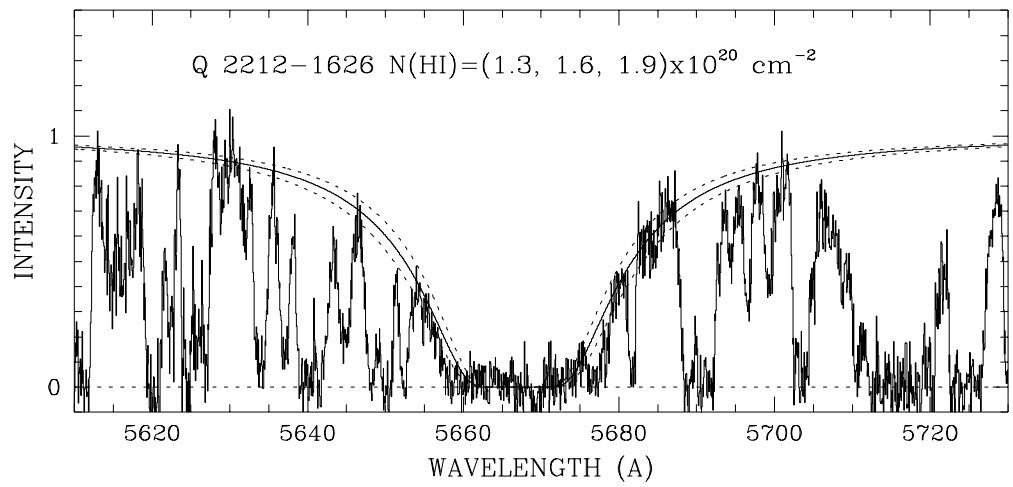


figure 17

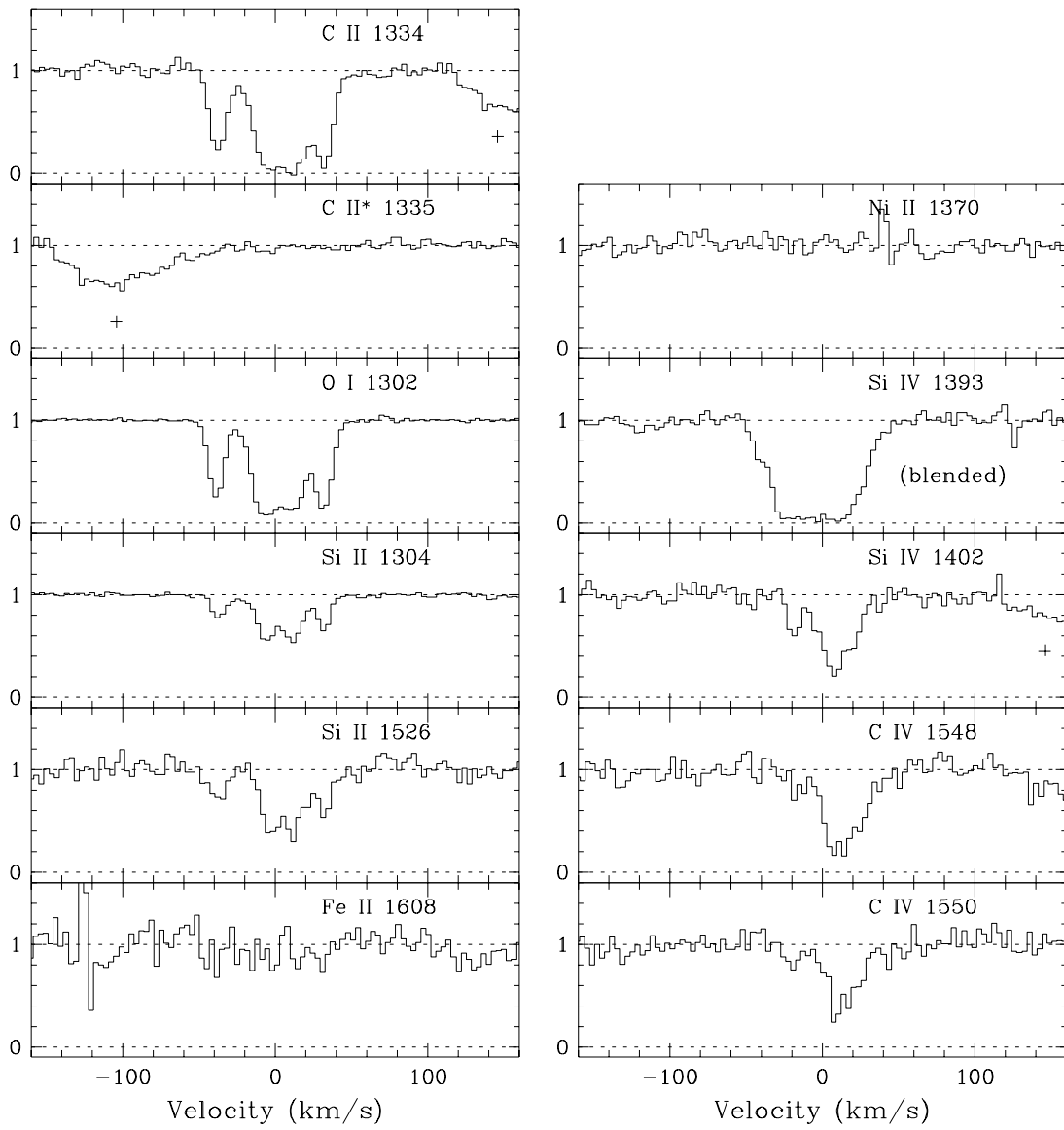


figure 18

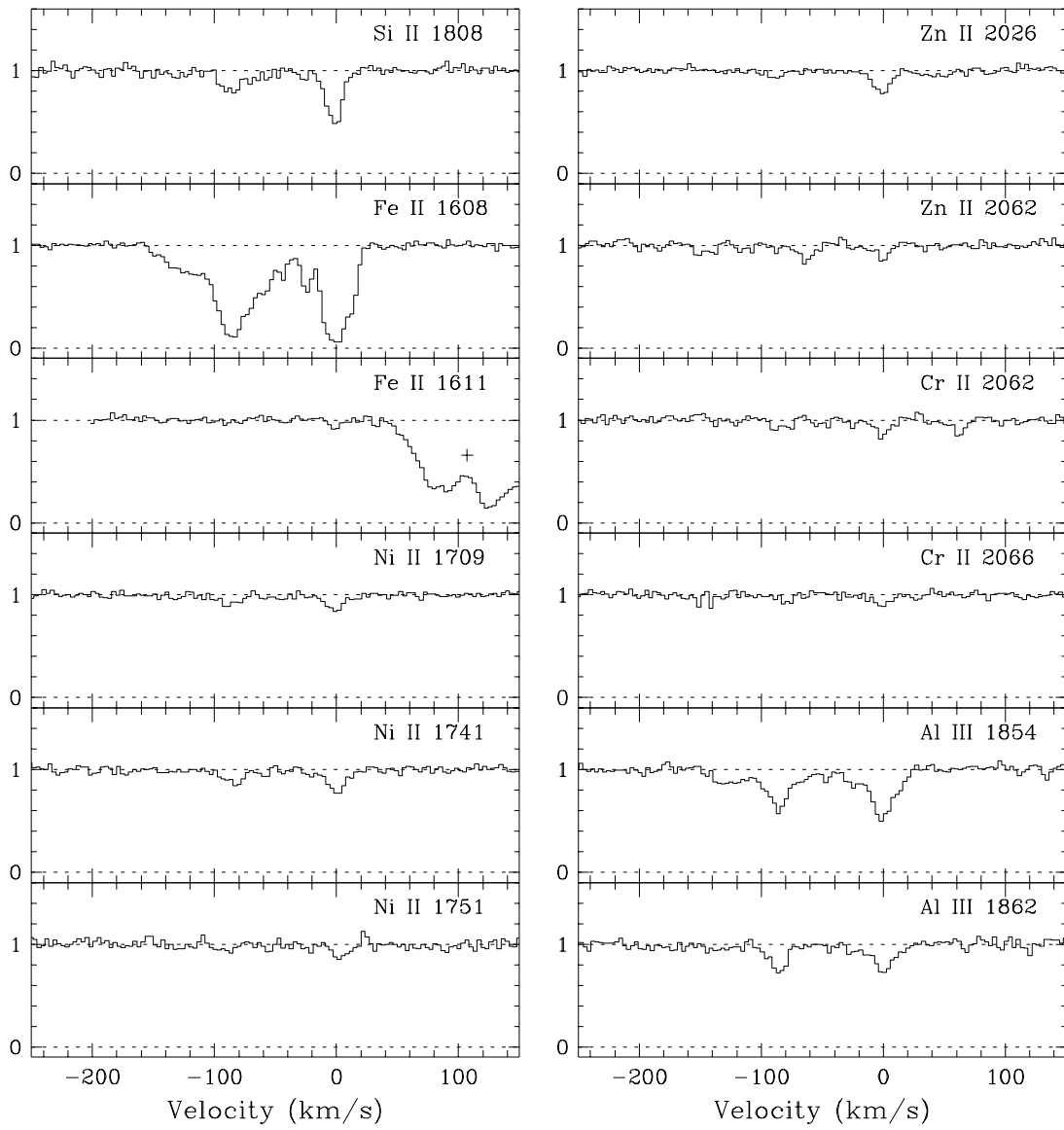


figure 19

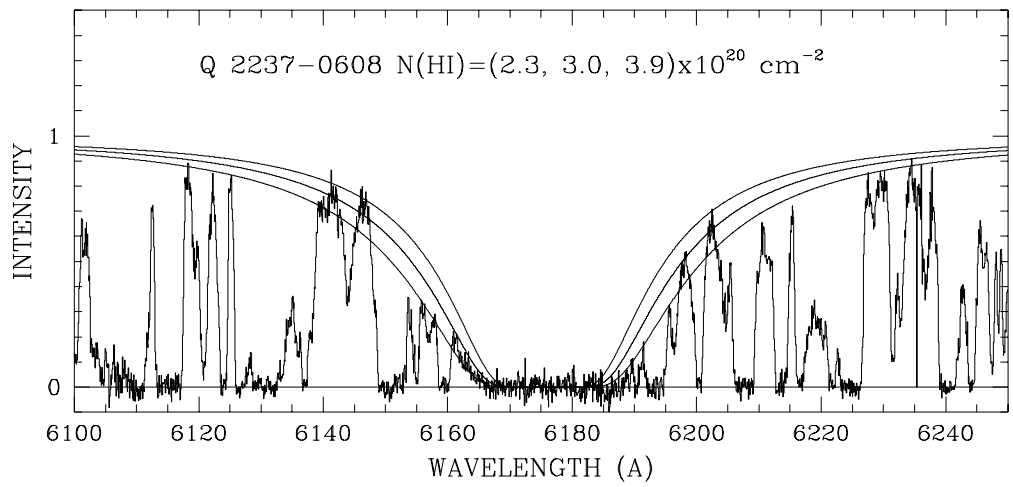


figure 20

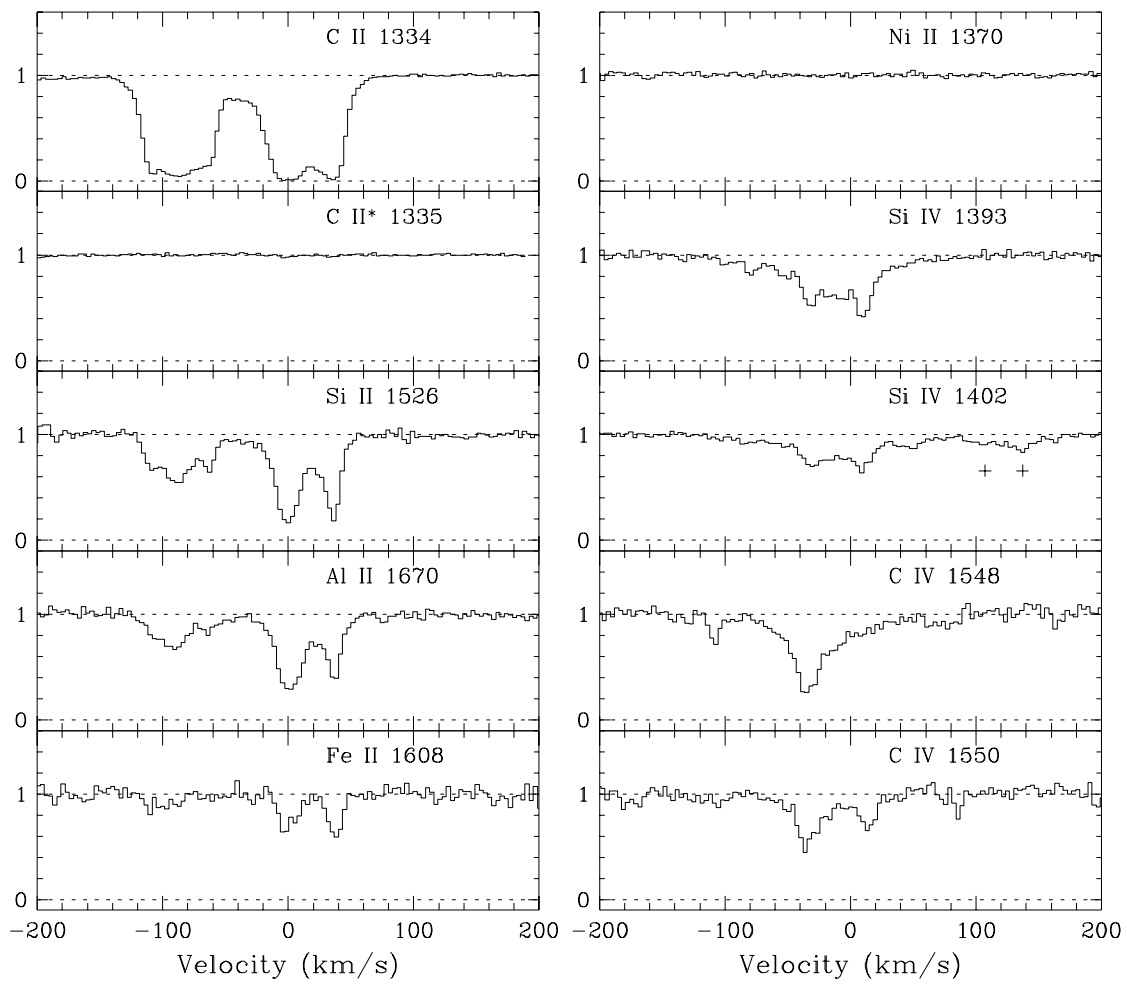


figure 21

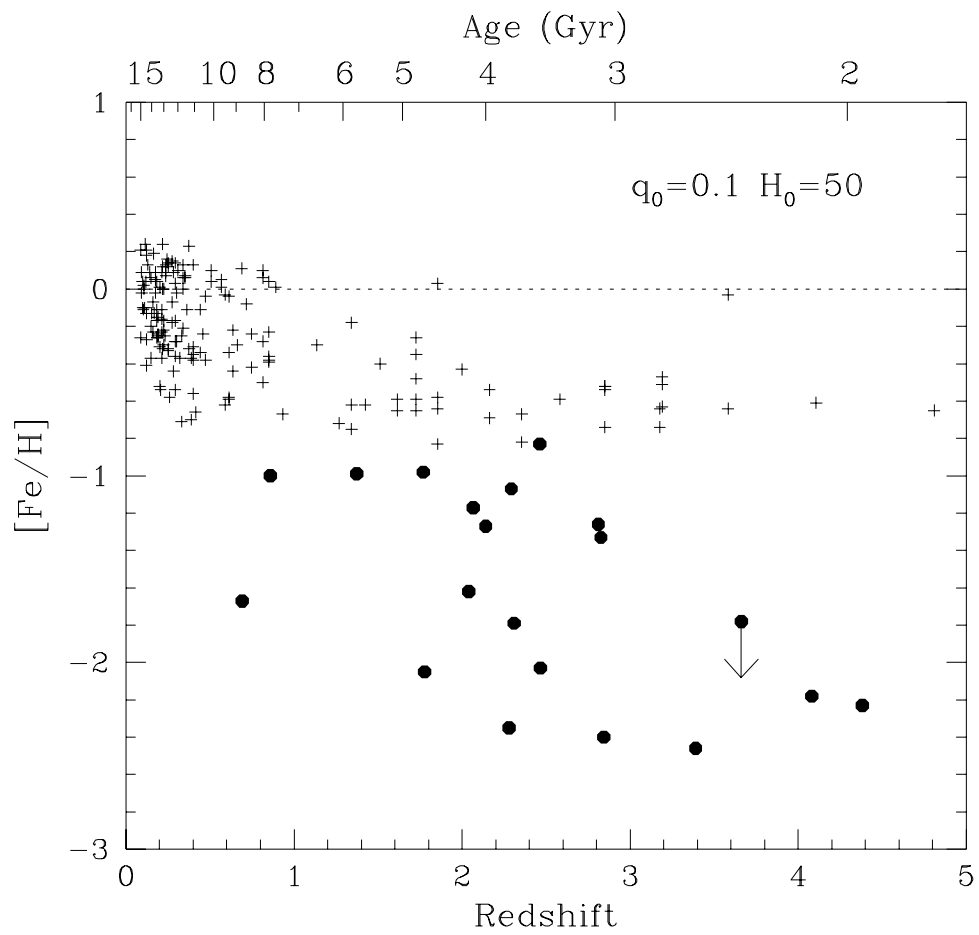


figure 22

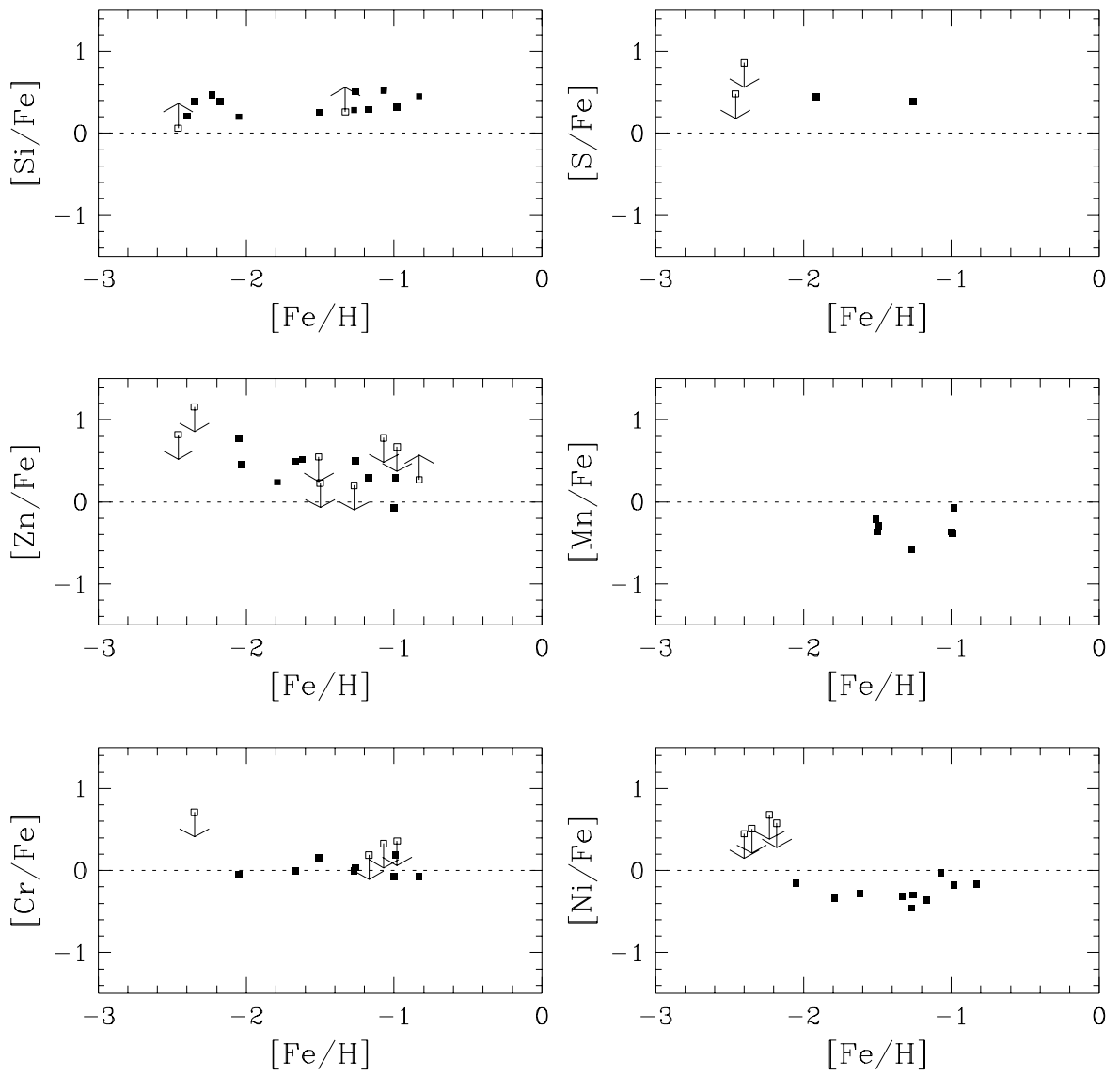


figure 23

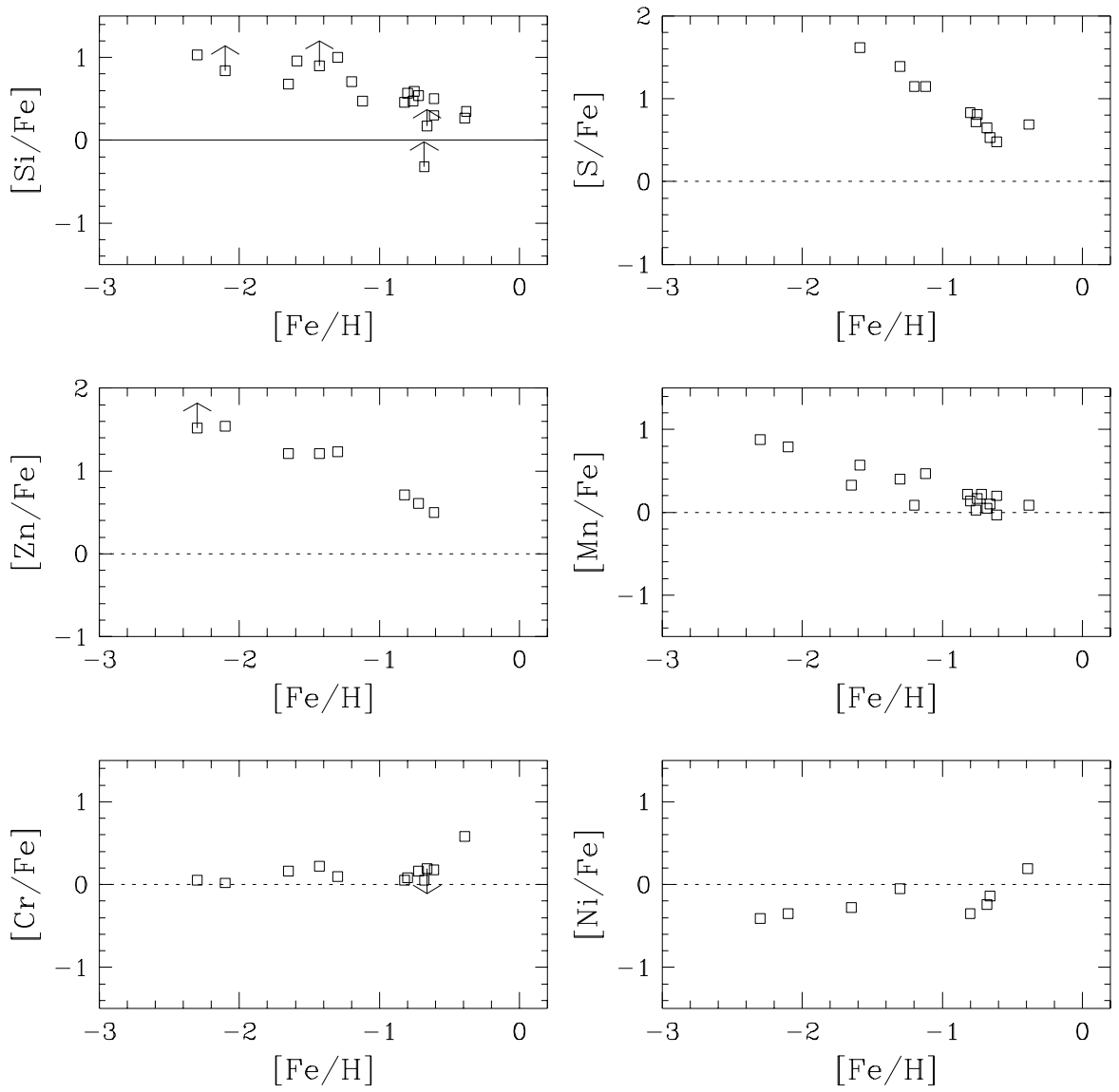


figure 24

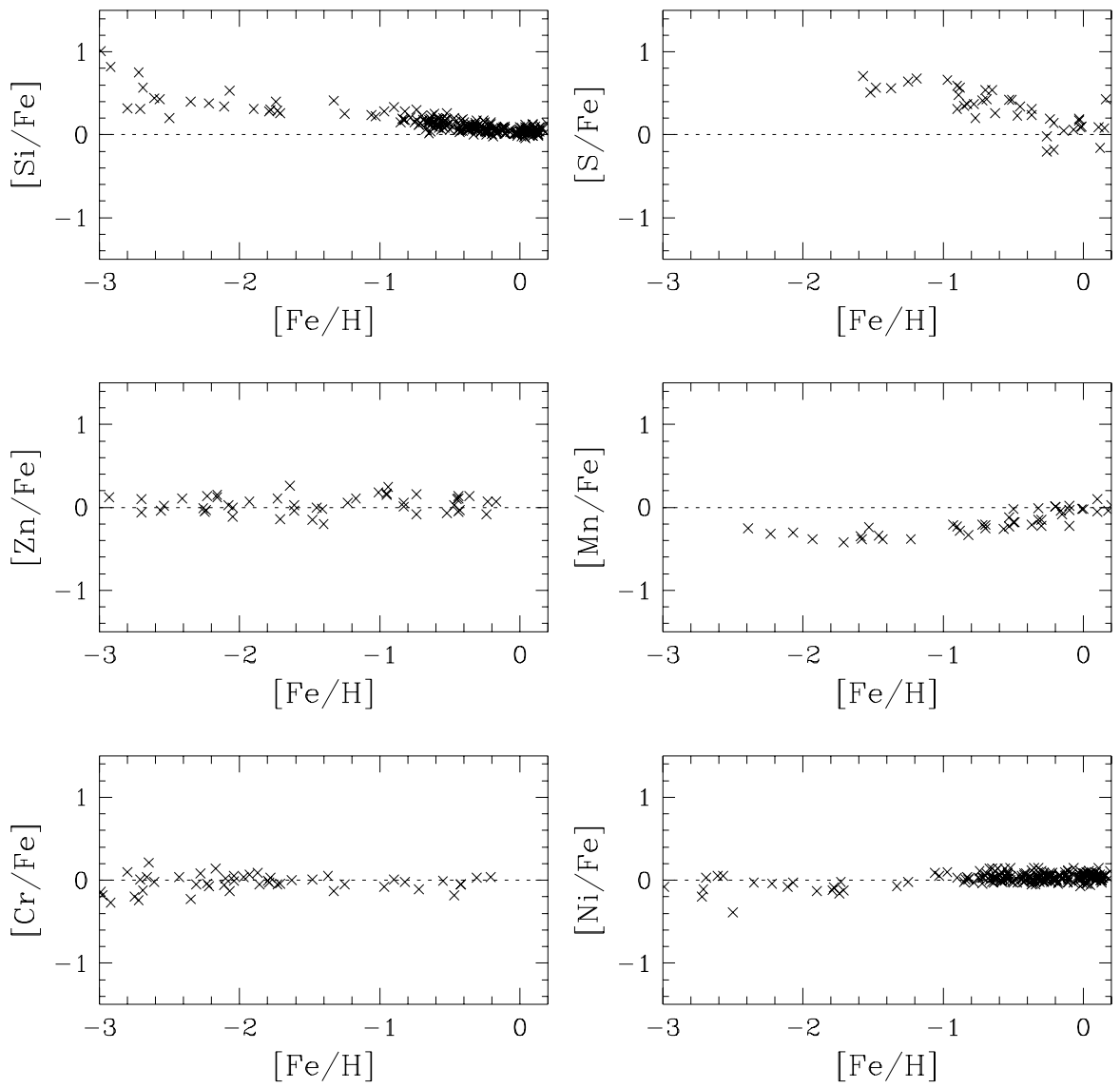


figure 25

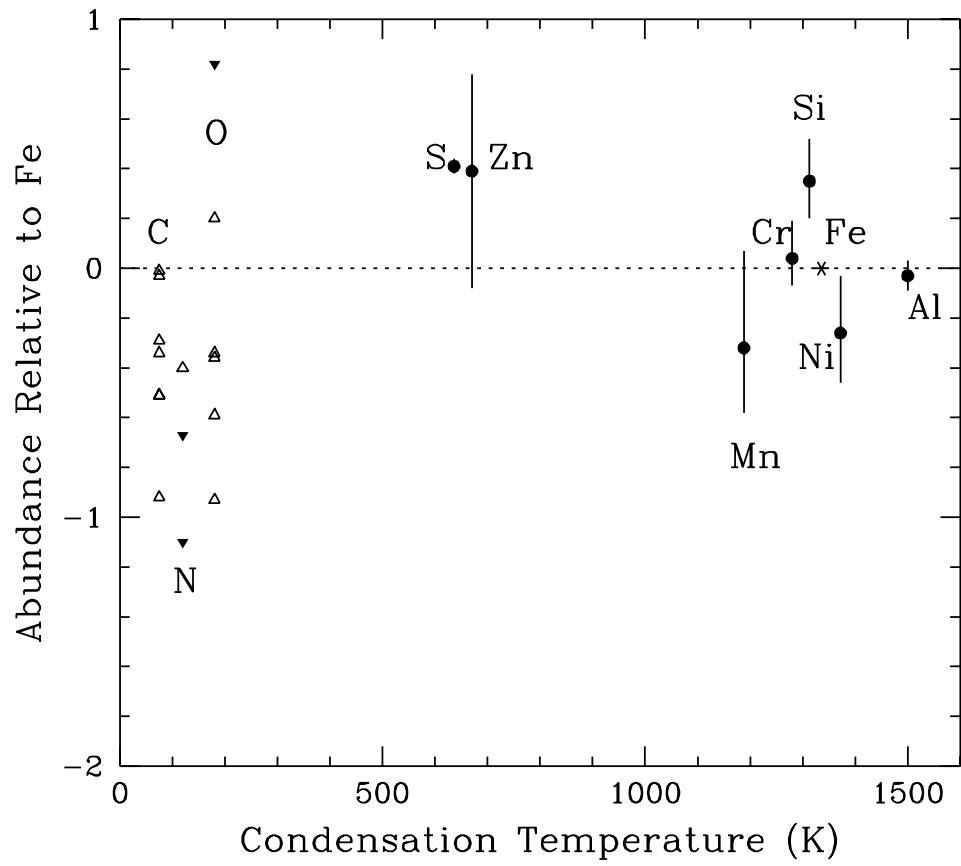


figure 26

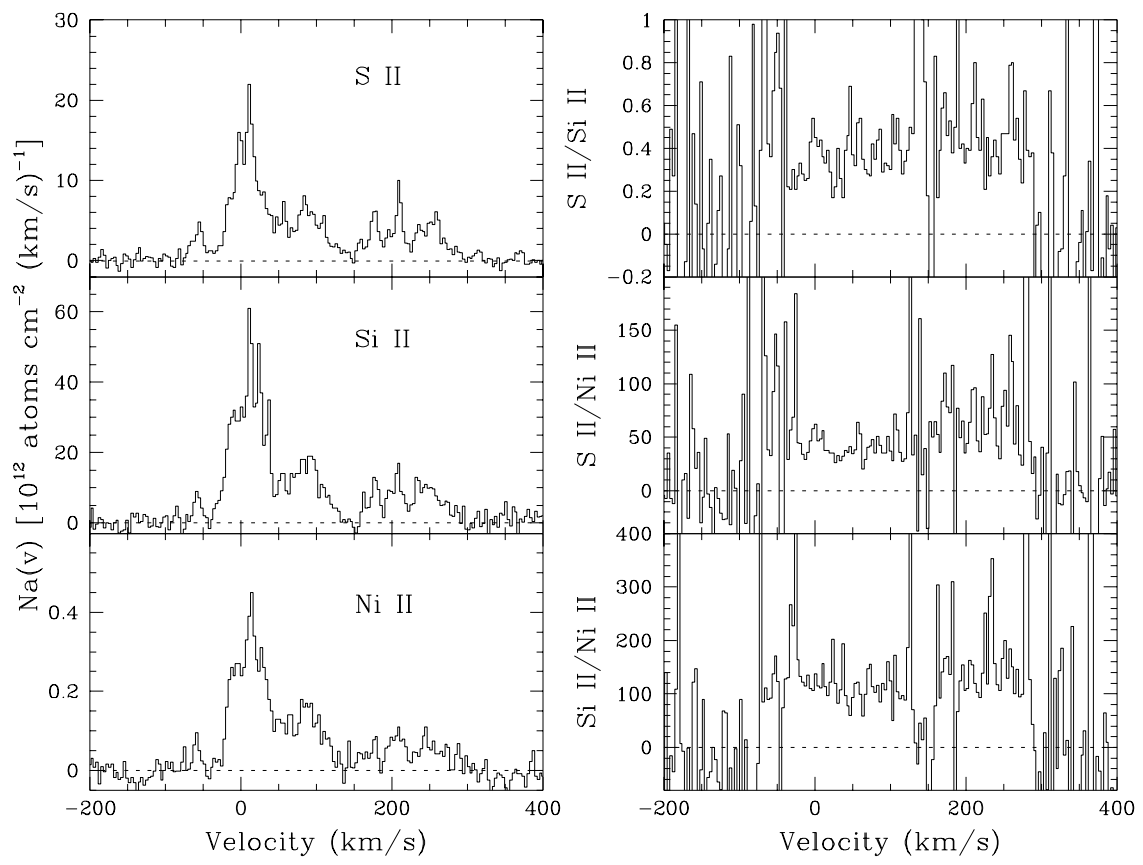


figure 27

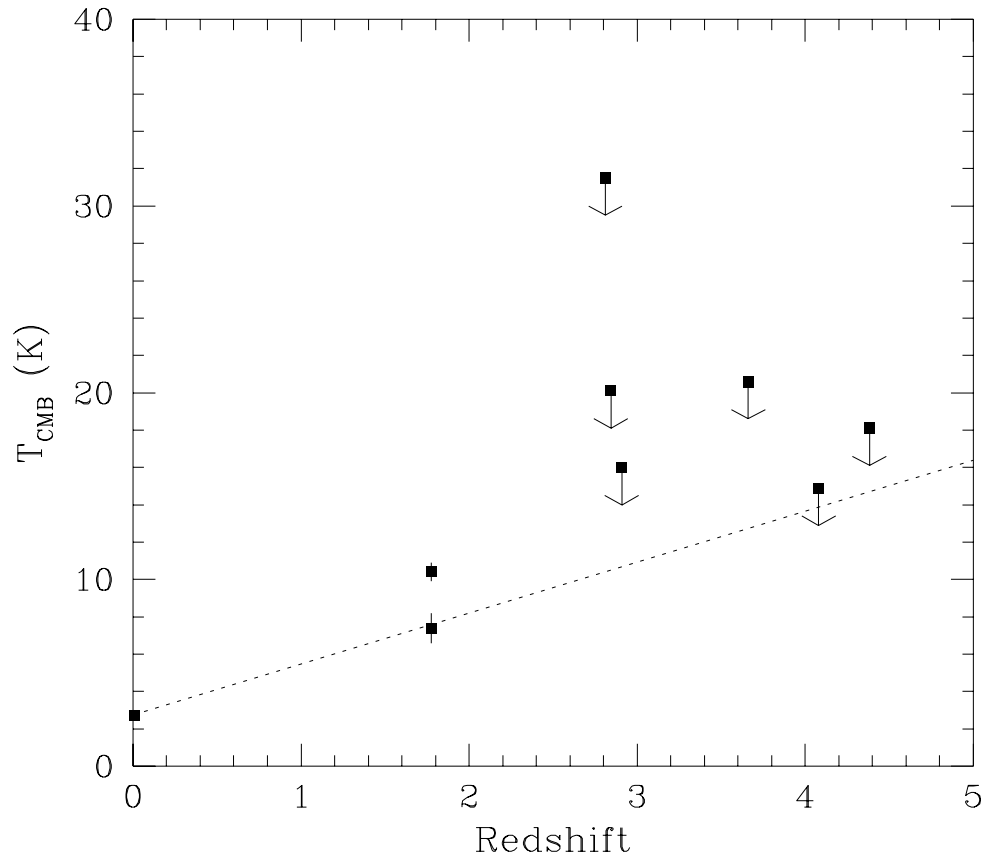


figure 28

TABLE 16

Elemental Abundances of Damped Lyman-alpha Galaxies

QSO	z_{em}	z_{damp}	$\log N(\text{H I})$	[C/H]	[N/H]	[O/H]	[Al/H]	[Si/H]	[S/H]	[Cr/H]	[Mn/H]	[Fe/H]	[Ni/H]	[Zn/H]	ref
0000-2620	4.108	3.3901	21.41	> -2.74	> -2.40	< -1.98 ^a	-2.46	...	> -2.44	...	< -1.64	1,2
0100+1300	2.686	2.3090	21.40	< -0.97	-1.79	-2.13	-1.55	9
0201+3634	2.912	2.4620	20.38	-0.38	...	-0.90	...	-0.83	-1.00	> -0.56	5
0216+0803	2.992	2.2931	20.45	> -1.05	-0.55	...	< -0.74	...	-1.07	-1.10	< -0.29	1
		1.7688	20.00	-0.66	...	< -0.62	-1.05	-0.98	-1.16	< -0.31	1
0449-1326	3.097	1.2667	... ^b	-1.78 ^b	-1.50 ^b	1
0450-1312	2.253	1.1743	... ^b	-1.35 ^b	-1.72 ^b	-1.50 ^b	...	< -0.96	1
0458-0203	2.286	2.0395	21.65	-1.62	-1.90	-1.10	11,12
0454+0356	1.350	0.8598	20.76	-1.07	-1.36	-1.00	...	-1.08	8
0528-2505	2.779	2.8110	21.20	> -2.18	...	> -2.19	> -1.48	-0.75	-0.88	-1.23	...	-1.26	-1.56	-0.76	1
		2.1410	20.70	> -1.72	-0.99	...	-1.28	-1.85	-1.27	-1.73	< -1.07	1
0935+4143	1.966	1.3726	20.30	-0.80	-1.38	-0.99	...	-0.70	4
1202-0725	4.700	4.3829	20.60	> -2.20	...	> -2.03	> -2.13	-1.76	-2.23	< -1.55	...	3
1223+1753	2.918	2.4658	21.52	-2.03	-1.58	11
1328+3045	0.849	0.6922	21.28	-1.68	...	-1.67	...	-1.18	7
1331+1704	2.084	1.7764	21.18	-1.85	...	-2.10	...	-2.05	-2.20	-1.27	10
1425+6039	3.173	2.8268	20.30	> -1.67	> -1.73	...	> -1.23	> -1.07	-1.33	-1.65	...	1
1946+7658	2.994	2.8443	20.27	> -2.69	< -3.50	> -2.74	-2.49	-2.19	< -1.54	-2.40	< -1.95	...	1
		1.7382	... ^b	-1.24 ^b	...	-1.35 ^b	-1.86 ^b	-1.50 ^b	...	< -1.27 ^b	1,6
2212-1626	3.992	3.6617	20.20	> -2.29	...	> -2.37	...	-1.90	< -1.78	< -2.01	...	1
2231-0015	3.018	2.0662	20.56	-0.88	...	< -0.98	...	-1.17	-1.53	-0.88	1
2237-0608	4.559	4.0803	20.52	> -2.19	-2.15	-1.80	-2.18	< -1.60	...	1
2348-1444	2.940	2.2794	20.57	...	< -3.02	> -2.71	...	-1.97	-1.91	< -1.64	...	-2.35	< -1.84	< -1.19	13

REFERENCES: (1) This paper; (2) Pettini *et al.* 1995b; (3) Lu *et al.* 1996a; (4) Meyer, Lanzetta, & Wolfe 1995; (5) Prochaska & Wolfe 1996; (6) Lu *et al.* 1995b; (7) Meyer & York 1992; (8) Steidel *et al.* 1995; (9) Wolfe *et al.* 1994; (10) Wolfe 1995; (11) Pettini *et al.* 1994; (12) Meyer & Roth 1990; (13) Pettini, Lipman, & Hunstead 1995a.

Notes to Table 16:

^a Taking the S II column density discussed in §3.1 as an upper limit given the possibility of contamination by Ly α forest absorption.

^b The $N(\text{H I})$ of the system is unknown (see discussion in §3). The elemental abundances are given for an assumed $[\text{Fe}/\text{H}] = -1.50$, which is typical of the sample galaxies.

TABLE 17

Elemental Abundances of Diffuse ISM Clouds

Star	Component ^a	[Si/H]	[S/H]	[Cr/H]	[Mn/H]	[Fe/H]	[Ni/H]	[Zn/H]	ref
ζ Oph	A ^b	-0.97	...	-1.49	-1.32	-1.65	-1.93	-0.44	1,2
	B ^c	-1.27	...	-2.25	-1.42	-2.30	-2.71	> -0.78	1,2
μ Col	A	-0.30	+0.09	-1.20	-0.90	-1.30	-1.35	-0.07	3
	B	-0.12	...	+0.19	...	-0.39	-0.20	...	3
HD 167756	A+B+C	> -0.53	...	-1.21	...	-1.43	...	-0.22	4
HD 93521	1	-0.03	+0.31	...	-0.29	-0.38	5
	3	-0.16	+0.06	...	-0.58	-0.75	5
	4	-0.31	-0.13	...	-0.64	-0.61	5
	6	-0.29	-0.04	...	-0.73	-0.76	5
	8	-0.49	-0.05	...	-1.11	-1.20	5
γ ² Vel	6	-0.63	+0.03	...	-1.02	-1.59	6
	7	-0.65	+0.03	...	-0.65	-1.12	6
HD 149881	2 ^d	-0.22	...	-0.54	-0.52	-0.72	...	-0.11	7
	6 ^d	-0.47	...	-0.88	-0.88	-0.93	...	-0.11	7
	8 ^d	-0.29	...	-0.67	-0.67	-0.83	...	-0.11	7
HD 116852	Group 2 ^e	> -1.00	-0.03	-0.63	-0.63	-0.68	-0.92	...	8
	Group 3 ^e	> -0.49	-0.13	< -0.47	-0.56	-0.77	-0.80	...	8
HD 18100	[-60,60]	-0.23	+0.03	-0.72	-0.66	-0.80	-1.15	...	8
ξ Per		> -1.26	...	-2.08	-1.31	-2.10	-2.45	-0.56	9

REFERENCES: (1) Savage, Cardelli, & Sofia 1992; (2) Sofia, Cardelli, & Savage 1994; (3) Sofia, Savage, & Cardelli 1993; (4) Cardelli, Sembach, & Savage (1994); (5) Spitzer & Fitzpatrick 1993; (6) Fitzpatrick & Spitzer 1994; (7) Spitzer & Fitzpatrick 1995; (8) Sembach & Savage 1996; (9) Cardelli et al. 1991b.

Notes to Table 17:

^a This refers to the component name or number given in the original paper. In the case of ξ Per, the measurements refer to the entire absorption.

^b Reference 1 assigned a $\log N(\text{H I})=19.74$ to component A, while reference 2 used $\log N(\text{H I})=20.16$. The values given here are for $\log N(\text{H I})=20.16$.

^c Reference 1 assigned a $\log N(\text{H I})=21.12$ to component B, while reference 2 used a $\log N(\text{H I})=20.09$. Here we adopt $\log N(\text{H I})=20.09$.

^d Reference 7 found $[\text{Zn}/\text{H}]=-0.11 \pm 0.08$ for the entire absorption, and gave depletions of other elements relative to Zn in each component in order to avoid the difficulty of assigning $N(\text{H I})$ to each component. Here we assume $[\text{Zn}/\text{H}]=-0.11$ for each individual components, and convert the depletions relative to Zn back to abundances relative to hydrogen.

^e Due to difficulties of assigning $N(\text{H I})$ to each group, the abundance measurements in reference 10 were given relative to Zn assuming Zn is undepleted in these warm clouds.